

EVALUATION OF CHLORIDE THRESHOLD FOR STEEL FIBER REINFORCED
CONCRETE COMPOSITES IN AGGRESSIVELY CORROSIVE ENVIRONMENTS

by

Dietrich H. Vogel

A Thesis Submitted to the Faculty of

The College of Engineering and Computer Science

In Partial Fulfillment of the Requirements for the Degree of

Masters of Science

Florida Atlantic University

Boca Raton, FL

May 2016

Copyright 2016 by Dietrich H. Vogel

EVALUATION OF CHLORIDE THRESHOLD FOR STEEL FIBER REINFORCED
CONCRETE COMPOSITES IN AGGRESSIVELY CORROSIVE ENVIRONMENTS

by

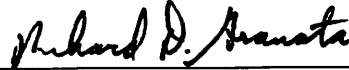
Dietrich H Vogel

This thesis was prepared under the direction of Dr. Francisco Presuel Moreno, Department of Ocean and Mechanical Engineering, and has been approved by the members of his supervisory committee. It was submitted to the faculty of the College of Engineering and Computer Science and was accepted in partial fulfillment of the requirements for the degree of Master of Science.

SUPERVISORY COMMITTEE:



Francisco Presuel-Moreno, Ph.D.
Thesis Advisor



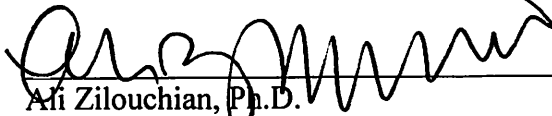
Richard Granata, Ph.D.



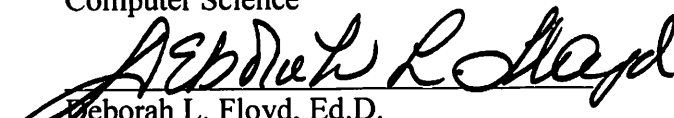
Hassan Mahfuz, Ph.D.



Javad Hashemi, Ph.D.
Chair, Department of Ocean and
Mechanical Engineering



Ali Zilouchian, Ph.D.
Dean, College of Engineering and
Computer Science



Deborah L. Floyd, Ed.D.
Dean, Graduate College

04/20/2016

Date

ACKNOWLEDGEMENTS

The author would like to thank Florida Atlantic University for providing the opportunity to research and learn. Thank you Florida Department of Transportation for providing incentive and the research relevance. For providing pipe samples as a part of testing, thank you Rinker Materials Concrete Construction. The author would like to acknowledge the senior graduate student Hariharan Balasubramanian for help and guidance; lab partner Alexander Lummus for humor and criticism. Most of all thank you to my research advisor Dr. Francisco Presuel Moreno for always being available to discuss ideas and provide suggestions. Lastly the author could not have completed the research without the unconditional love and support from his family.

ABSTRACT

Author: Dietrich H. Vogel
Title: Evaluation of Chloride Threshold for Steel Fiber Reinforced Concrete Compositing in Aggressively Corrosive Environments
Institution: Florida Atlantic University
Thesis Advisor: Dr. Francisco Presuel-Moreno
Degree: Masters of Science
Year: 2016

Highway drainage pipes utilize concrete reinforced with steel wire to help mitigate water, earth, and traffic loads. Drainage pipes reinforced with zinc electroplated steel fibers offer a lower steel alternative to traditional steel wire cage reinforcements. The objective of the thesis research was to determine the physical and electrochemical characteristics of zinc electroplated steel fiber corrosion propagation. Experimental programs include: Fracture analysis of zinc electroplated steel fibers embedded in dry-cast concrete pipes exposed to varying chloride concentrations; Visual analysis of zinc electroplated steel fibers embedded in concrete exposed to varying chloride concentrations; Electrochemical analysis of zinc electroplated steel fibers embedded in concrete exposed to varying chlorides; Chloride threshold determination for zinc electroplated steel fibers immersed in simulated pore solution. Between the four experimental programs the most significant conclusion is that oxygen, moisture, and chlorides past the chloride threshold must be present for corrosion to propagate significantly on the zinc electroplated steel fibers.

EVALUATION OF CHLORIDE THRESHOLD FOR STEEL FIBER REINFORCED
CONCRETE COMPOSITES IN AGGRESSIVELY CORROSIVE ENVIRONMENTS

| | |
|--|----|
| List of Tables | x |
| List of Figures | xi |
| 1 Introduction, Literature Review, Research Objectives | 1 |
| 1.1 Introduction..... | 1 |
| 1.2 Literature Review..... | 7 |
| 1.3 Thesis Objective..... | 12 |
| 2 Experimental Program: Fracture analysis of zinc electroplated steel fibers embedded in dry cast concrete pipes exposed to varying chlorides | 14 |
| 2.1 Introduction..... | 14 |
| 2.2 Experimental Procedure..... | 15 |
| 2.2.1 No Chloride Exposure - NC..... | 21 |
| 2.2.2 Exterior Chloride Exposure - CE..... | 21 |
| 2.2.3 Interior Chloride Exposure- CI..... | 23 |
| 2.2.4 Seawater Exposure..... | 23 |
| 2.2.5 Sodium Sulfate and Intercostal water Exposure | 24 |
| 2.3 Results and Analysis | 24 |

| | |
|--|----|
| 2.4 Conclusion | 39 |
| 3 Experimental Program: Visual Analysis of Zinc Electroplated steel fibers embedded in concrete exposed to varying chloride concentrations..... | 40 |
| 3.1 Introduction..... | 40 |
| 3.2 Experimental Procedure..... | 42 |
| 3.2.1 Non Instrumented Concrete Cylinders..... | 42 |
| 3.3 Results and Discussion | 48 |
| 3.3.1 Cylinders Cast Without Chlorides for Migration Testing (SFNCA, NCB) | 48 |
| 3.3.2 Cylinders Cast Without Chlorides (NC, NC1) | 52 |
| 3.3.3 Cylinders Cast With Chlorides (C2, C3, HC1, HC2) | 55 |
| 3.3.4 Conclusions..... | 63 |
| 4 Experimental Program: electrochemical analysis of zinc electroplated steel fibers embedded in concrete exposed to varying chloride..... | 64 |
| 4.1 Introduction..... | 64 |
| 4.2 Experimental Procedure..... | 65 |
| 4.2.1 Instrumented samples cast with no chlorides..... | 67 |
| 4.2.2 Instrumented samples cast with chlorides C4, C7, C8 | 75 |
| 4.3 Results and Discussion | 76 |
| 4.3.1 C1, C5, C6 Control Samples..... | 77 |

| | | |
|-------|--|-----|
| 4.3.2 | LWCA, LWCB, HWC Passive Transport Samples | 80 |
| 4.3.3 | P1, P2 Passive Transport Poke Samples | 85 |
| 4.3.4 | MLWC A, MLWC B; Migration Cylinders | 90 |
| 4.3.5 | B1, B2; Migration Blocks | 95 |
| 4.3.6 | Instrumented samples cast with chlorides C4, C7, C8 | 102 |
| 4.4 | Conclusions..... | 109 |
| 5 | Experimental Program: Chloride threshold determination for zinc electroplated steel fibers immersed in simulated pore solution..... | 110 |
| 5.1 | Introduction..... | 110 |
| 5.2 | Experimental Procedure..... | 111 |
| 5.2.1 | A1- Bare Fibers; pH 12.6..... | 111 |
| 5.2.2 | A2- Bare Fibers; pH 13.3..... | 112 |
| 5.2.3 | A3- 13.3 pH mortar coating on fibers | 113 |
| 5.3 | Results and Discussion | 114 |
| 5.3.1 | A1- Bare Fibers; pH 12.6..... | 114 |
| 5.3.2 | A2- Bare Fibers; pH 13.3..... | 117 |
| 5.3.3 | A3- 13.3 pH mortar coating on fibers | 119 |
| 5.4 | Conclusions..... | 122 |
| 6 | Summary and Conclusions | 124 |
| 6.1 | Summary | 124 |

| | | |
|-------|--|-----|
| 6.2 | Conclusions..... | 126 |
| 6.2.1 | Fracture Analysis of Zinc Electroplated Steel Fibers Embedded in Dry-cast Concrete Pipes Exposed to Varying Chlorides..... | 126 |
| 6.2.2 | Visual Analysis of Zinc Electroplated Steel Fibers Embedded in Concrete Exposed to Varying Chloride Concentrations..... | 127 |
| 6.2.3 | Electrochemical Analysis of Zinc Electroplated Steel Fibers Embedded in Concrete Exposed to Varying Chlorides | 127 |
| 6.2.4 | Chloride Threshold Determination for Zinc Electroplated Steel Fibers Immersed in Simulated Pore Solution | 127 |
| 7 | Appendix..... | 129 |
| 8 | References..... | 233 |

LIST OF TABLES

| | |
|--|----|
| Table 2-1 Chloride penetration distances measured using a caliper and the non-steady state migration coefficient | 26 |
| Table 2-2 Chloride penetration distances measured using a caliper and the non-steady state migration coefficient | 28 |
| Table 2-3 Average modulus of rupture for each beam type | 32 |
| Table 2-4 Summary table of modulus of rupture and fiber count..... | 38 |
| Table 3-1 Concrete Compositions and water to cement ratios | 43 |
| Table 3-2 Resistivity of concrete sample SFNCA..... | 48 |
| Table 3-3 Resistivity of concrete sample NCB units in kohms*cm | 48 |
| Table 3-4 Non-Steady State Diffusion Coefficient..... | 50 |

LIST OF FIGURES

| | |
|--|----|
| Figure 1.1 Zinc Electroplated Steel Fibers; 28mm in length, .35mm X.6mm helix cross sectional area Photograph by Dietrich Vogel copyright 2016 by Dietrich Vogel..... | 5 |
| Figure 1.2 Metallographic microscope close-up of the zinc layer highlighted in green with an etching solution; the layer thickness was estimated to be nearly 1µm Photograph by Dietrich Vogel copyright 2016 by Dietrich Vogel..... | 5 |
| Figure 2.1 ASTM C78 test setup for beam bending [10] | 15 |
| Figure 2.2 Pipe section S-2 made to be the no chloride control sample for beam bending Photograph by Dietrich Vogel copyright 2016 by Dietrich Vogel | 18 |
| Figure 2.3 Pipe section after interior face chloride migration Photograph by Dietrich Vogel copyright 2016 by Dietrich Vogel..... | 18 |
| Figure 2.4 Pipe sample exposed to exterior chloride migration Photograph by Dietrich Vogel copyright 2016 by Dietrich Vogel | 19 |
| Figure 2.5 Graph of concrete resistivity over time in large pipe sections Photograph by Dietrich Vogel copyright 2016 by Dietrich Vogel | 25 |
| Figure 2.6 Sample CI3 sprayed with AgCl to indicate chloride migration Photograph by Dietrich Vogel copyright 2016 by Dietrich Vogel | 27 |
| Figure 2.7 Beam CE1 sprayed with silver nitrate to indicate chloride penetration Photograph by Dietrich Vogel copyright 2016 by Dietrich Vogel..... | 27 |

| | |
|---|----|
| Figure 2.8 Sample SW2 after being sprayed with silver nitrate Photograph by Dietrich Vogel copyright 2016 by Dietrich Vogel | 29 |
| Figure 2.9 Beam NC2; modulus of rupture 1030 PSI Photograph by Dietrich Vogel copyright 2016 by Dietrich Vogel | 30 |
| Figure 2.10 Beam sample CE2; modulus of rupture 910 PSI Photograph by Dietrich Vogel copyright 2016 by Dietrich Vogel..... | 30 |
| Figure 2.11 Beam sample CI2; modulus of rupture 805 PSI Photograph by Dietrich Vogel copyright 2016 by Dietrich Vogel..... | 31 |
| Figure 2.12 Beam sample SW2; modulus of rupture 895 PSI Photograph by Dietrich Vogel copyright 2016 by Dietrich Vogel..... | 31 |
| Figure 2.13 Beam Sample S2; modulus of rupture 940 PSI Photograph by Dietrich Vogel copyright 2016 by Dietrich Vogel..... | 32 |
| Figure 2.14 Beam sample CI2 with the fibers mapped and analyzed: 21 fibers, 5 brittle fractures and 3 corroded pullout fibers Photograph by Dietrich Vogel copyright 2016 by Dietrich Vogel | 33 |
| Figure 2.15 Stereographic microscope picture of a brittle fracture observed in beam CI2 Photograph by Dietrich Vogel copyright 2016 by Dietrich Vogel | 34 |
| Figure 2.16 Companion brittle fiber to a brittle fracture observed on beam CI2 Photograph by Dietrich Vogel copyright 2016 by Dietrich Vogel..... | 34 |
| Figure 2.17 Beam sample CI3 with fibers mapped and the conditions analyzed Photograph by Dietrich Vogel copyright 2016 by Dietrich Vogel..... | 35 |

| | |
|---|----|
| Figure 2.18 Pullout failure despite the onset of corrosion; fiber observed in sample CI1 observed under the stereographic microscope Photograph by Dietrich Vogel copyright 2016 by Dietrich Vogel..... | 36 |
| Figure 2.19 Increased corrosion in a large concrete pore from sample CI2 Photograph by Dietrich Vogel copyright 2016 by Dietrich Vogel | 36 |
| Figure 2.20 Beam sample CE3with the fibers mapped and the conditions indicated by color Photograph by Dietrich Vogel copyright 2016 by Dietrich Vogel..... | 37 |
| Figure 3.1 Single test setup for a chloride migration test indicated by NT build 492 | 41 |
| Figure 3.2 Non-instrumented samples cast without chlorides (NC, NCI) Photograph by Dietrich Vogel copyright 2016 by Dietrich Vogel | 46 |
| Figure 3.3 Non-instrumented samples cast with chlorides (HC1, HC2, C2, C3) Photograph by Dietrich Vogel copyright 2016 by Dietrich Vogel | 47 |
| Figure 3.4 Core 4 from NCB after RMT picture taken months after being split Photograph by Dietrich Vogel copyright 2016 by Dietrich Vogel | 49 |
| Figure 3.5 2mm slices taken from slice 2 of sample NCB after 4 weeks of lab humidity and oxygen exposure Photograph by Dietrich Vogel copyright 2016 by Dietrich Vogel..... | 51 |
| Figure 3.6 Fibers extracted from the 10mm depth slice taken from sample 2 of NCB Photograph by Dietrich Vogel copyright 2016 by Dietrich Vogel | 52 |
| Figure 3.7 Sample NC after first slice taken 6 months after casting Photograph by Dietrich Vogel copyright 2016 by Dietrich Vogel | 53 |
| Figure 3.8 Disk from sample NC after 5 weeks of outdoor exposure Photograph by Dietrich Vogel copyright 2016 by Dietrich Vogel | 54 |

| | |
|---|----|
| Figure 3.9 Fibers taken from the NC disk stored outdoors for 5 weeks Photograph by Dietrich Vogel copyright 2016 by Dietrich Vogel | 55 |
| Figure 3.10 Sample HC1 after the first slice Photograph by Dietrich Vogel copyright 2016 by Dietrich Vogel..... | 56 |
| Figure 3.11 Sample C3 after the first slice Photograph by Dietrich Vogel copyright 2016 by Dietrich Vogel..... | 57 |
| Figure 3.12 Four slices of sample HC1 taken in early February Photograph by Dietrich Vogel copyright 2016 by Dietrich Vogel | 58 |
| Figure 3.13 Extracted samples from sample C3 shortly after a disk was sliced off of the cylinder Photograph by Dietrich Vogel copyright 2016 by Dietrich Vogel ... | 59 |
| Figure 3.14 Disk sample HC1 after 5 weeks of outdoor exposure Photograph by Dietrich Vogel copyright 2016 by Dietrich Vogel | 60 |
| Figure 3.15 Fibers extracted from the HC1 disk sample exposed to outside conditions Photograph by Dietrich Vogel copyright 2016 by Dietrich Vogel..... | 60 |
| Figure 3.16 Disk HC1 exposed to inside conditions for 5 weeks Photograph by Dietrich Vogel copyright 2016 by Dietrich Vogel | 61 |
| Figure 3.17 Disk HC1 Exposed to high humidity and restricted oxygen for 5 weeks Photograph by Dietrich Vogel copyright 2016 by Dietrich Vogel..... | 62 |
| Figure 4.1 Instrumented Samples without chlorides(Left to right:C1, C5, C6) Photograph by Dietrich Vogel copyright 2016 by Dietrich Vogel..... | 68 |
| Figure 4.2 Instrumented samples cast without chlorides (Left to right: HWC, LWCA, LWCB) Photograph by Dietrich Vogel copyright 2016 by Dietrich Vogel | 69 |

| | |
|--|----|
| Figure 4.3 Instrumented samples with the poke method(Left to right: P2, P1) | |
| Photograph by Dietrich Vogel copyright 2016 by Dietrich Vogel | 71 |
| Figure 4.4 Instrumented Migration samples (Left to right: MLWCB, MLWCA) | |
| Photograph by Dietrich Vogel copyright 2016 by Dietrich Vogel | 72 |
| Figure 4.5 Migration block samples. (Left to right: B2, B1) Photograph by Dietrich | |
| Vogel copyright 2016 by Dietrich Vogel..... | 74 |
| Figure 4.6 Instrumented sample cast with chlorides(Left-C8, Center-C7, Right-C4) | |
| Photograph by Dietrich Vogel copyright 2016 by Dietrich Vogel | 76 |
| Figure 4.7 Corrosion potential graph of sample C1..... | 77 |
| Figure 4.8 Corrosion potential graph of sample C5..... | 78 |
| Figure 4.9 Corrosion potential graph of sample C6..... | 78 |
| Figure 4.10 Fiber SF1 from sample C6 Photograph by Dietrich Vogel copyright 2016 | |
| by Dietrich Vogel..... | 79 |
| Figure 4.11 Carbon steel wire from sample C1 Photograph by Dietrich Vogel | |
| copyright 2016 by Dietrich Vogel | 79 |
| Figure 4.12 Corrosion potential graph of sample LWCA..... | 80 |
| Figure 4.13 Corrosion potential graph of sample LWCB..... | 80 |
| Figure 4.14 Corrosion potential graph of sample HWC..... | 81 |
| Figure 4.15 Apparent polarization resistance measurements graphed for sample | |
| LWCA..... | 82 |
| Figure 4.16 Apparent polarization resistance measurements graphed for sample | |
| LWCB | 82 |

| | |
|--|----|
| Figure 4.17 Apparent polarization resistance measurements graphed for sample HWC | 83 |
| Figure 4.18 Forensic analysis of fiber LWCA SF1 Photograph by Dietrich Vogel copyright 2016 by Dietrich Vogel | 83 |
| Figure 4.19 Forensic analysis of LWCB SF2 Photograph by Dietrich Vogel copyright 2016 by Dietrich Vogel | 84 |
| Figure 4.20 Forensic analysis of HWC SF2 Photograph by Dietrich Vogel copyright 2016 by Dietrich Vogel..... | 84 |
| Figure 4.21 Corrosion potential for sample P1 | 86 |
| Figure 4.22 Corrosion potential for sample P2..... | 86 |
| Figure 4.23 Apparent polarization resistance for sample P1 | 87 |
| Figure 4.24 Apparent polarization resistance for sample P2 | 87 |
| Figure 4.25 Carbon steel wires protruding from sample P2 Photograph by Dietrich Vogel copyright 2016 by Dietrich Vogel..... | 88 |
| Figure 4.26 Forensic analysis of P1 CW1 Photograph by Dietrich Vogel copyright 2016 by Dietrich Vogel..... | 88 |
| Figure 4.27 Forensic analysis of P2 SF 1 depth 40mm Photograph by Dietrich Vogel copyright 2016 by Dietrich Vogel | 89 |
| Figure 4.28 Forensic analysis of P2 SF2 depth 30mm Photograph by Dietrich Vogel copyright 2016 by Dietrich Vogel | 89 |
| Figure 4.29 Corrosion potential for migration cylinder MLWCA | 91 |
| Figure 4.30 Corrosion potential for migration cylinder MLWCB..... | 91 |
| Figure 4.31 Polarization resistance for sample MLWCA..... | 92 |

| | |
|---|-----|
| Figure 4.32 Polarization resistance for MLWCB | 92 |
| Figure 4.33 Forensic analysis of MLWCA SF 11; cover depth 10mm Photograph by Dietrich Vogel copyright 2016 by Dietrich Vogel | 93 |
| Figure 4.34 Forensic evaluation of MLWCA SF 13; cover depth 10mm Photograph by Dietrich Vogel copyright 2016 by Dietrich Vogel | 94 |
| Figure 4.35 Forensic evaluation of MLWCB 32; cover depth 30mm Photograph by Dietrich Vogel copyright 2016 by Dietrich Vogel | 94 |
| Figure 4.36 Forensic analysis of MLWCB SF 31; cover depth 30mm Photograph by Dietrich Vogel copyright 2016 by Dietrich Vogel | 95 |
| Figure 4.37 Corrosion potential for migration block B1 | 96 |
| Figure 4.38 Corrosion potential for block B2..... | 97 |
| Figure 4.39 Polarization resistance for migration block B1 | 98 |
| Figure 4.40 Polarization resistance for migration block B2 | 98 |
| Figure 4.41 Forensic analysis of B1 SF1; cover depth 10mm Photograph by Dietrich Vogel copyright 2016 by Dietrich Vogel..... | 99 |
| Figure 4.42 Forensic analysis of B1 SF2; cover depth 20mm Photograph by Dietrich Vogel copyright 2016 by Dietrich Vogel..... | 99 |
| Figure 4.43 Forensic analysis of B1 SF3; cover depth 30mm Photograph by Dietrich Vogel copyright 2016 by Dietrich Vogel..... | 100 |
| Figure 4.44 Forensic analysis of B1 SF4; cover depth 40mm Photograph by Dietrich Vogel copyright 2016 by Dietrich Vogel..... | 101 |
| Figure 4.45 Forensic analysis of B2 SF 3; cover depth 12.5mm Photograph by Dietrich Vogel copyright 2016 by Dietrich Vogel | 101 |

| | |
|---|-----|
| Figure 4.46 Forensic analysis of B2 SF 5; cover depth 10mm Photograph by Dietrich Vogel copyright 2016 by Dietrich Vogel..... | 102 |
| Figure 4.47 Corrosion potential of chloride cylinder C4..... | 103 |
| Figure 4.48 Corrosion potential of chloride cylinder C7 | 103 |
| Figure 4.49 Corrosion potential of chloride cylinder C8..... | 104 |
| Figure 4.50 Apparent polarizations resistance for chloride cylinder C4 | 105 |
| Figure 4.51 Apparent polarizations resistance for chloride cylinder C7 | 105 |
| Figure 4.52 Apparent polarizations resistance for chloride cylinder C8 | 106 |
| Figure 4.53 Forensic analysis of sample C4 SF 1 on top, SF 2 on the bottom Photograph by Dietrich Vogel copyright 2016 by Dietrich Vogel..... | 106 |
| Figure 4.54 Forensic analysis of chloride cylinder C7 pictured left SF 1 pictured right SF2 Photograph by Dietrich Vogel copyright 2016 by Dietrich Vogel..... | 107 |
| Figure 4.55 Forensic analysis of sample C8 SF1 Photograph by Dietrich Vogel copyright 2016 by Dietrich Vogel | 108 |
| Figure 4.56 Forensic analysis of C8 SF 2 Photograph by Dietrich Vogel copyright 2016 by Dietrich Vogel..... | 108 |
| Figure 5.1 Corrosion potential for simulated pore solution A1 | 115 |
| Figure 5.2 Apparent polarization resistance measurements for simulated pore solution sample A1 | 116 |
| Figure 5.3 Forensic analysis for A1 SF2 Photograph by Dietrich Vogel copyright 2016 by Dietrich Vogel..... | 116 |
| Figure 5.4 Forensic analysis for A1 SF 5 Photograph by Dietrich Vogel copyright 2016 by Dietrich Vogel..... | 117 |

| | |
|--|-----|
| Figure 5.5 Corrosion potential for simulated pore solution A2 | 118 |
| Figure 5.6 Apparent polarization resistance measurements for simulated pore solution sample A2 | 119 |
| Figure 5.7 Corrosion potential for simulated pore solution A3 | 120 |
| Figure 5.8 Apparent polarization resistance measurements for simulated pore solution sample A3 | 121 |
| Figure 5.9 Forensic analysis of simulated pore solution A3 SF 1 Photograph by Dietrich Vogel copyright 2016 by Dietrich Vogel | 122 |
| Figure 7.1 No chloride exposure pipe section | 129 |
| Figure 7.2 Chloride exposure to the pipe exterior post RMT | 129 |
| Figure 7.3 Chloride exposure to pipe interior post RMT | 130 |
| Figure 7.4 Pipe sections CE (left) and CI (right) subject to environmental conditioning | 130 |
| Figure 7.5 Beam NC1 post ASTM C78..... | 130 |
| Figure 7.6 Failure plane 1 for beam NC1 | 131 |
| Figure 7.7 Failure plane 2 for beam, NC1 | 131 |
| Figure 7.8 Combined failure planes for NC1..... | 132 |
| Figure 7.9 Beam NC2 post ASTM C78..... | 132 |
| Figure 7.10 Failure plane 1 for beam NC2 | 133 |
| Figure 7.11 Failure plane 2 for beam NC2 | 133 |
| Figure 7.12 Combined failure planes NC2 | 134 |
| Figure 7.13 Beam crack comparison NC2..... | 134 |
| Figure 7.14 Beam NC3 post ASTM C78..... | 135 |

| | |
|---|-----|
| Figure 7.15 Failure plane 1 for beam NC3 | 135 |
| Figure 7.16 Failure plane 2 for beam NC3 | 136 |
| Figure 7.17 Combined failure planes NC3 | 136 |
| Figure 7.18 Beam CE1 post ASTM C78 | 137 |
| Figure 7.19 Combined failure planes CE1 | 137 |
| Figure 7.20 Beam crack comparison CE1 | 138 |
| Figure 7.21 Beam CE1 sprayed with silver nitrate | 138 |
| Figure 7.22 Beam CE2 post ASTM C78 | 139 |
| Figure 7.23 Failure plane 1 for beam CE2..... | 139 |
| Figure 7.24 Failure plane 2 for beam CE2..... | 140 |
| Figure 7.25 Companion failure faces CE2..... | 140 |
| Figure 7.26 Beam CE2 crack comparison | 141 |
| Figure 7.27 Beam CE3 post ASTM C78 | 141 |
| Figure 7.28 Failure plane 1 for beam CE3..... | 142 |
| Figure 7.29 Failure plane 2 for beam CE3..... | 142 |
| Figure 7.30 Companion failure faces for beam CE3 | 143 |
| Figure 7.31 Crack comparison for beam CE3 | 143 |
| Figure 7.32 Beam CI1 post ASTM C78 | 144 |
| Figure 7.33 Failure plane 1 for beam CI1 | 144 |
| Figure 7.34 Failure plane 2 for beam CI1 | 145 |
| Figure 7.35 companion failure planes for beam CI1 | 145 |
| Figure 7.36 Failure plane from beam CI1 sprayed with silver nitrate | 146 |
| Figure 7.37 CI 2 | 146 |

| | |
|--|-----|
| Figure 7.38 Failure plane 1 for beam CI2..... | 147 |
| Figure 7.39 Failure plane 2 for beam CI2..... | 147 |
| Figure 7.40 Companion failure faces for beam CI2 | 148 |
| Figure 7.41 Microscope picture of a brittle fracture in beam sample CI2..... | 148 |
| Figure 7.42 companion face to the previous picture..... | 149 |
| Figure 7.43 microscopic picture of corrosion propagation on a pullout failure fiber..... | 149 |
| Figure 7.44 Beam CI3 post ASTM C78 | 149 |
| Figure 7.45 Failure plane 1 for beam CI3..... | 150 |
| Figure 7.46 Failure plane 2 for beam CI3..... | 150 |
| Figure 7.47 companion failure planes for beam CI3 | 151 |
| Figure 7.48 Beam SW1 post ASTM C78 | 151 |
| Figure 7.49 Failure plane 1 for beam SW1..... | 152 |
| Figure 7.50 Failure plane 2 for beam SW1..... | 152 |
| Figure 7.51 Companion failure faces for beam SW1 | 153 |
| Figure 7.52 Beam SW2 post ASTM C78 | 153 |
| Figure 7.53 Failure plane 1 for beam SW2..... | 154 |
| Figure 7.54 Failure plane 2 for beam SW2..... | 154 |
| Figure 7.55 Companion failure planes for beam SW2 | 155 |
| Figure 7.56 Beam S1 post ASTM C78..... | 155 |
| Figure 7.57 Failure plane 1 for beam S1..... | 156 |
| Figure 7.58 Failure plane 2 for beam S1..... | 156 |
| Figure 7.59 companion failure planes for beam S1 | 157 |
| Figure 7.60 Beam S2 post ASTM C78..... | 157 |

| | |
|---|-----|
| Figure 7.61 Failure plane 1 for beam S2..... | 158 |
| Figure 7.62 Failure plane 2 for beam S2..... | 158 |
| Figure 7.63 Companion failure planes for beam S2 | 159 |
| Figure 7.64 Remaining pipe section pieces NC, CI, CE (left to Right)..... | 159 |
| Figure 7.65 Concrete mold with 4 inch diameter and 8 inch length..... | 159 |
| Figure 7.66 Slice 1 From NCB after being sprayed with silver nitrate | 160 |
| Figure 7.67 Slice 4 From NCB after being sprayed with silver nitrate | 160 |
| Figure 7.68 Slices approximately 2mm thick from RMT sample 2 after elevated temperature conditioning | 161 |
| Figure 7.69 Fibers extracted from slice 8mm to 10mm cover depth RMT sample 2..... | 161 |
| Figure 7.70 Slices approximately 2mm thick from RMT sample 3 after elevated temperature conditioning | 162 |
| Figure 7.71 Fibers extracted from slice 8mm to 10mm cover depth RMT sample 3..... | 162 |
| Figure 7.72 Slices approximately 2mm thick from RMT sample B after elevated temperature conditioning | 163 |
| Figure 7.73 Fibers extracted from slice 8mm to 10mm cover depth RMT sample B | 163 |
| Figure 7.74 Slices approximately 2mm thick from RMT sample C after elevated temperature conditioning | 164 |
| Figure 7.75 Fibers extracted from slice 8mm to 10mm cover depth RMT sample C | 164 |
| Figure 7.76 Non-instrumented no chloride control samples NC and NCI | 165 |
| Figure 7.77 Four slices from sample NCI..... | 165 |
| Figure 7.78 Fibers extracted after a NCI slice was crushed immediately after cutting.. | 166 |
| Figure 7.79 Three slices from sample NC | 166 |

| | |
|---|-----|
| Figure 7.80 Fibers extracted after a NC slice was crushed immediately after cutting ... | 167 |
| Figure 7.81 Slice NC exposed outdoors 5 weeks after cutting | 167 |
| Figure 7.82 Slice NC exposed outdoors 5 weeks after cutting side 2..... | 168 |
| Figure 7.83 Fibers extracted from slice NC left outdoors | 168 |
| Figure 7.84 Slice NCI exposed outdoors 5 weeks after cutting..... | 169 |
| Figure 7.85 Slice NCI exposed outdoors 5 weeks after cutting side 2 | 169 |
| Figure 7.86 Fibers extracted from slice NCI left outdoors | 170 |
| Figure 7.87 Slice NC exposed to lab humidity 5 weeks after cutting..... | 170 |
| Figure 7.88 Slice NC exposed to lab humidity 5 weeks after cutting side 2 | 171 |
| Figure 7.89 fibers extracted from slice NC left in lab humidity..... | 171 |
| Figure 7.90 Slice NCI exposed to lab humidity 5 weeks after cutting | 172 |
| Figure 7.91 Slice NC exposed to lab humidity 5 weeks after cutting side 2 | 172 |
| Figure 7.92 Fibers extracted from slice NCI after lab humidity exposure | 173 |
| Figure 7.93 Slice NC exposed to high moisture and low oxygen for 5 weeks after cutting | 173 |
| Figure 7.94 Slice NC exposed to high moisture and low oxygen for 5 weeks after cutting side 2 | 174 |
| Figure 7.95 Fibers extracted from slice NC exposed to high moisture and low oxygen | 174 |
| Figure 7.96 Slice NCI exposed to high moisture and low oxygen for 5 weeks after cutting | 175 |
| Figure 7.97 Slice NCI exposed to high moisture and low oxygen for 5 weeks after cutting side 2 | 175 |

| | |
|---|-----|
| Figure 7.98 Fibers extracted from slice NCI exposed to high moisture and low oxygen..... | 176 |
| Figure 7.99 Non-instrumented samples cast with chlorides | 176 |
| Figure 7.100 Four slices taken from high chloride sample HC1 | 177 |
| Figure 7.101 Fibers taken from a crushed slice immediately after cutting..... | 177 |
| Figure 7.102 Slice HC1 after 5 weeks of outdoor exposure | 178 |
| Figure 7.103 Slice HC1 after 5 weeks of outdoor exposure side 2..... | 178 |
| Figure 7.104 fibers extracted from the HC1 slice left outdoors | 179 |
| Figure 7.105 Slice HC1 after 5 weeks of lab humidity exposure | 179 |
| Figure 7.106 Slice HC1 after 5 weeks of lab humidity exposure side 2..... | 180 |
| Figure 7.107 Fibers extracted from slice HC1 exposed to lab humidity | 180 |
| Figure 7.108 Slice HC1 after 5 weeks of high moisture and limited oxygen exposure . | 181 |
| Figure 7.109 Slice HC1 after 5 weeks of high moisture and limited oxygen exposure side 2 | 181 |
| Figure 7.110 Fibers extracted from slice HC1 exposed to high humidity and low oxygen..... | 182 |
| Figure 7.111 Four slices from cylinder HC2 4 months after casting..... | 182 |
| Figure 7.112 fibers extracted from a slice immediately after cutting..... | 183 |
| Figure 7.113 Slice HC2 after 5 weeks of outdoor exposure | 183 |
| Figure 7.114 Slice HC2 after 5 weeks of outdoor exposure side 2..... | 184 |
| Figure 7.115 Fibers extracted from slice HC2 left outdoors | 184 |
| Figure 7.116 Slice HC2 after 5 weeks of lab humidity exposure | 185 |
| Figure 7.117 Slice HC2 after 5 weeks of lab humidity exposure side 2..... | 185 |

| | |
|---|-----|
| Figure 7.118 Fibers extracted from the HC2 slice left in lab humidity | 186 |
| Figure 7.119 Slice HC2 after 5 weeks of high moisture and low oxygen exposure..... | 186 |
| Figure 7.120 Slice HC2 after 5 weeks of high moisture and low oxygen exposure side 2 | 186 |
| Figure 7.121 Fibers extracted from slice HC2 exposed to high moisture and low humidity | 187 |
| Figure 7.122 Four chloride slices from sample C2 taken 6 months after casting..... | 187 |
| Figure 7.123 Fibers extracted from a slice C2 immediately after cutting | 188 |
| Figure 7.124 Slice C2 after 5 weeks of outdoor exposure | 188 |
| Figure 7.125 Slice C2 after 5 weeks of outdoor exposure side 2 | 189 |
| Figure 7.126 Fibers extracted from slice C2 left outdoors | 189 |
| Figure 7.127 Slice C2 exposed to lab humidity for 5 weeks after cutting..... | 190 |
| Figure 7.128 Slice C2 after 5 weeks of outdoor exposure side 2 | 190 |
| Figure 7.129 Fibers extracted from slice C2 after lab humidity exposure..... | 191 |
| Figure 7.130 Slice C2 exposed to high moisture and low oxygen for 5 weeks after cutting | 191 |
| Figure 7.131 Slice C2 exposed to high moisture and low oxygen for 5 weeks after cutting side 2 | 192 |
| Figure 7.132 Fibers extracted from slice C2 exposed to high moisture and limited oxygen..... | 192 |
| Figure 7.133 Four slices from cylinder C3 cut 6 months after casting with chlorides... | 193 |
| Figure 7.134 fibers extracted from a slice immediately after cutting | 193 |
| Figure 7.135 Slice C3 exposed outdoors for 5 weeks after cutting | 194 |

| | |
|--|-----|
| Figure 7.136 Slice C3 exposed outdoors for 5 weeks after cutting side 2..... | 194 |
| Figure 7.137 Fibers extracted from slice C3 left outdoors | 195 |
| Figure 7.138 Slice C3 exposed to lab humidity for 5 weeks after cutting..... | 195 |
| Figure 7.139 Slice C3 exposed to lab humidity for 5 weeks after cutting side 2 | 195 |
| Figure 7.140 Fibers extracted from slice C3 exposed to lab humidity | 196 |
| Figure 7.141 Slice C3 exposed to high moisture and low oxygen for 5 weeks after cutting | 196 |
| Figure 7.142 Slice C3 exposed to high moisture and low oxygen for 5 weeks after cutting side 2..... | 197 |
| Figure 7.143 Fibers extracted from slice C3 exposed to high moisture and low oxygen..... | 197 |
| Figure 7.144 All samples cast by the researcher used in the experimental programs | 198 |
| Figure 7.145 Instrumented cylinders cast without chlorides for experimental control .. | 198 |
| Figure 7.146 No chloride cylinder C1 | 199 |
| Figure 7.147 CW1 from C1 | 199 |
| Figure 7.148 SF1 from C1 | 199 |
| Figure 7.149 Cylinder C6 | 200 |
| Figure 7.150 SF1 from C6..... | 200 |
| Figure 7.151 SF2 from C6 | 200 |
| Figure 7.152 Cylinders subject to passive chloride migration HWC right, LWCA center and LWCB right..... | 201 |
| Figure 7.153 SF 1 from cylinder LWCA..... | 201 |
| Figure 7.154 CW from LWCA..... | 201 |

| | |
|---|-----|
| Figure 7.155 SF 2 from LWCA | 201 |
| Figure 7.156 LWCB after pond removal | 202 |
| Figure 7.157 SF1 from cylinder LWCB | 202 |
| Figure 7.158 SF2 from LWCB | 202 |
| Figure 7.159 CW from LWCB | 202 |
| Figure 7.160 SF1 from HWC..... | 203 |
| Figure 7.161 CW from HWC..... | 203 |
| Figure 7.162 SF2 from HWC..... | 203 |
| Figure 7.163 Poke instrumentation cylinders P1 left P2 right | 204 |
| Figure 7.164 Carbon steel wires from poke sample P1 9 months after casting..... | 204 |
| Figure 7.165 CW1 at 40mm cover depth from sample P1 | 205 |
| Figure 7.166 CW2 at 30mm cover depth from sample P1 | 205 |
| Figure 7.167 CW3 at 20mm cover depth from sample P1 | 205 |
| Figure 7.168 Steel fiber face from poke sample P1 | 206 |
| Figure 7.169 SF1 at 40mm cover depth from sample P1 | 206 |
| Figure 7.170 SF2 at 30mm cover depth from sample P1 | 206 |
| Figure 7.171 SF3 at 20mm cover depth from sample P1 | 206 |
| Figure 7.172 Carbon steel wires exposed on sample P2 8 months after casting | 207 |
| Figure 7.173 CW1 at 40mm cover depth from sample P2 | 207 |
| Figure 7.174 CW2 at 30mm cover depth from sample P2 | 207 |
| Figure 7.175 CW3 at 20mm cover depth from sample P2 | 207 |
| Figure 7.176 CW4 at 10mm cover depth from sample P2 | 208 |
| Figure 7.177 steel fibers while exposed from sample P2 | 208 |

| | |
|--|-----|
| Figure 7.178 SF1 40mm cover depth sample P2 | 208 |
| Figure 7.179 SF2 30mm cover depth sample P2 | 208 |
| Figure 7.180 SF3 20mm cover depth sample P2 | 209 |
| Figure 7.181 SF4 10mm cover depth sample P2 | 209 |
| Figure 7.182 MLWC1 left and MLWC2 right while ponded | 210 |
| Figure 7.183 SF 11 cover depth 10mm from MLWC1 | 210 |
| Figure 7.184 CW 12 cover depth 10mm from MLWC1 | 210 |
| Figure 7.185 SF 13 cover depth 10mm from MLWC1 | 211 |
| Figure 7.186 SF 21 cover depth 20mm from MLWC1 | 211 |
| Figure 7.187 CW 22 cover depth 20mm from MLWC1 | 211 |
| Figure 7.188 SF 23 cover depth 20mm from MLWC1 | 211 |
| Figure 7.189 SF 31 cover depth 30mm from MLWC1 | 212 |
| Figure 7.190 CW 32 cover depth 30mm from MLWC1 | 212 |
| Figure 7.191 SF 33 cover depth 30mm from MLWC1 | 212 |
| Figure 7.192 SF 11 cover depth 10mm from MLWC2 | 212 |
| Figure 7.193 SF 12 cover depth 10mm from MLWC2 | 213 |
| Figure 7.194 CW 13 cover depth 10mm from MLWC2 | 213 |
| Figure 7.195 SF 21 cover depth 20mm from MLWC2 | 213 |
| Figure 7.196 SF 22 cover depth 20mm from MLWC2 | 213 |
| Figure 7.197 CW 23 cover depth 20mm from MLWC2 | 213 |
| Figure 7.198 SF 31 cover depth 30mm from MLWC2 | 214 |
| Figure 7.199 SF 32 cover depth 30mm from MLWC2 | 214 |
| Figure 7.200 CW 33 cover depth 30mm from MLWC2 | 214 |

| | |
|---|-----|
| Figure 7.201 Sample B1 left and sample B2 right shown with reservoir ponds | 215 |
| Figure 7.202 SF1 at 10mm cover depth taken from sample B1 | 215 |
| Figure 7.203 Instrumented SF2 at 20mm cover depth taken from sample B1 | 215 |
| Figure 7.204 SF2 at 20mm cover depth taken from sample B1 | 216 |
| Figure 7.205 SF3 at 30mm cover depth taken from sample B1 | 216 |
| Figure 7.206 Instrumented SF4 at 40mm cover depth taken from sample B1 | 216 |
| Figure 7.207 SF4 at 40mm cover depth taken from sample B1 | 217 |
| Figure 7.208 CW1 at 40mm cover depth taken from sample B1 | 217 |
| Figure 7.209 Instrumented CW2..... | 217 |
| Figure 7.210 CW2 at 30mm cover depth taken from sample B1 much of the fiber was destroyed by the milling process to obtain a chloride profile..... | 217 |
| Figure 7.211 CW 3 at 20mm cover depth taken from sample B1 | 218 |
| Figure 7.212 CW 4 at 10mmcover depth taken from sample B1 | 218 |
| Figure 7.213 Sample B2 after the first step of forensic analysis | 218 |
| Figure 7.214 Instrumented CW1 at 10mm cover depth taken from sample B2 | 219 |
| Figure 7.215 Instrumented CW2 at 20mm cover depth taken from sample B2 | 219 |
| Figure 7.216 Instrumented SF1 at 12.5mm cover depth taken from sample B2 | 219 |
| Figure 7.217 SF1 at 12.5mm cover depth taken from sample B2 | 219 |
| Figure 7.218 Instrumented SF2 at 20mm cover depth taken from sample B2 | 219 |
| Figure 7.219 SF2 at 20mm cover depth taken from sample B2 | 220 |
| Figure 7.220 Instrumented SF3 at 10mm cover depth taken from sample B2 | 220 |
| Figure 7.221 SF3 at 10mm cover depth taken from sample B2 | 220 |
| Figure 7.222 Samples cast with chlorides C8 left, C7 center, and C4 right | 221 |

| | |
|---|-----|
| Figure 7.223 SF1 from sample C4..... | 221 |
| Figure 7.224 SF2 with instrumentation from sample C4..... | 221 |
| Figure 7.225 SF2 from sample C4..... | 222 |
| Figure 7.226 Assorted non-instrumented fibers embedded in sample C4 | 222 |
| Figure 7.227 SF1 and SF2 from sample C4..... | 222 |
| Figure 7.228 Sample C7 before forensic analysis | 223 |
| Figure 7.229 Both steel fibers from sample C7, SF1 left, SF2 right | 223 |
| Figure 7.230 Steel fiber 1 from sample C7..... | 224 |
| Figure 7.231 Steel fiber 2 from sample C7..... | 224 |
| Figure 7.232 Carbon steel wire embedded in C8 with instrumentation | 224 |
| Figure 7.233 Carbon steel wire embedded in C8 without instrumentation | 225 |
| Figure 7.234 SF1 from sample C8..... | 225 |
| Figure 7.235 SF2 from sample C8..... | 225 |
| Figure 7.236 Assorted non-instrumented fibers embedded in sample C8 | 226 |
| Figure 7.237 Simulated pore solution samples A1 A2 A3 left to right | 226 |
| Figure 7.238 Fiber group from simulated pore solution A1 | 227 |
| Figure 7.239 A1 fiber 1..... | 227 |
| Figure 7.240 A1 fiber 2..... | 228 |
| Figure 7.241 A1 fiber 3..... | 228 |
| Figure 7.242 A1 fiber 4..... | 228 |
| Figure 7.243 A1 fiber 5..... | 229 |
| Figure 7.244 A1 fiber 6..... | 229 |
| Figure 7.245 Fiber group immediately after immersion sample A3..... | 229 |

| | |
|---|-----|
| Figure 7.246 A3 fiber 1 coated in mortar | 230 |
| Figure 7.247 A3 fiber 1..... | 230 |
| Figure 7.248 A3 fiber 2 coated in mortar post immersion..... | 230 |
| Figure 7.249 A3 fiber 2..... | 230 |
| Figure 7.250 A3 fiber 3 coated in mortar post immersion..... | 230 |
| Figure 7.251 A3 fiber 3 without mortar..... | 230 |
| Figure 7.252 A3 fiber 4 after immersion | 231 |
| Figure 7.253 A3 fiber 4..... | 231 |
| Figure 7.254 Carbon steel wire coated in mortar; A3 fiber 5 | 231 |
| Figure 7.255 Carbon steel wire: A3 fiber 5 | 232 |

1 INTRODUCTION, LITERATURE REVIEW, RESEARCH OBJECTIVES

1.1 Introduction

Concrete is the literal foundation on which modern society is built. Starting in the Roman Empire, architects began to incorporate concrete into construction of domes and arches to avoid the cost and complexity of keystones and stacking bricks¹. Romans relied on concrete to hold under compressive stresses, under tensile loadings concrete would crumble. Many early concrete structures are still standing in modern day Italy. After the Roman Empire broke apart, the uses of concrete slowed due to its brittle properties. Early Europeans preferred to construct using carved stones and wrought iron arches.

It was not until 1849 where French gardener Joseph Monier developed the method of reinforcing concrete with steel. Joseph first used iron mesh to reinforce planter pots. Reinforced concrete uses quickly expanded and Monier designed the first iron reinforced cement bridge built in 1875². Reinforced concrete is significantly more resistant to breaking apart under tension. Displacements due to tensile stresses in Monier's bridge were decimated by using metal rebar to support the concrete. Due to the discovery of casting reinforcements into concretes, uses of the technology are very common in modern construction.

Historically, concrete has been reinforced with rebar. Rebar is a steel cylinder with a type of rib to increase the surface area and the contact strength between the concrete and the reinforcement. Traditional rebar thicknesses are 3/8" to 5/8" however

smaller and larger variations exist and are used commonly. For structure construction, bars are bent into shapes and placed or welded into molds or configurations. Once the reinforcement cage is set in place, the concrete is poured and it is set to cure around the reinforcement. The steel reinforced concrete in service will be more elastic and resistant to tensile stresses than unreinforced concrete. Over time, aggressive ions may penetrate the concrete and after the corrosion has propagated for some time; corrosion can diminish the structural integrity of reinforcements.

Structures exposed to atmospheric marine environments are subject to chloride deposition and other structures in non-marine environments are subject to carbon dioxide exposure. Chlorides and atmospheric gasses like CO₂ facilitate the onset of corrosion and the migration of oxidation products. After additional service time in most aggressive environments, corrosives will penetrate the concrete and initiate corrosion in the rebar reinforcements upon exceeding a critical chloride concentration. During the corrosion propagation, corrosion products of the rebar causes a volume expansion which cracks or spalls the concrete allowing oxides to stain the exterior. Upon observation of cracks and spalling, the structure must be maintained to ensure safety.

In order to delay the negative effects of corrosion in reinforcements engineers have developed alloys and coatings for specific applications. Some common coatings are spray on epoxies, tapes, or paints. For aggressive environments, rebar are oftentimes protected with a galvanized layer, now it is more common to use metallurgy or organic coatings to protect reinforcements. The galvanization is a thin layer of zinc oxide created from various cathodic protection systems². Over time the layer can be dissolved by excessive chlorides exposing the bare steel. Stainless steel rebar is a steel alloy

containing chromium and nickel³. Although expensive, alloying the rebar will prevent corrosion in specific environments. Designs for structures that employ concrete reinforcement are tailored to their specific environment; reinforcement and concrete composition are chosen carefully. In addition to the budget and load bearing requirements, engineers consider the pH, chloride deposition rate, oxygen availability, and the construction method that applies to the environment. Reinforced concrete systems are tailor made for their operating environment and concrete mixture.

Over time precise concrete mixtures have been developed to fit specialized applications. Almost all concretes are made from different percentages of aggregate, cementitious materials (cement, fly ash, silica fume, slag), and water. The dry cement and fly ash are dispersed through different size aggregates then water hydrates the dry particles creating a paste which connects and binds aggregate particles. After the paste hardens the resulting concrete can take the rigid form in which it was molded. After molded, the concrete is cured in a moist environment to increase strength and prevent shrinkage cracks. Concrete can be cast either dry or wet. Wet cast concrete is typically more than 40% water to cement ratio and it is mixed and poured into molds. Wet cast concrete is less expensive for one time castings but for mass produced concrete pipes, dry cast is more efficient. Dry cast concrete pipe systems use approximately 38%⁴ water to cementitious ratio and require a steam cure. Dry cast concretes set quicker so molds can be used more efficiently to mass produce items such as pipes. The bulk of this thesis report will center upon zinc electroplated steel fibers embedded in dry cast concrete.

While the concrete is set, there is an abundance of calcium, potassium, and sodium hydroxide in the mixture which elevates the pH in concrete to 12-13. The

elevated pH can cause reinforcements to behave differently. Iron based alloys are covered with a passive layer when surrounded by a high pH. The resistance is observed by a protective oxide layer which passivates the surface by inhibiting direct metal contact with the environment. The pure metal is mostly shielded by oxides with low solubility in the high pH environment⁶. The protective layer is broken when the chlorides in the environment exceed a critical level; thus the metal can corrode. The typical rebar steel corrosion products will expand within the concrete causing breaks and cracks; typical steel fiber reinforcements corrode then oxidation products dissolve into the porous structure of the concrete delaying expansion cracking. Structure longevity depends on the critical chloride concentration because solubility of the reinforcement passive layer is a function of the chloride concentration.

The recent development of adding zinc-electroplated steel fibers in the concrete composite can effectively increase the critical chloride concentration. Because the fibers have a smaller diameter and surface area than conventional reinforcing steel, the critical chloride content increases⁵. The fibers in the figure 1.1 are zinc electroplated steel fibers; the fibers are 28mm long and the cross section is a 0.35 mm by 0.6 mm rectangle that has been twisted into a helix; the fiber manufacturer calls the fibers helix micro-rebars. The fibers are covered with a very thin electroplated zinc layer highlighted in figure 1.2. A uniform zinc layer is indicated by the faint green glow on the edge of the fiber. The uniform zinc electro coat acts as a sacrificial anode prolonging the corrosion of the supportive steel.

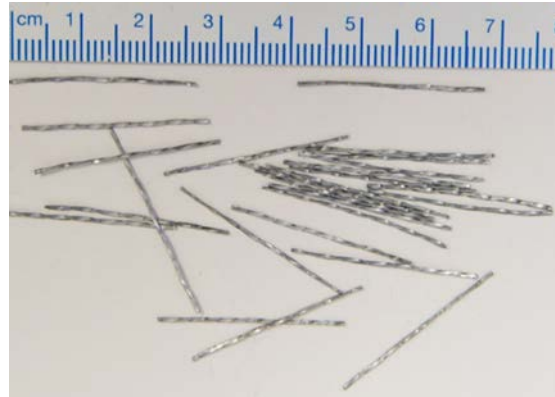


Figure 1.1 Zinc Electroplated Steel Fibers; 28mm in length, .35mm X.6mm helix cross sectional area Photograph by Dietrich Vogel copyright 2016 by Dietrich Vogel

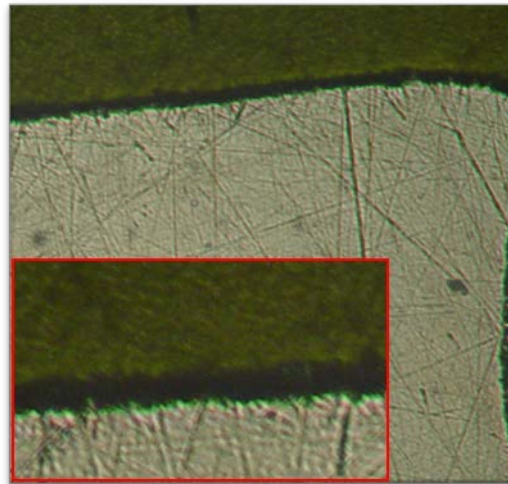


Figure 1.2 Metallographic microscope close-up of the zinc layer highlighted in green with an etching solution; the layer thickness was estimated to be nearly 1 μ m Photograph by Dietrich Vogel copyright 2016 by Dietrich Vogel

Exchanging uniform skeleton reinforcements for short fibers can increase the longevity of composites by increasing the corrosion resistance. An advantage for fiber reinforced concretes is its ability to isolate reinforcements at different depths. In traditional reinforcement systems, corrosion of rebar in one location will take electrons from the rest of the structure reinforcement. Structure reinforcement will eventually loose strength at corrosion sites even though some areas may not experiencing the critical

chloride concentration. In fiber reinforced concrete, corrosion may be observed near the surface but the internal fibers remain untouched even after aggressive chloride deposits. In addition to isolation, steel fibers have a higher chloride threshold or; are more resistant to corrosion than rebar due to a favorable volume to surface area ratio, better coverage by interfacial transition zone, and small cathode to anode ratio. Steel fiber metal microstructure is different compared to carbon steel rebar due to a multiple drawing process needed to achieve the fiber dimensions. Where traditional steel rebar can expand and contract causing tensile and compressive forces to crack concrete and accelerate corrosion of the rebar, the fiber composites offer more plasticity and the concrete is more resistant to cracking. Longevity of structures reinforced with steel fibers is difficult to determine because once corrosion initiates on the fiber it may take a short time to corrode. Because fibers have a range of critical chloride concentrations it is unclear when enough fibers have corroded to cause concern for reduced mechanical properties.⁶

Private companies have pilot programs in which they have produced water drainage pipes that contain the above described steel fibers. Dry cast concrete is known to have a higher porosity than wet cast concrete. Thus, in order to implement them in higher risk situations and areas, the materials need to be verified for resistance to corrosion related failure. Verification will come from experimental analysis of the critical chloride content, bulk diffusion coefficient, and 4 point bending test. The research that follows intends to provide a physical and electrochemical overview of the steel fiber behavior as it corrodes in concrete. The research is presented as a result of a Florida Department of Transportation grant.

1.2 Literature Review

For this thesis a literature review was conducted to find a better understanding of the properties of fiber reinforced concretes. Literature concerning the migration or deposition of chlorides in cementitious materials were of particular interest; however many other texts and papers were consulted even if not used in the following review. The literature review serves as a justification for the experimental conditioning procedures and a gauge of expected results.

Despite its general durability, concrete can be made vulnerable by environmental influence. Environments can physically attack concrete with chemical attacks (sulfates/chlorides/carbonation), freezing-thawing cycles, erosion, or wetting and drying. Cracks in the concrete can greatly exaggerate the negative effects environments have on structures. Environments can chemically attack concrete steel reinforcement through chloride deposition, acidification, and eventual corrosion. To protect concrete from physical attacks, reinforcements are added internally or externally. The use of steel fibers in concrete are gaining popularity due to its pre and post cracking behaviors which lead to increased concrete durability. Over time, the chemical degradation induced by the environment will destroy the reinforcement and the physical attack will destroy the concrete; if cracks can be avoided then overall durability will increase.

Transport of ions is made possible by the porous nature of concrete composites [4]. Chlorides penetrating porous concrete samples is a well-documented problem in concrete materials science [3,4,5]. Private companies recently started producing potential solutions to the issue by fabricating water drainage pipes that contain small steel fibers. Many steel fibers laid in concrete can provide comparable strength to traditional steel

wire cage reinforcement. Typically less than 2% by volume of steel is used.⁷ However, the separated fibers allow corrosion to attack each fiber individually once a critical chloride concentration is exceeded rather than allowing the entire support diminishing at once. This one by one attack of the fibers increases the longevity of the structure by allowing the concrete to depend on small isolated strands of steel rather than large reinforcements. Upon the corrosion onset of the steel fibers, the corrosion products are able to seep into the concrete pores; effectively preventing tensile stresses caused by corrosion product expansion typically observed on rebars [7].

Moreover, because of the small dimension of fibers (smaller surface area, smaller number of flaws) it has been suggested that the concentration of chlorides needed to start corrosion is higher. Not only does the physical presence of a smaller reinforcement raise the critical chloride content, the mechanical process of drawing the fibers increases the uniformness of the surface and microstructure. Testing and evaluation of dry-cast concrete reinforced with steel fiber exposed in aggressively corrosive environments is not a well-researched field. In order to implement dry-cast concrete steel fiber structures in higher risk situations and areas, the materials need to be characterized for resistance to corrosion related failure. The metric used to determine material characterization with respect to corrosion is the chloride threshold on samples and the corresponding physical behaviors after the onset of corrosion.

Determinations of the critical chloride content are made after analysis of steel fiber potential over time and linear polarization resistance measurements over time. The potential tests check the potential difference between the instrumented fiber and a saturated calomel reference electrode (SCE). Results from the potential tests will provide

a quick insight to what is going on electrochemically with the fiber. From the potential tests, the type of corrosion or lack thereof can be estimated. For example, research suggests that the zinc is active on potential ranges from -800mV to -1.2V and steel is active between a larger region -250 mV and -700mV vs. a saturated calomel electrode[4]. The potential tests will offer a primary measuring technique to determine the instrumented sample behavior without breaking the concrete and forensically examining the state of the sample.

In addition to the potential difference measurements, linear polarization resistance measurements were conducted monthly or bi monthly to track corrosion progress on each instrumented sample. The apparent polarization resistance noted as R_{papp} indicates electrochemical activity at low values and indicates passivity at high values. The R_{papp} value can be modified with surface area calculations to reveal the corrosion current density. A feature of anodic controlled corrosion processes is that the fiber potential will decrease and the corrosion current will increase. If the fiber is observing cathodic corrosion control the current range will shrink indicating no loss of reinforcement [8]. Over the course of the research, the steel fibers will be the focus of electrochemical observation and forensic analysis. The zinc in the fibers is expected to be initially active; indicated by a low potential while it forms a passive layer in the high pH of the concrete. After passivating, the corrosion potential should increase towards passive values. Samples introduced to chlorides should see the potential decrease as the chlorides break down the passive layer and initiate electrochemical activity in the steel fiber.

According to past research on the critical chloride content, there are 4 methods of determining critical chloride content [6]. Although the goal is to find the critical chloride

threshold for zinc electroplated steel fiber corrosion, the temperature and humidity surrounding the concrete will greatly influence the onset of corrosion. Each method of determining the critical chloride threshold requires different conditions and time scales until completion.

The first method is a chloride migration, either passive or active. Passive transport implies that chloride ions are transported into the concrete via capillary action or diffusion; active transport implies the application of an electric field (via a DC power supply) to accelerate chloride transport via electro-migration into the concrete.

Throughout the migration process and the environmental conditioning that will occur after, measurements of steel fiber corrosion potential and LPR measurements will indicate the effect the chlorides have on the electrochemical activity at the zinc electroplated steel fiber surface. Once the chlorides are present, a forensic analysis of the fiber condition will determine if the chloride threshold has been reached. There are no published results on the critical chloride concentration of zinc electroplated steel fiber reinforced concrete composites by means of chloride migration. There are however studies published on the diffusion and electro-migration of chlorides in concrete. A rapid migration test or RMT is a standard test where chlorides are migrated over a specific period of time under certain electric field conditions [9].

The second method of determining the critical chloride content is adding chlorides to the water used to cast the concrete. Casting the multiple concrete samples with varied chloride concentrations mixed into the cement ensures that chlorides are uniform and present in the concrete matrix. After the chlorides are cast into the concrete, the samples must be exposed to oxygen and humidity before the fibers can react to the

chlorides. The measurements of fiber corrosion potential and linear polarization resistance will reveal if the threshold was passed. If a threshold was passed, forensic analysis will indicate the chloride content and the fiber condition. Experiments on low carbon steel fibers conducted by Halvorsen et al indicate that the chloride concentration where de-passivation occurs is 0.15% to 0.6% by weight of cementitious components [5]. Some tests have also concluded that chloride concentrations in excess of 2% by weight of cementitious components have shown no corrosion of steel fibers [5].

The third method of determining the critical chloride threshold for micro helix rebars (zinc electroplated steel fibers) is a simulated concrete pore solution. This method does not require concrete casting. A simulated pore solution consisting of different amounts of calcium hydroxide, potassium hydroxide, and sodium hydroxide could be used to soak the fibers. Over time, chlorides are gradually added until potential measurements and linear polarization resistances indicate a breakdown of a protective layer and electrochemical activity at the surface. Once a breakdown in the layer is observed and re-passivation has not occurred, a critical chloride content is determined. In a solution of pH 12.6, the critical chloride content is expected to be between 30 and 40 milli-molar, but it could be higher. In solutions containing pH 13.3, the critical chloride content is expected to fall between 750 and 1000 milli-molar [6].

The fourth and last published method of critical chloride threshold determination is the most time consuming. The last method requires dozens of years while samples collect chlorides, oxygen, water, and pollutants naturally. After the concrete specimen exhibits clear evidence of electrochemical activity indicated by either measurements or observations; the sample is terminated for forensic analysis. The forensic analysis of the

concrete will yield the chloride content of the concrete at different depths and the condition of the internal fibers at the chloride concentrations. The method of waiting for natural exposure is not practical in the time constraints imposed by this thesis research. To hasten results, the water to cementitious ratio or the temperature could be elevated.

The standard indication of corrosion resistance is the determination of the chloride threshold and the concrete pH. The long term mechanical properties such as toughness and flexural strength are sometimes determined after the onset of corrosion and the properties are used to evaluate the corrosion in steel fiber reinforced concrete. For this thesis, methods outlined in ASTM standard C78 will be used to determine the modulus of rupture for beams exposed to different levels of chlorides. To determine the modulus of rupture for the steel fiber reinforced concrete composite, beams are subjected to a four point loading. The top of the beam is under compression and the bottom of the beam is subjected to increasing tensile stresses until the concrete cracks; upon cracking the loading is immediately stopped. For non-reinforced concrete beams, the flexural test will crack and typically break the beam in two at the midpoint. Steel fiber reinforced concrete beams will not always break in similarly sized halves, the flexural test will break the sample where the reinforcement is weakest. The influence of chlorides on the reinforcements may affect the location of fracture if corrosion has been initiated. Fracture analysis is necessary to determine the condition of reinforcement after flexural strength testing.

1.3 Thesis Objective

The objective of the thesis is to support a Florida Department of Transportation grant to determine the critical chloride content of dry cast concrete containing zinc

electroplated helix micro rebar fibers and material properties after corrosion onset. To confidently determine the critical chloride content the thesis details multiple test methods for comparison. The experiments include a rapid migration test (RMT) accompanied by concrete resistivity measurements which help to characterize the bulk chloride diffusivity and conductivity of the dry cast concrete. Additionally, a modified RMT experiment where chlorides were transported faster onto concrete cast with instrumented fibers at different depths. It is expected that this will help to determine the penetrative nature of the chlorides and the electrochemical effect on the fibers in the concrete. Other samples, cast with chlorides detail the electrochemical results of chloride induced corrosion onset. All instrumented samples underwent regular potential measurement and linear polarization resistance against a standard calomel reference electrode to determine electrochemical trends over time. The last method for critical chloride characterization is a concrete environment simulation test. Bins were set up with an aqueous mixture similar in pH to concrete; over time chlorides were incrementally added to the concrete pore solution. Throughout the experimentation, fibers corrosion potential (vs. SCE) and linear polarization resistance was measured until the critical chloride content has been passed and corrosion of the fibers was observed. The goal of each experiment was to provide evidence of corrosion onset so that results could be used to predict long term material behavior using short term testing techniques. It is the objective of the thesis to correlate the experiments to confidently comment on the corrosion resistance of micro helix steel fibers in dry cast concrete composites.

2 EXPERIMENTAL PROGRAM: FRACTURE ANALYSIS OF ZINC
ELECTROPLATED STEEL FIBERS EMBEDDED IN DRY CAST CONCRETE
PIPES EXPOSED TO VARYING CHLORIDES

2.1 Introduction

Physical durability after corrosion initiation is not well known with dry cast concrete embedded with zinc electroplated steel fiber technology. Some strength studies have been done on fiber reinforced concrete exposed to environmental conditioning focusing on the interfacial shear strength between concrete matrix and reinforcing fibers. This experiment will focus on the tensile strength of concrete containing zinc electroplated steel fibers, after the onset of corrosion rather than the interfacial shear between matrix and fibers. A UF final report for the Florida Department of Transportation details the durability of hooked end steel fiber reinforced concrete that has been immersed in saltwater for 27 months [11]. Flexural strength measurements were taken after the environmental conditioning; values for steel fiber reinforced beams were between 679-806 PSI. In comparison, the previous study tested concrete reinforced with 39 kg/m³ of steel fibers; the concrete used in the experiment that follows used 8.9 kg/m³ zinc electroplated steel fibers.

Due to the disparity in the steel fiber concentration, it is expected that the beams with less fibers may take less force to flex and crack than the higher concentration counterparts. Further, beams subject to the onset of corrosion are expected to flex under less force than those without the presence of corrosion. The experiment that follows has

examined these expectations. Beams were tested and compared using methods outlined in ASTM C78 after preliminary varying chloride (passive and accelerated) and oxygen exposure.

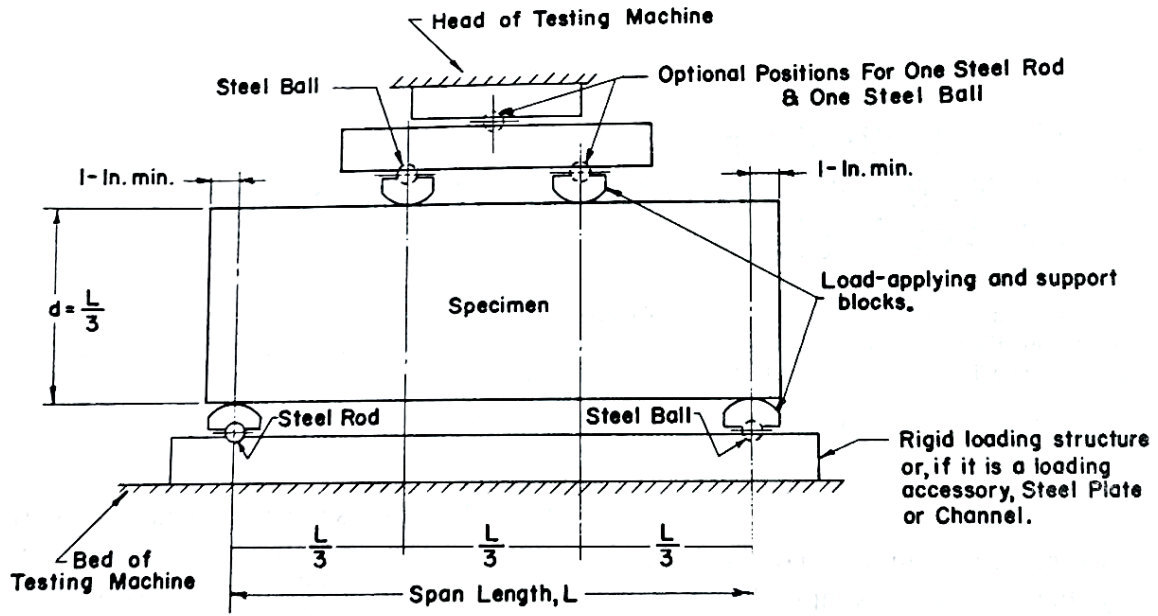


Figure 2.1 ASTM C78 test setup for beam bending [10]

After strength testing, a forensic analysis has determined the effect of steel fiber corrosion on the failure mode following the flexural strength test. Each fiber in the failure plane was observed for the onset of corrosion and physical condition.

Conclusions were made based on the analysis of results.

2.2 Experimental Procedure

Several 8 ft long highway drainage pipe samples with 24 inch interior diameter were dry-cast with 8.9 kg/m^3 zinc electroplated steel fibers. These pipes were produced at a manufacturer's facility. One of the pipes was cut by the manufacturer into smaller 90 degree sections that were approximately 2 feet in length. Eight large pipe samples were

directly obtained from the manufacturer as a representation of the mass produced steel fiber reinforced highway drainage pipe. The objective of this experiment was to determine the failure method of steel fibers under varying degrees of corrosion. The zinc electroplated steel fibers were exposed to chlorides as to hasten the corrosion propagation while they were embedded in the concrete. The modulus of rupture was determined by beam bending tests (ASTM C78). In addition to determining the failure method, research has attempted to determine the relationship between diffusivity of chlorides in concrete.

The samples for flexural strength testing were originally large (27”X22”) pipe sections. Some of the drainage pipe sections were subject to modified rapid migration, environmental conditioning, and then materials testing. Four of the pipe sections provided by the manufacturer were used for the specimens described below. The first pipe section selected was cut into small beams; three beams were immersed in elevated temperature sea water and the other three were immersed in brackish water and sodium sulfate added. Each half pipe section was capable of producing three beams for flexural strength testing; however only two were tested. The other three pipe sections were monitored for some time; one section was left as a no chloride control, the second and third sections underwent rapid chloride deposition via a modified rapid migration test approach. Each of these three samples (No chlorides-NC, Chlorides External-CE, Chlorides internal-CI) were maintained as whole pipe sections. Each pipe section was received and maintained at 100% humidity. Sample CE was exposed to a high humidity environment 60 days before NC and CI. Over the 120 and 60 days respectively the concrete resistivity was measured using the 4 point measurement technique with 2cm probe spacing at 20 evenly spaced places over the entire interior concrete face. After the

regimen of resistivity measurements, samples CE and CI were equip with plastic reservoirs and sample NC was moved to lab humidity. The ponded samples CE and CI were subject to accelerated chloride migration modified from NT Build 492. The modifications outlined below were intended to transport chlorides through the concrete slab in order to induce corrosion in the steel fiber reinforcements. First the reservoir for the CI sample and the bin for the CE sample were filled with 15% NaCl. Opposite the chloride solution, the anolyte solution was added. Then a titanium mix metal oxide wire mesh was placed below the pipe section and one was placed inside the reservoir. The wire mesh electrodes were connected to a DC power supply in July of 2015. The pipe sections were subject to 30 V for three days, 20 V for two days and then the sections were left disconnected for a month. Then in early September, the pipe sections were turned back on at 12 V for 10 days. After the sections were subject to nearly 15 days of electric field induced chloride migration, the pipe sections were moved outdoors. Figures 2.3 and 2.4 depict the conditions of the pipe section faces that were exposed to chloride migration. Once outdoors, the top reservoirs of both pipe sections were filled with 15% NaCl solution. Sections CE and CI were conditioned outdoors to stimulate corrosion through increased temperature, humidity, and oxygen exposure. The sections were left outdoors with the solution for over 2 months; from October through December. All the while, the pipe section without chlorides was maintained at lab humidity.



Figure 2.2 Pipe section S-2 made to be the no chloride control sample for beam bending
Photograph by Dietrich Vogel copyright 2016 by Dietrich Vogel

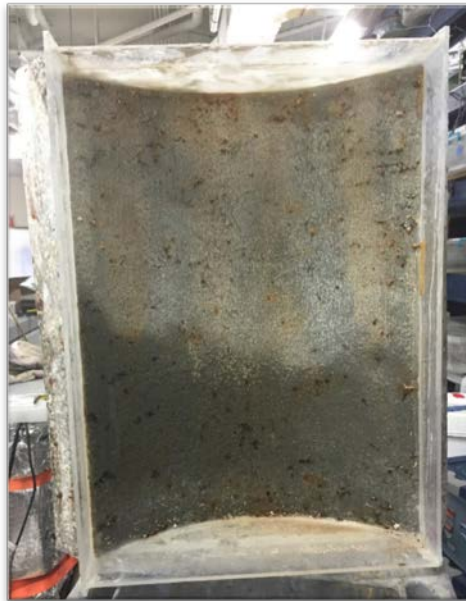


Figure 2.3 Pipe section after interior face chloride migration Photograph by Dietrich Vogel copyright 2016 by Dietrich Vogel



Figure 2.4 Pipe sample exposed to exterior chloride migration Photograph by Dietrich Vogel copyright 2016 by Dietrich Vogel

Upon the conclusion of conditioning, a portion of the pipe sections were cut into beams for flexural strength testing. Figure 2.2 depicts the pipe section NC in the environment which it was conditioned in. For the purpose of flexural testing and evaluation; two beams were selected from the seawater and the brackish water sections, and six beams were taken from the NC, CE, and CI pipe section samples. Three beams were used of the six obtained from the larger sections; three beams remain of NC, CE, and CI for future evaluation.

The beams from the pipe sections were cut to be 14" long with a target 4" width. The pipe sections have a shorter width on the interior side and a longer width on the exterior side, the 4 inches were measured on the exterior side in most cases. The cross section of the beam samples vary in size due to saw limitations and the curvature of the pipe sample. The shape of the cross sections are similar to a trapezoid. The beams were

tested by the FDOT in Gainesville Florida under the ASTM C-78 standard [1]. The samples were bent until deflection and the modulus of rupture was recorded for each sample. After the FDOT had cracked the beams, the beams were brought back to FAU SeaTech lab in Dania Beach. In the lab, the crack location and width were noted with pictures; then the samples were separated into two. After wiggling on the cracked area, the concrete faces could be examined from each separated beam. Once apart, the interior faces of the sample exposed by the crack were documented with pictures. After initial documentation, a careful examination of each exposed fiber determined its method of failure; either pull out, brittle fracture, or a clear cross section loss due to corrosion onset. A pull out is defined by a fiber that is protruding from one face of the concrete and has a clean end. A brittle fracture is fiber that has broken in two along the crack. The brittle fracture was determined by examining the fibers exposed that exhibited a companion rust stain on both sides of the cracked fiber. Lastly, there were fibers that exhibited clear cross section loss due to corrosion however the fiber pulled out from one side without fracture. Oxidation products may be evident on the companion beam face from the pullout of the steel fiber. Selected areas from some of the samples were examined further in a stereo microscope to further verify their internal and surface condition.

Fiber failure condition was observed within 48 hours of the flexural strength test. The diffusivity of chlorides into the concrete depends on the non-steady state diffusion coefficient; after flexural strength testing the chloride penetration was measured in each beam and the coefficients were determined. After the fibers were examined and documented, one face from each sample exposed to chlorides was sprayed with silver nitrate. Silver nitrate highlights the regions where chlorides have penetrated the concrete

pore structure. For each sample, seven careful distance measurements were taken along the width of the concrete from the base to the edge of chloride penetration. The chloride penetration distance can be correlated to the concrete diffusivity using the methods outlined in NT Build 492. Analysis will focus on relationships between chloride penetration, corrosion of steel fibers, and flexural strength

2.2.1 No Chloride Exposure - NC

Sample NC is a non-chloride control pipe section. For 60 days the sample was maintained at 100% humidity and its resistivity was monitored. After high moisture conditioning, it was removed from high humidity and it was exposed to lab humidity, not ponded. The sample NC was cut into cores and 14"x4" beams for physical property measurements such as the beam bending test for the flexural strength. Of the six samples collected, three samples were NC_1, NC_2, NC_3. Three samples were given to the FDOT in December and stayed in a fog curing room for a month. The beams were tested in early January. Soon after, when the samples were returned; the condition of the steel fibers were observed at the site of failure. The samples were kept in lab humidity for 2 months for visual observations.

2.2.2 Exterior Chloride Exposure - CE

Sample CE was obtained from the manufacturer and it was kept at 100% humidity for 120 days. After the resistivity was measured over that period, the sample was placed in lab humidity and prepared for ponding. Plastic panes were cut from sheets and affixed to the top of the pipe sample with marine goop epoxy. The reservoir covered the entire interior surface of the sample, the reservoir was checked for water tightness with water,

then filled with saturated calcium hydroxide. The sample was placed in a larger mortar tub-container which was filled with 15% sodium chloride.

The pipe section was then subject to chloride migration where the chlorides were migrated from the bottom to the top as facilitated by two titanium mix metal oxide (MMO) meshes connected to a power supply. After a total of 15 days exposed to a range of 30-12V applied potential between the two TiMMO mesh, the sample was removed from the solution and placed outdoors for seasoning. The sample was conditioned outdoors with chloride solution exposed to the interior face. After the sample was seasoned for 5 weeks, it was cut to obtain the beams to be used for bending and modulus of rupture measurements. The 6 beams were between 14” and 15” in length and they were close to 4” in width; the height of each beam was dictated by the pipe wall thickness. Beams that were created for flexural strength were CE_1, CE_2, and CE_3; abbreviated for the chloride exposure to the exterior of the pipe.

The three cut samples were given to the FDOT for flexural strength testing in Gainesville. After testing, the samples were returned cracked with the accompanying the modulus of rupture. Within a day of the bending test, the samples were photographed and broken in two for analysis. The fiber location and condition were documented. After careful documentation of the fiber location and condition, the samples were sprayed with silver nitrate to verify the presence of chlorides in the concrete. Spraying the concrete with silver nitrate highlighted the regions with chlorides then the chloride penetration distance was measured. For each beam sample the modulus of rupture was measured, the chloride penetration was measured, and the fiber conditions were determined.

2.2.3 Interior Chloride Exposure- CI

The third sample from the manufacturer was maintained at 100% humidity and the resistivity along the inside of the pipe was sampled periodically for 60 days. After the resistivity values were repeatable over time, the sample was ponded similar to CE. The interior pipe section of specimen CI was filled with 15% sodium chloride solution and then placed in a container filled with calcium hydroxide.

Then the sample was subject to accelerated chloride migration. Titanium mesh on the top and the bottom of the concrete were connected to opposite ends of the power supply. For CI, the chlorides traveled from the top down over 15 days at 30-12V. After the migration, the sample was removed from the container and placed for 5 weeks outdoors in high humidity. After the environment has seasoned the samples, cuts and cores were made to create samples for standardized testing. Six beams were cut from the sample and three were sent to the FDOT for flexural strength testing. Once returned, the tested samples were broken in two and the condition of the fibers were examined. Some samples were photographed with a stereoscopic microscope to examine the condition of fibers and the severity of corrosion. After careful documentation of surface condition, the cracked faces were sprayed with 0.1 molar silver nitrate solution to reveal the chloride ingress. The chloride penetration distance was measured and documented.

2.2.4 Seawater Exposure

The fourth type of beam sample was one half of a pipe section sample received initially, four beams were cut from the pipe section. The beam samples were immersed in elevated temperature seawater (60°C). The freshly cut beams were immersed in the seawater for over 180 days. The immersion in elevated temperature seawater increased

the chloride diffusivity compared to the diffusivity of room temperature seawater exposure. Two of the beams selected were removed from the tank then transported to the FDOT testing site for flexural strength testing. Once the beams arrived back at SeaTech, the beams were separated at the crack; then the failure planes were analyzed for fiber condition and chloride penetration.

2.2.5 Sodium Sulfate and Intercostal water Exposure

The last type of beam samples were exposed to an intercostal water and sodium sulfate solution. The beams were exposed for over 180 days and the beams were cut from the pipe sections before immersion. The seawater immersion samples are the companion beams to the same pipe section. The immersion in sulfate solution was an alternate aggressively corrosive environment for the steel concrete interaction. The solution was chosen to purposely attempt to break down the connective bonds between the steel fibers and mortar and reduce the interfacial shear stress needed to pull the fiber out. After the 180 days of immersion, the samples were subjected to the flexural test to determine if the introduction of sulfates and chlorides from the brackish water has reduced the strength of the reinforcement in the concrete. Post strength testing, the samples were separated at the failure plane and the fiber condition and location were observed and documented. Lastly, the samples were sprayed with silver nitrate to reveal the chloride penetration into the beam.

2.3 Results and Analysis

Many measurements make up the results of this experiment. The first measurement taken was the concrete resistivity of the pipe sections. Pipe sections were received after prolonged outdoor exposure and over time, in the lab exposure to 100% humidity

moistened the concrete. The moisture addition can be seen in the plot of the concrete resistivity over time. The plot (figure 2.5) was generated by averaging all resistivity measurements over the interior face for each sample. After the concrete was made moist, the resistivity values dropped and stabilized.

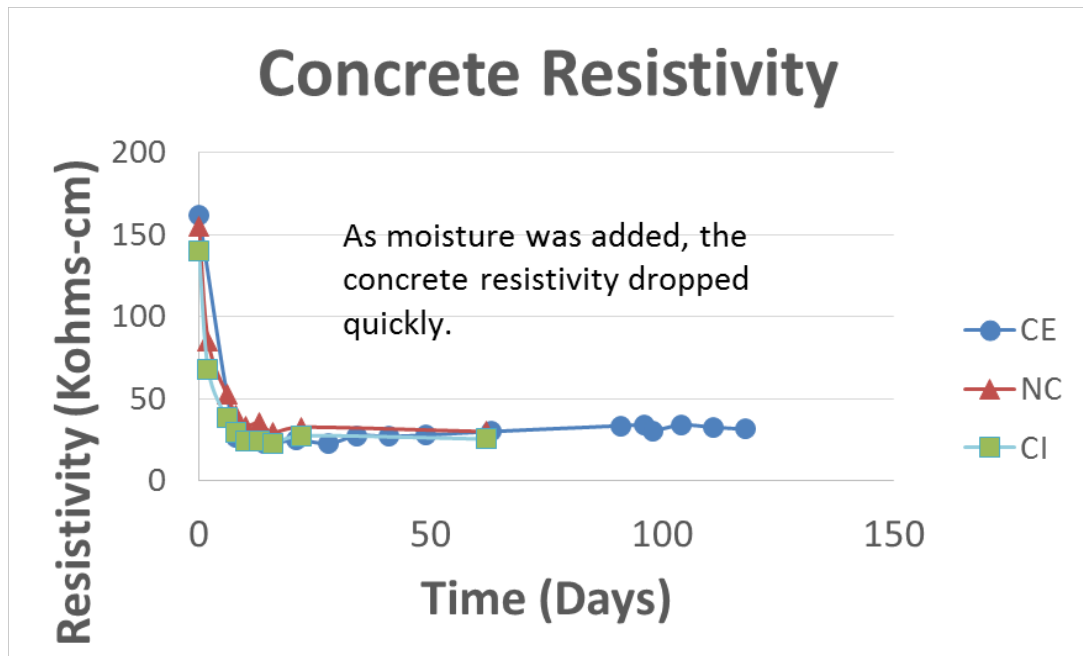


Figure 2.5 Graph of concrete resistivity over time in large pipe sections Photograph by Dietrich Vogel copyright 2016 by Dietrich Vogel

An average resistivity for each sample was calculated over the last three weeks of the measured values. Table 2-1 contains the final three week average resistivity which is characteristic of the concrete resistivity for a concrete cast with 20% fly ash by weight cementitious.

Table 2-1 Chloride penetration distances measured using a caliper and the non-steady state migration coefficient

| Range 4, Spacing 2cm | |
|----------------------|---------------------|
| Sample | Average Resistivity |
| NC Kohms*cm | 32.7 |
| CE Kohms*cm | 32.8 |
| CI Kohms*cm | 25.6 |

The resistivity values measured are higher than most dry cast concretes. Past studies have measured dry cast concretes containing OPC only to have resistivity's near 10 Kohms*cm on wet samples. Higher resistivity measured in these pipe sections was attributed to the presence of 18% fly ash and the concrete age. Sample highway drainage pipes were cast in April of 2014 and resistivity measurements were conducted in spring 2015; so the pozzolanic reaction has had time to progress. The pozzolanic reaction due to the presence of fly ash effectively reduces the porosity of the concrete making the transport of ions more difficult. A reduction in porosity increases concrete resistivity even when saturated with water. Concrete moisture can also dictate the concrete resistivity; dry concrete is very resistive. Concrete resistivity affects the diffusivity of chlorides; presented next are the results of chloride migration.

The CI and CE beams were split after they returned from flexural strength testing and they were sprayed with 0.1M AgNO₃. Silver nitrate highlights regions where chlorides are absent as seen in figures 2.6 and 2.7. The coefficients are found using the standard equation found in the NT build 492 modified for increased time, increased potential difference, and a thicker section.



Figure 2.6 Sample CI3 sprayed with AgCl to indicate chloride migration Photograph by Dietrich Vogel copyright 2016 by Dietrich Vogel

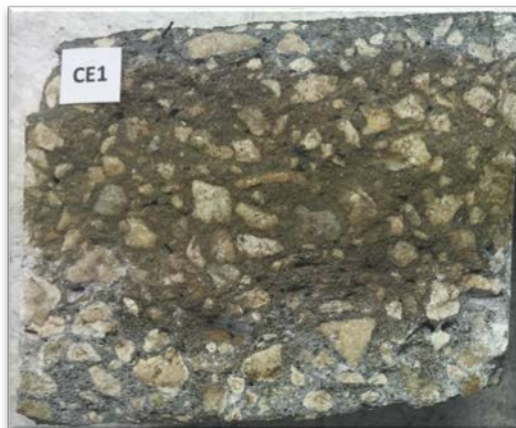


Figure 2.7 Beam CE1 sprayed with silver nitrate to indicate chloride penetration Photograph by Dietrich Vogel copyright 2016 by Dietrich Vogel

Table 2-2 Chloride penetration distances measured using a caliper and the non-steady state migration coefficient

| Sample | Avg. Depth (mm) | Dnssm * 10 ⁻¹² m ² /s |
|--------|-----------------|---|
| CE | 21.66 | 0.537 |
| CI | 55.99 | 3.91 |

Previous research done on this type of concrete pipe has found the Dnssm to be 8.43×10^{-12} m²/s from the inner surface and 7.8×10^{-12} m²/s from the exterior for concrete fully saturated prior to applied potential. In comparison with table 2-2, the previous measurements indicate higher diffusivity. Those previously mentioned values were obtained after the concrete was water saturated; the decreased water content due to lab humidity exposure in the large section specimens prior to electric field application might have slowed the chloride penetration. During the electric field migration, the pipe sections were not completely immerse in solution(figures 2.3 and 2.4). The lower moisture content likely allowed an increase in resistivity, which would explain a much smaller diffusion coefficient for beam samples in comparison to previous measurements. Pipe section CE has the smallest Dnssm because it had been moist first and was left to dry in lab humidity where it may have lost additional moisture.

Although the beams immersed in seawater were not subject to electric migration of chlorides, spraying the beam face with silver nitrate revealed the penetration of chlorides into the concrete (figures 2.8). The elevated temperature seawater has accelerated the transport, chlorides penetrated the concrete from all sides.



Figure 2.8 Sample SW2 after being sprayed with silver nitrate Photograph by Dietrich Vogel copyright 2016 by Dietrich Vogel

It is important to note that chloride penetration was measured to be more from the interior surface than the exterior surface. Beams immersed in brackish water and sodium sulfate were sprayed with silver nitrate however there was no measurable indication of chlorides. Chlorides may have been present in concentrations below the silver nitrate indicator threshold. The room temperature brackish water did not have the same aggressive affect as the elevated temperature seawater.

The presence of chlorides has been verified in samples CE, CI, and SW. All beam specimens to be tested were transported to FDOT SMO early December 2015, and flexural strength testing took place in early January 2016. In between transport and testing, the beam samples were stored in a fog room. The beams were then transported to FAU SeaTech to assess chloride penetration and failure type. After the chloride presence has been determined, the results from the flexural strength test (ASTM C78) were compared. For the beams cracked, the side exposed to the tensile stresses had the largest separation distance. The test did not break the beam in to two pieces, as some fibers kept the beam together despite the cracked concrete.



Figure 2.9 Beam NC2; modulus of rupture 1030 PSI Photograph by Dietrich Vogel
copyright 2016 by Dietrich Vogel

Seen in figure 2.9, the flexural test created a crack on specimen NC2 that did not propagate through the entire beam. The crack was seen to be over 1” off the center of the beam.



Figure 2.10 Beam sample CE2; modulus of rupture 910 PSI Photograph by Dietrich Vogel
copyright 2016 by Dietrich Vogel

Figure 2.10 shows the beam CE2 post flexural strength testing. Rust stains could be seen on the exterior surface due to chloride exposure. Steel fiber corrosion may have been responsible for a lower modulus of rupture when compared to the no chloride sample. The failure crack occurred over 1.5” from the center of the beam.



Figure 2.11 Beam sample CI2; modulus of rupture 805 PSI Photograph by Dietrich Vogel copyright 2016 by Dietrich Vogel

Seen in figure 2.11, beam sample CI2 had one of the lowest modulus of raptures measured. Chlorides were migrated from the interior face and the effects of corrosion can be radially seen as red rust. The failure crack is around 2” away from the centerline of the beam; the beam broke at the weakest spot.



Figure 2.12 Beam sample SW2; modulus of rupture 895 PSI Photograph by Dietrich Vogel copyright 2016 by Dietrich Vogel

Seen in figure 2.12, the beam sample SW2 does not have any exterior evidence of corrosion. The modulus of rupture for the sea water sample was less than the no chloride control which suggests that the seawater modestly influenced the physical properties.



Figure 2.13 Beam Sample S2; modulus of rupture 940 PSI Photograph by Dietrich Vogel copyright 2016 by Dietrich Vogel

Beam S2 seen in figure 2.13 as also free of visible corrosion products. Failure crack on the S2 sample was very slim and did not pass through the entire beam. The beams were cracked between $L/3$ and $L/2$ confirming that the test results are valid for each beam. In line with expectations, the sample NC averaged the highest modulus of rupture. The table 2-3 displays the average modulus of rupture for the beams of each type of chloride exposure.

Table 2-3 Average modulus of rupture for each beam type

| Beam Type | NC | S | SW | CE | CI |
|---------------------|------|------|------|------|-------|
| Avg. Mod of Rupture | 1030 | 985 | 985 | 945 | 872 |
| Standard Deviation | 65.3 | 45.0 | 90.0 | 79.5 | 154.3 |

Chloride penetration was greatest in the CI beams and those samples tested the smallest flexural strength. Initial analysis shows that the chlorides have adversely affected the flexural strength of the concrete. Next, further analysis needs to be conducted on the beams to determine the method of failure and the degree of fiber degradation. Careful examination of beam failure planes determined the method of failure for each fiber. As mentioned in the experimental procedure section; fractures are either brittle (red circles), clean pullout (green circles), and pullout fibers with the onset of corrosion (blue circles) as depicted in figure 2.14 for beam CI2.

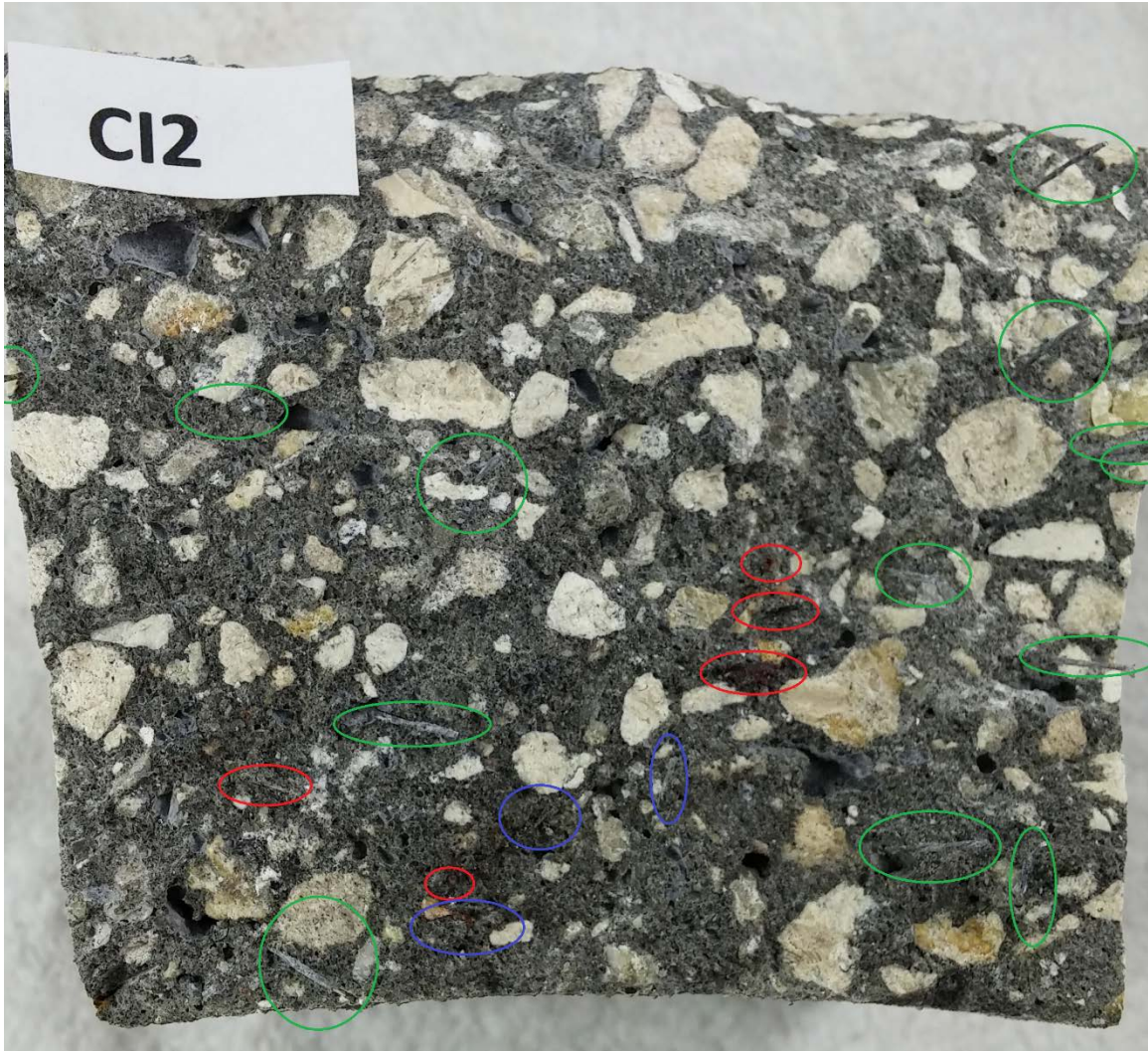


Figure 2.14 Beam sample CI2 with the fibers mapped and analyzed: 21 fibers, 5 brittle fractures and 3 corroded pullout fibers Photograph by Dietrich Vogel copyright 2016 by Dietrich Vogel

The most interesting beams to observe were CI beams. In each CI beam, many fibers have been affected by the onset of corrosion seen in figure 2.14. The beams with the most brittle failures were the CI samples. The brittle failures due to corrosion onset might in part explain the lower flexural strength observed in the CI beams.

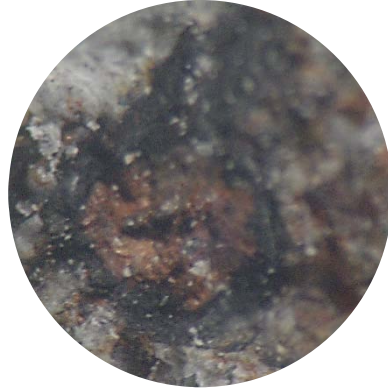


Figure 2.15 Stereographic microscope picture of a brittle fracture observed in beam CI2
Photograph by Dietrich Vogel copyright 2016 by Dietrich Vogel

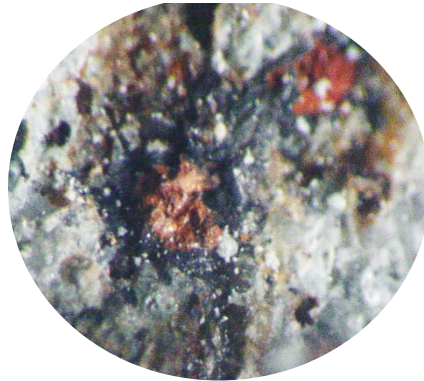


Figure 2.16 Companion brittle fiber to a brittle fracture observed on beam CI2
Photograph by Dietrich Vogel copyright 2016 by Dietrich Vogel

The stereo microscope pictures of both sides of a brittle fracture found in sample CI2 clearly show a brittle steel fiber failure mechanism in figures 2.15 and 2.16. The onset of corrosion caused the oxidation products to diffuse into the surrounding pores, the fiber cross section was barely recognizable due to the oxidation products staining the area. All fractures were determined to be brittle only if a fractured companion fiber was found in the opposite beam face. Some samples were determined to be corroded pullouts; due to black/red rust stains and no fiber found on the companion face.

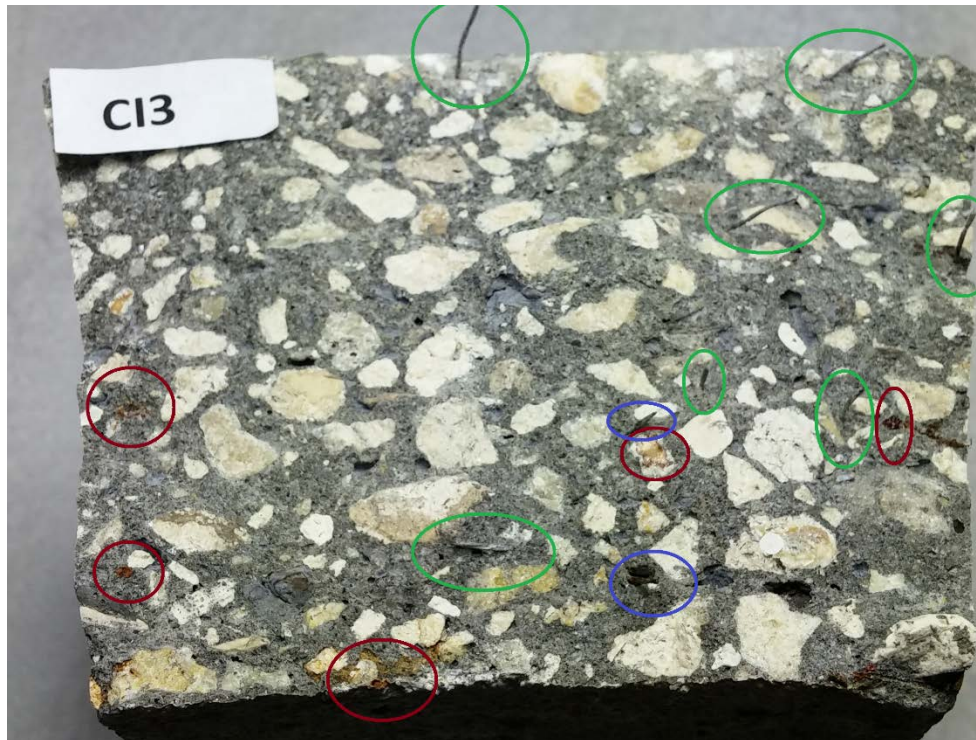


Figure 2.17 Beam sample CI3 with fibers mapped and the conditions analyzed
Photograph by Dietrich Vogel copyright 2016 by Dietrich Vogel

Mapped fiber failure for beam CI2 could be seen in figure 2.17. It is interesting however that there is a fiber that did not reach its chloride threshold despite being in the chloride penetration region. That particular fiber indicated by the green circle closest to the bottom of the picture did not corrode in the presence of chlorides alone. The moisture or oxygen content at that location did not satisfy the chloride threshold. Alternatively, the chloride threshold may have been reached however the sacrificial zinc may not have been completely consumed. Some fibers might have reached the chloride threshold but were not diminished enough to fracture when stressed and rather showed pullout failure.



Figure 2.18 Pullout failure despite the onset of corrosion; fiber observed in sample CI1 observed under the stereographic microscope Photograph by Dietrich Vogel copyright 2016 by Dietrich Vogel

The above figure 2.18 depicts a fiber that has reached the chloride threshold but was strong enough to resist brittle fracture. Increased oxygen exposure and longer time before the flexural strength testing would have allowed the corrosion to propagate further weakening the fiber. Different degrees of corrosion propagation were observed at different depths of chloride penetration. Fibers found in large pores (figure 2.19) were observed to corrode more than fibers surrounded in mortar.

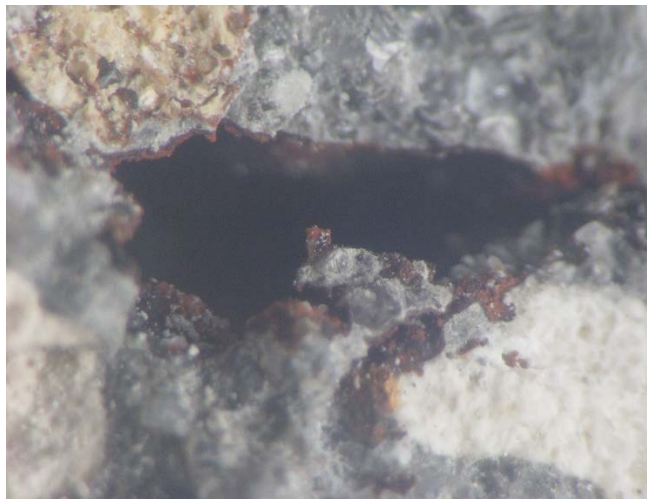


Figure 2.19 Increased corrosion in a large concrete pore from sample CI2 Photograph by Dietrich Vogel copyright 2016 by Dietrich Vogel

Even though chloride transport was accelerated from the exterior and passively introduced from the interior, the CE beams showed very little chloride influence and minimal corrosion of fibers. The chloride penetration in sample CE was measured to be much less than the CI beams. Chloride penetration is highly dependent on concrete resistivity; since beams pipe section CE was dried out before chloride migration the resistivity had increased. Fibers in CE beams were exposed to less chlorides and less moisture; two critical factors in determining the chloride threshold. During modified RMT chlorides and moisture moved through the CE section but they did not penetrate as far as the CI section.

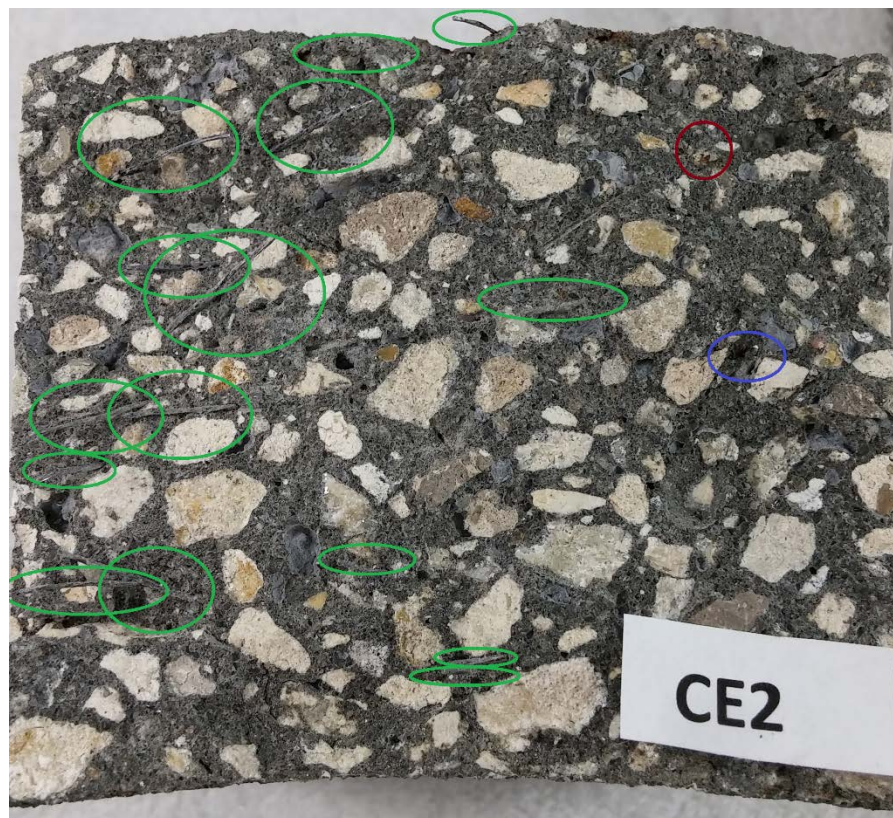


Figure 2.20 Beam sample CE3 with the fibers mapped and the conditions indicated by color Photograph by Dietrich Vogel copyright 2016 by Dietrich Vogel

Seen in figure 2.20, the beam CE2 had clean pullouts very near the surface of chloride exposure. Similar to one fiber in the sample CI3, despite the presence of

chlorides; corrosion of many steel fibers did not initiate due to a lack of oxygen or moisture or chloride threshold not being exceeded. In two areas of beam sample the chloride threshold was met and corrosion was able to diminish the strength of the fibers. The red circle is a brittle fracture with a companion spot on the other face, and the blue indicated the onset of corrosion but insignificant fiber cross section loss.

Beams NC, SW, and S did not have fibers affected as much by corrosion; the vast majority of fiber failures were clean pullout and there were zero brittle fractures observed. A summary of the experiment concerning the modulus of rupture, cross sectional area and fiber condition was tabulated in table 2-4 by counting each failure type in each beam face.

Table 2-4 Summary table of modulus of rupture and fiber count

| Sample | Mod of Rupture (psi) | Cross Sectional Area in ² | Number of Fibers, Sides 1 and 2 | | Number of Brittle Fractures |
|--------|----------------------|--------------------------------------|---------------------------------|----|-----------------------------|
| NC1 | 950 | 7.87 | 7 | 5 | 0 |
| NC2 | 1030 | 12.35 | 9 | 15 | 0 |
| NC3 | 1110 | 11.90 | 2 | 12 | 0 |
| CE1 | 1055 | 8.30 | 5 | 7 | 2 |
| CE2 | 910 | 11.90 | 17 | 17 | 1 |
| CE3 | 870 | 13.34 | 8 | 13 | 0 |
| CI1 | 1085 | 7.45 | 11 | 10 | 6 |
| CI2 | 805 | 11.94 | 21 | 17 | 5 |
| CI3 | 725 | 13.16 | 14 | 16 | 5 |
| SW1 | 1075 | 10.62 | 10 | 4 | 0 |
| SW2 | 895 | 12.11 | 6 | 11 | 0 |
| S1 | 1030 | 9.38 | 6 | 4 | 0 |
| S2 | 940 | 10.79 | 6 | 5 | 0 |

Tabulating the results (table 2-4) has summarized the experiment. The strongest beams tested were the no chloride control NC beams. The weakest beams tested were the interior chloride exposure beams due to the onset of corrosion and brittle fiber fracture observed on several fibers in the beam fracture plane.

2.4 Conclusion

- Upon the presence of corrosion propagation, the modulus of rupture for concrete reinforced with zinc electroplated steel fibers is adversely affected
- Beams without chlorides observed zero brittle fractures
- The preferred method of steel fiber failure was pull out, however brittle fractures and cross sectional loss was observed in beams with chlorides
- The fiber reinforcements resist corrosion propagation in the presence of chlorides alone; corrosion propagation is only possible in the presence of oxygen and humidity when the chloride concentration exceeds the threshold.
- Beams conditioned with chlorides may not have been dry long enough for oxygen to reach the fiber and allow corrosion propagation
- Oxidation products from corroded fibers appear to have traveled through the concrete pore structure which may make identifying fibers difficult
- The moisture content of concrete greatly affects ion diffusion and concrete resistivity
- Some fibers in the chloride penetration zone did not reach the chloride threshold of did not consume the sacrificial zinc electroplate

3 EXPERIMENTAL PROGRAM: VISUAL ANALYSIS OF ZINC ELECTROPLATED STEEL FIBERS EMBEDDED IN CONCRETE EXPOSED TO VARYING CHLORIDE CONCENTRATIONS

3.1 Introduction

Highway drainage pipes must be built tough enough to mitigate water, earth and traffic loads for decades without corroding and failing. Drainage pipes in service use a steel wire cage to reinforce the concrete from tensile stresses. Over time aggressively corrosive ions will penetrate the pores of the concrete and attack the metal reinforcement. Corrosion on the surface of the reinforcement will diminish in strength as the metal oxidizes and corrosion products expands during the propagation stage. The expansion pressures can crack and spall the concrete further exposing reinforcement to corrosives exacerbating the loss in structural support. Once the corrosion has diminished the reinforcement cross sectional area, the pipe strength could greatly decrease and failure is more probable. This experiment has observed the condition of steel fibers after the onset of corrosion.

Steel fiber reinforced drainage pipes are a new lower steel alternative to steel wire cage reinforced concrete pipes. Steel fiber reinforcement offers increased corrosion resistance to typical steel reinforced structures by having a more uniform micro-structure and a smaller volume to surface area ratio. Using a concrete testing standard (NT Build 492), chlorides can be migrated into concrete to initiate corrosion in the reinforcing steel fibers by applying an electric field that drives the chlorides via electro-migration.

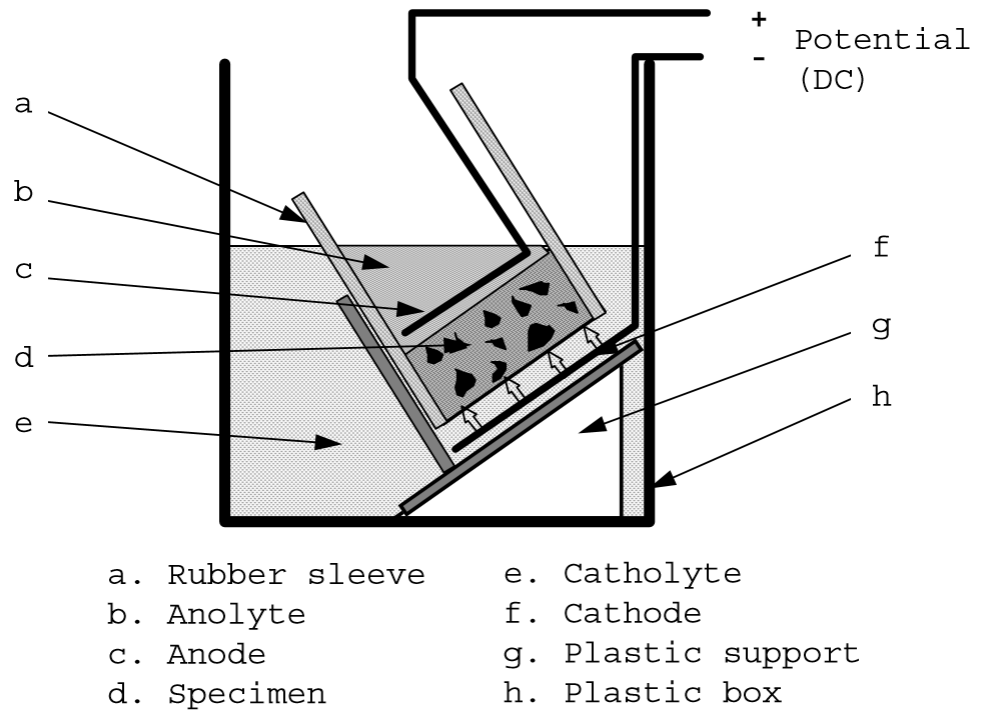


Figure 3.1 Single test setup for a chloride migration test indicated by NT build 492

In addition to stimulating the onset of corrosion in the steel fibers the non-steady state migration coefficient could be determined through chloride penetration measurements following NT-492. Figure 3.1 is a quick visual representation of the test setup where chlorides are migrated into concrete. Modified test methods were used throughout this thesis research to accommodate varying concrete geometry and fiber instrumentation.

Concrete specimens were cast in the lab with steel fibers that were mixed into the aggregate. The concrete samples were exposed to varying levels of chlorides to stimulate the onset of corrosion. Some concrete samples cast contained chlorides in the water, some samples had chlorides migrated into the concrete (accelerated and natural diffusion), and other samples were left as no chloride controls. Non instrumented

cylinders were cast then conditioned in high humidity for 9 months where their concrete resistivity was measured using the 4 point technique. Concrete resistivity was measured to track the progress of the pozzolanic reaction caused by adding fly ash to the concrete. Two 4"x8" cylinders were designated for RMT testing per NT build 492. The other cylinders were maintained in high humidity and lab temperature or high humidity and elevated temperature for environmental conditioning. Disks were then sliced off of each cylinder; one disk was crushed immediately for analysis and other disks were left outdoors, in high humidity, and lab humidity. The disks were then compared for steel fiber condition; all were eventually crushed so that fibers could be removed for further analysis. Steel fiber condition after the onset of corrosion and the chloride concentration were the focus of this experiment.

3.2 Experimental Procedure

3.2.1 Non Instrumented Concrete Cylinders

Observing the steel fiber condition after the onset of corrosion was the main objective of this research. Non instrumented samples were used for concrete characterization and forensic evaluation. Non-instrumented samples were cast in either 3"x6" or 4"x8" cylinder molds, but not always filled to the mold length. The larger cylinders were later used for RMT and Bulk diffusivity testing. The smaller diameter cylinders were either cast with chlorides or without chlorides. The purpose of creating the smaller cylinders is to inspect visually the difference between the surface and internal condition of the fibers after increased chlorides, oxygen and moisture. Concrete compositions were based on the steel fiber reinforced dry cast concrete pipe.

| Concrete Mixes and Properties | | | | |
|-------------------------------|--------------------------|-----------------------------|---------------------------------|------------------------------------|
| Type | Cementitious Content (g) | Water to Cementitious Ratio | Chloride as a % of Cementitious | Samples |
| Target | | 0.38 | 0 | Pipe |
| SFNC | 705 | 0.44 | 0 | <u>SFNCA</u> , NC, NCI, <u>NCB</u> |
| SFLC | 705 | 0.37 | 3.60% | C2, C3 |
| SFHC | 705 | 0.37 | 4.30% | HC1, HC2 |

Table 3-1 Concrete Compositions and water to cement ratios

3.2.1.1 Cylinders cast with fibers no chlorides for RMT (SFNCA, NCB)

Two cylinders were cast with zinc electroplated steel fibers, both cylinders were 4” diameter and 8” length; they are intended to simulate the dry cast concrete. Although all the concrete presented is wet cast, a simulation is necessary to measure corrosion activity of the steel fibers under comparable concrete conditions. Both cylinders are of similar composition. The cylinders were wet cast with zinc electroplated steel fibers obtained from two sources; fibers that were found from coring a pipe sample and new fibers obtained from the manufacturer. Some fibers were taken from lumped fiber spots found while coring in steel fiber reinforced concrete samples obtained from manufactures. SFNCA was cast on 2/20/2015. It was cast without chlorides and with helix steel fibers. NCB was cast on 3/26/2015 without chlorides and with fibers. The target water to cementitious ratio was 0.44 for the samples SFNCA and NCB. The samples were cast and the resistivity for each were measured throughout curing in a high humidity chamber. Resistivity measurements were taken to explore relationships between non-steady state migration coefficient and concrete resistivity.

After 60 days SFNCA and 30 days NCB in a high humidity environment, the cylinders were cut into four sections, each 2” (40-50mm) thick for a total of eight

cylinder slices. At the beginning of January, the eight samples were subject to accelerated chloride transport for 48 hours per modified NT build 492. The test took 48 hours and during that time, there was a steady diffusion of chloride ions into the concrete facilitated by an induced electric field. A power supply was used to apply a 15 V potential difference between two stainless steel mesh electrodes to drive the chlorides through the exposed faces of the concrete cut. After the 48 hour migration period, the four interior samples (2, 3, B, C) were placed in high humidity-elevated temperature environment. The four remaining samples including the top and bottom of SFNCA and NCB were mechanically cracked using a chisel and hammer. The cracked samples were sprayed with [0.1M] Silver Nitrate to expose the chloride penetration distance. The distance was measured with a caliper and 10 values were averaged over the span of the broken piece. *Figure 5.1* shows the split core #4 and the chloride ingress. The coefficient of migration was calculated using an average of the penetration lengths and the equations provided in the standard. After six months of elevated temperature exposure the remaining 4 samples were sliced and sprayed with silver nitrate; the exposure was expected to increase chloride penetration into the concrete. The chloride penetration distance was measured and the D_{nssm} was calculated. After demonstrating chloride penetration, four 3 mm concrete slices were taken from each of the samples 2,3,B, and C. The slices were dried in lab humidity for four weeks of oxygen exposure. The slices at the 10mm depth from chloride exposure were titrated for chloride concentration and the steel fiber condition was analyzed. A visual comparison of the steel fibers extracted from each sample and an analytical comparison of chloride content has helped to determine if the chloride threshold was reached.

3.2.1.2 Cylinders cast without chlorides and with fibers for Observation (NC, NCI)

To serve as a reference for non-corrosive behavior, two non-instrumented cylinders were cast without chlorides. The absence of chlorides provided a baseline for the in-service characteristics of the commercial steel fiber reinforced concrete pipe. The cylinders without chlorides were cast so that the condition of steel fibers and the presence of oxidation products could be compared to cylinders cast with chlorides.

On 3/26, the no chloride samples NC and NC I were cast. Sample NCI contained iron flakes in the aggregate, and sample NC had the iron flakes removed before casting. Iron flakes in the aggregate was caused by poor aggregate storage conditions outdoors; particles from the roof have added impurities to the aggregate. The metal particles were cast in the NCI concrete sample. Careful examination has distinguished the steel fiber oxidation from the impure metal additives.



Figure 3.2 Non-instrumented samples cast without chlorides (NC, NCI) Photograph by Dietrich Vogel copyright 2016 by Dietrich Vogel

The samples seen in figure 3.2 were sliced once in December 2015 then another three times the following February 2016. One of the three fresh slices were immediately crushed and the fibers were examined for physical condition, a second disk was stored outdoors 100ft from the intercostal waterway, a third disk was stored in 100% humidity and the original disk was placed in lab humidity. After 5 weeks of separate environmental conditioning the samples were crushed and the fibers were separated for forensic analysis. Fiber conditions were compared between environmental exposures and casting composition.

3.2.1.3 Cylinders cast with chlorides and fibers for observation (C2,C3, HC1, HC2)

Other than the 4”X8” cylinders that were cast for the purpose of concrete characterization through rapid migration testing; a series of cylinders were cast with

chlorides and fibers for observation and chloride threshold reference. The chlorides were mixed into the water that was used when combining the cementitious materials, sand and course aggregate. Samples C2, C3 were cast on 2/27 and HC1, HC2 were cast on 3/26. These samples were intended to be a shortcut to corrosion onset; the chlorides were mixed with the fibers at the time of casting.



Figure 3.3 Non-instrumented samples cast with chlorides (HC1, HC2, C2, C3)
Photograph by Dietrich Vogel copyright 2016 by Dietrich Vogel

In November 2015, after corrosion was observed on the surface of the chloride samples (seen in figure 3.3); a single cut was taken from each sample for observation of internal steel fiber condition. Two months later, four perpendicular cuts were made to obtain four 5/16 inch thick disks of each sample. The sections were immediately examined for any signs of corrosion; one section was crushed and examined for chloride concentration. Then the other three sections were placed into different environments for three weeks of atmospheric exposure. One was placed outdoors 100 ft from an intercostal waterway and approximately 150 yards from the Atlantic Ocean, one was placed in lab humidity, and one sample was placed inside a Ziploc sandwich bag to maintain humidity and restrict oxygen exposure. The condition of the fibers after

environmental conditioning as well as the sample chloride concentration have assisted in determining the chloride threshold of the steel fibers cast in the dry cast concrete.

3.3 Results and Discussion

3.3.1 Cylinders Cast Without Chlorides for Migration Testing (SFNCA, NCB)

Sample resistivity was measured using the 4 point method. The resistivity was measured at 4 places around the circumference of the cylinder. The resistivity wand was set to 2 cm spacing to accommodate the geometry of the cylinders measured. The resistivity meter range was set to 4; geometric corrections did not significantly change the measured resistivity.

Table 3-2 Resistivity of concrete sample SFNCA

| Days | 0 | 6 | 13 | 20 | 26 | 33 | 48 | 55 | 73 |
|---------|--------------|-------------|--------------|-------------|--------------|------------|--------------|--------------|------------|
| SFNCA | 4.5 | 4.6 | 4.4 | 4.9 | 5.5 | 6 | 7.1 | 8.6 | 9.2 |
| | 4 | 3.7 | 4.2 | 5.5 | 5.1 | 5.9 | 7.1 | 7.8 | 3.8 |
| | 3.4 | 4.4 | 4.4 | 5.3 | 6.5 | 7.1 | 6.5 | 8.8 | 11.1 |
| | 2.8 | 3.9 | 4.1 | 4.9 | 6 | 6.2 | 7.8 | 7.9 | 8.7 |
| Average | 3.675 | 4.15 | 4.275 | 5.15 | 5.775 | 6.3 | 7.125 | 8.275 | 8.2 |

Table 3-3 Resistivity of concrete sample NCB units in kohms*cm

| Days | 14 | 29 | 36 | 54 |
|---------|------------|--------------|--------------|--------------|
| NCB | 3.1 | 4 | 4.6 | 6 |
| | 2.9 | 3.7 | 4.4 | 5.4 |
| | 2.9 | 3.2 | 4.4 | 5.4 |
| | 2.7 | 4 | 5.1 | 6.3 |
| Average | 2.9 | 3.725 | 4.625 | 5.775 |

Over time the resistivity of the concrete samples was increasing as seen in both tables 3-2 and 3-3. The increasing resistivity over time was attributed to the progression of the pozzolanic reaction. The pozzolanic reaction due to fly ash mixed into the concrete reduces the pore size and a decreased pore size increases the concrete resistivity.

The resistivity for NCB was measured to be lower than SFNCA; further chloride penetration distance was expected when subject to RMT.



Figure 3.4 Core 4 from NCB after RMT picture taken months after being split

Photograph by Dietrich Vogel copyright 2016 by Dietrich Vogel

The figure 3.4 depicts sample 4 from NCB after the cylinder was subject to 48 hours of chloride migration as a part of the standard RMT test. After the RMT testing the samples were split within 48 hours using a hammer and chisel then sprayed with silver nitrate. The photo shown was taken 2 months after the cylinder was split and sprayed with silver nitrate. Using calipers, the distance of chloride ingress was measured at 7 evenly spaced places and recorded. The average distances were used to calculate the non-steady state diffusion coefficient for each cylinder.

Table 3-4 Non-Steady State Diffusion Coefficient

| Core | Average thickness (mm) | Cl depth (mm) | D_{nssm}^* 10^{-12} m^2/s |
|------|------------------------|---------------|---------------------------------------|
| A | 41.31 | 10.41 | 9.30 |
| B | 41.20 | 13.10 | 12.11 |
| C | 42.10 | 11.57 | 10.69 |
| D | 44.05 | 6.89 | 5.95 |
| 1 | 42.16 | 11.57 | 10.70 |
| 2 | 42.13 | 17.23 | 16.85 |
| 3 | 42.20 | 13.17 | 12.44 |
| 4 | 42.16 | 10.73 | 9.80 |

Cylinder 1 SFNCA- Cast 2/20/15 contributed samples A,B,C,D

Cylinder 2 NCB- Cast 3/26/15 contributed samples 1,2,3,4

Table 3-4 presents the non-steady state migration coefficient of the concrete used in the majority of samples included in this research. The sample D was the thickest slice and observed the least chloride penetration. Chloride penetration may have also been inhibited by better compaction; as slice D was the bottom section from the cylinder. Cylinders B,C,2,3 were seasoned in elevated temperature and high humidity for an additional six months before being split and checked for chlorides. The increased temperature and moisture allowed the chlorides that penetrated as a part of RMT to seep further into the concrete than the samples split immediately after rapid migration testing. No correction was applied to account for the six month exposure to elevated temperature and high humidity.

Samples B,C,2,3 were further analyzed for fiber condition and chloride concentration. Four slices approximately 2mm in thickness were taken from each cylinder.



Figure 3.5 2mm slices taken from slice 2 of sample NCB after 4 weeks of lab humidity and oxygen exposure Photograph by Dietrich Vogel copyright 2016 by Dietrich Vogel

For each sample: B,C,2,3; the slice at the 10mm depth was crushed and the steel fibers were extracted. Figure 3.5 shows one side the 4 slices that were taken from sample 2 for further analysis. Steel fiber condition was analyzed and the chloride concentration was measured. The steel fibers that were oxidized had a stronger bond to the concrete than fibers free of corrosion; bond strength was an observational or qualitative characteristic based on the comparative difficulty of extracting fibers from the concrete. The presence of oxidation products created a stronger bond between the steel fiber and the surrounding cement matrix. Corroded fibers were consistently more difficult to extract from the concrete and upon removal, rust stains were evident on the concrete.

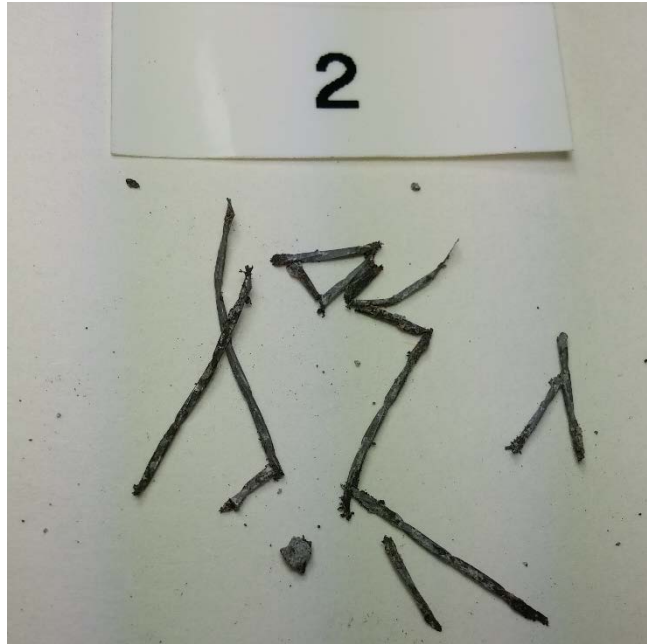


Figure 3.6 Fibers extracted from the 10mm depth slice taken from sample 2 of NCB
Photograph by Dietrich Vogel copyright 2016 by Dietrich Vogel

The fibers extracted from the each of the slices had varying degrees of corrosion as seen in figure 3.6 for one of the slices. There were oxidation stains as well as visible cross section loss on many fibers. While most of the fibers have clear effects of corrosion, at the same depth other fibers did not show red oxidation stains. The chloride threshold was passed for the fibers observed to be stained in oxidation. For other fibers the steel substrate was not exposed and thus there were not red stains. It is not clear if these fibers have reached the chloride threshold as some of the zinc layer may have been consumed.

3.3.2 Cylinders Cast Without Chlorides (NC, NC1)

Over the course of the experiment the cylinders without chlorides did not show any change in appearance. As seen in the picture 5.4, the slice from NC did not exhibit any evidence of discoloration. Discoloration or corrosion was not expected due to the

lack of chlorides in the concrete mixture.



Figure 3.7 Sample NC after first slice taken 6 months after casting Photograph by Dietrich Vogel copyright 2016 by Dietrich Vogel

After the first slice, the concretes without chlorides did not exhibit visual evidence of corrosion as seen in figure 3.7. Some of the fibers were seen as reflective silver spots where others appeared matte grey. The samples were maintained in high humidity for another six months before additional slices were cut. Four additional slices were obtained from each sample. The first slice was immediately crushed and analyzed for fiber analysis. At the time of crushing the first slice there was no corrosion observed in the steel fibers. The next slice was placed outside, 100 feet from the intercostal waterway in the south Florida heat and humidity. The third slice was placed in lab conditions and the last slice was placed in a bag to limit oxygen exposure and maintain moisture content. After 5 weeks of respective exposure the slices were photographed and the fibers were extracted and analyzed.



Figure 3.8 Disk from sample NC after 5 weeks of outdoor exposure Photograph by Dietrich Vogel copyright 2016 by Dietrich Vogel

The slice seen in figure 3.8 was from the no chloride sample and the picture was taken after 5 weeks of outdoor exposure. This was the sample that exhibited the most corrosion of the NC samples and was superficial to the exposed side. The fibers embedded in the samples without chlorides were free of corrosion regardless of environmental exposure. Many of the exposed fibers remain free of steel corrosion but two fibers were seen to have oxidized. Over the 5 weeks the south Florida heat and humidity combined with aerosol sea spray from the nearby ocean provided a naturally corrosive environment for the fibers embedded in the concrete and the exposed steel fiber faces. After the surface condition was documented the slice was smashed and the fibers were extracted for forensic evaluation.

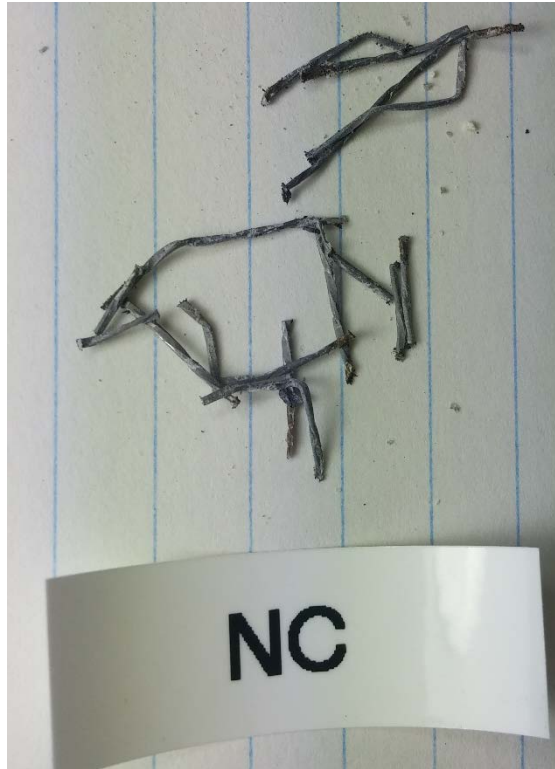


Figure 3.9 Fibers taken from the NC disk stored outdoors for 5 weeks Photograph by Dietrich Vogel copyright 2016 by Dietrich Vogel

Fiber condition after extraction was observed and documented. The fibers from the no chloride sample left outdoors were free of steel corrosion as seen in figures 3.8 and 3.9. No discoloration or cross section loss was observed in the majority of fibers. Three fibers had some red discoloration near the fiber tips; where the edges were exposed to the atmosphere. As expected, the no chloride samples (NC, NCI) were not corroded and intact. Some zinc corrosion products were evident on the surface of the fibers indicated by a white discoloration. See figures in appendix for the complete experimental photo story.

3.3.3 Cylinders Cast With Chlorides (C2, C3, HC1, HC2)

Non-instrumented cylinders cast with chlorides were maintained in high humidity to facilitate corrosion onset. After nearly 3 months, some surface discoloration could be

observed. The surface discoloration was seen as small red stains on the surface of the concrete cylinder.



Figure 3.10 Sample HC1 after the first slice Photograph by Dietrich Vogel copyright
2016 by Dietrich Vogel

The figure 3.10 shows that regardless of some exterior staining on sample HC1, interior fibers remain inactive at a 5 mm cover depth. Red discoloration was not seen in the slice after the cut. Two weeks after the first slice, oxidation products could be observed on the cut surface. It is speculated that inside the cylinder the fibers remained inactive; only when exposed to oxygen does the fiber begin to corrode.



Figure 3.11 Sample C3 after the first slice Photograph by Dietrich Vogel copyright 2016

by Dietrich Vogel

Similarly to HC1, figure 3.11 depicts C3 after the first slice. Once again, regardless of surface staining; the interior fibers remain unchanged in appearance. After two weeks of exposure to the atmosphere, the fibers uncovered by the slice exhibited a white frost, an indication of zinc oxidation but not steel fiber corrosion. After three weeks, the slice exhibited some red discoloration at the surface for some of the fibers.

Six months after the first slice and about a year after casting, four more slices from each sample were taken. Photos were taken of the cylinder cross section soon after slices were taken from the concrete.



Figure 3.12 Four slices of sample HC1 taken in early February Photograph by Dietrich Vogel copyright 2016 by Dietrich Vogel

All slices taken were observed for oxidation products, no corrosion was found as can be seen in figure 3.12 for HC1 slices. One slice of each sample type was immediately crushed and the fiber condition was analyzed. Despite the presence of chlorides cast inside the concrete for a year, corrosion was not evident on the surface of the steel fibers.

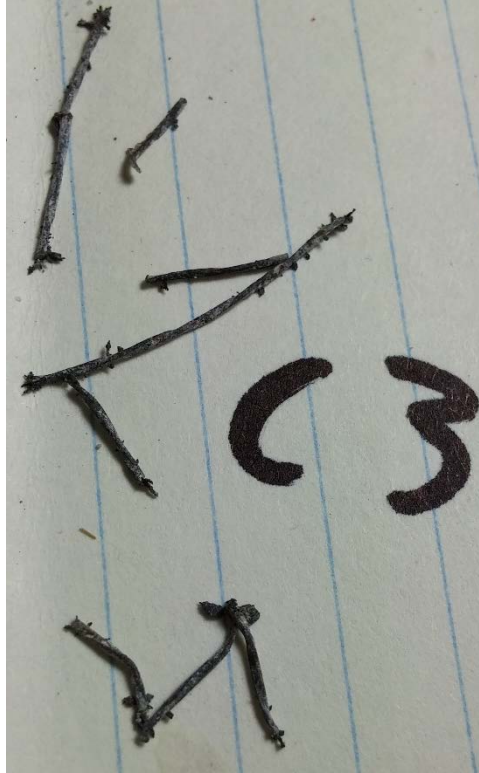


Figure 3.13 Extracted samples from sample C3 shortly after a disk was sliced off of the cylinder Photograph by Dietrich Vogel copyright 2016 by Dietrich Vogel

The fibers in the figure 3.13 were mostly corrosion free; other samples are pictured in the appendix. Some have isolated tarnish spots where the fiber appears black and not grey; no red discoloration was observed on any fibers. At those tarnish spots, cross section loss was not observed. The other slices were seasoned outdoors, indoors, and in high humidity for 5 weeks.

Slices left outdoors were exposed to oxygen and high humidity. A combination of the chlorides in the concrete, moisture from the dew cycle, oxygen availability and the high heat has initiated corrosion of the steel fibers. Steel fiber condition was documented with pictures before the slices were crushed and the fibers removed were then analyzed more closely.



Figure 3.14 Disk sample HC1 after 5 weeks of outdoor exposure Photograph by Dietrich Vogel copyright 2016 by Dietrich Vogel

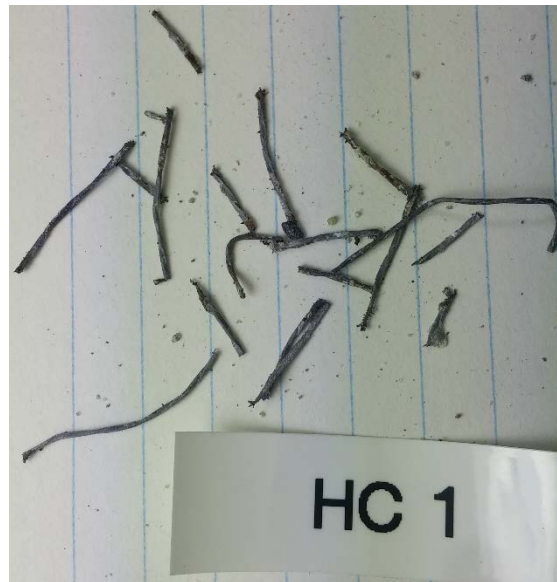


Figure 3.15 Fibers extracted from the HC1 disk sample exposed to outside conditions Photograph by Dietrich Vogel copyright 2016 by Dietrich Vogel

Slices left outdoors were observed to have the most corrosion. Many exposed fibers were rusted red and no bare metal was visible. Red oxidation products were

observed on all exposed fiber faces as seen in figure 3.14. After the slice was crushed and the fibers were extracted, their surface condition was analyzed. Many of the fibers seen in figure 3.15 were corroding before extraction from the slice. However some of the fibers remained without visible effects of steel fiber corrosion but with zinc oxidation products. While the chloride threshold was reached for some fibers, corrosion in other fibers might have not initiated. The samples maintained at lab humidity did not exhibit any comparable corrosion. Exposed fiber faces were shiny and free of corrosion after 5 weeks of lab humidity exposure.



Figure 3.16 Disk HC1 exposed to inside conditions for 5 weeks Photograph by Dietrich Vogel copyright 2016 by Dietrich Vogel

Despite the presence of chlorides and an abundance of oxygen, the lab humidity

was not high enough to stimulate oxidation of the steel fiber on slice HC1-2 seen in figure 3.16. The results from this experiment prove that the chloride threshold is a function of oxygen, moisture, and chloride presence; all three are required for steel fiber corrosion. To verify this result, the slices that were maintained in a plastic bag were analyzed. Pictures of the slices maintained at high humidity with limited oxygen exposure show fibers that remain mostly free of corrosion.



Figure 3.17 Disk HC1 Exposed to high humidity and restricted oxygen for 5 weeks
Photograph by Dietrich Vogel copyright 2016 by Dietrich Vogel

Limited oxygen has limited the steel fiber oxidation. Very few isolated oxidation stains could be seen on the edges of exposed fiber ends in figure 3.17. The isolated corrosion was stimulated by oxygen in the water droplets trapped near the steel fiber

surface. More oxygen and humidity were needed to oxidize the iron contained in the steel fibers. The level of chlorides in each cylinder was high enough to initiate corrosion in the presence of moisture and atmospheric exposure.

3.3.4 Conclusions

- Chlorides, oxygen, and moisture are required for corrosion of zinc electroplated steel fibers embedded in concrete
- The chloride threshold for the zinc electroplated steel fibers is a range of chloride concentrations and depends on the individual fiber
- The initial oxidation products create a stronger bond between the steel fiber and cement matrix

4 EXPERIMENTAL PROGRAM: ELECTROCHEMICAL ANALYSIS OF ZINC ELECTROPLATED STEEL FIBERS EMBEDDED IN CONCRETE EXPOSED TO VARYING CHLORIDE

4.1 Introduction

Corrosion of zinc electroplated steel fibers is an electrochemical process that the Florida Department of Transportation must consider when choosing construction materials. Materials are tailor made for the environment where they will be deployed for service. Few studies exist on the electrochemical activity of zinc electroplated steel fiber reinforcements after the onset of corrosion embedded in concrete. Typical rebar reinforcements are large enough to easily instrument while embedded in concrete and measure corrosion potential or corrosion rate. Individual steel fiber instrumentation is more difficult due to the concrete cover distance and the separation of fibers. Fiber instrumentation is necessary for electrochemical activity measurements.

Electrochemical corrosion activity can be initiated in reinforced steel concrete by introducing chlorides. Similar to the non-instrumented experiment, the concrete cylinders were exposed to varying chloride concentrations. Some samples were cast with chlorides, others were introduced to chlorides after casting, and others were no chloride exposure control samples. All fibers with instrumentation were measured for corrosion potential and linear polarization resistance over the course of one year. After a year of measurements, the fibers were extracted from the concrete for visual inspection of the

corrosion propagation. The electrochemical trends after the onset of corrosion is the focus of this research; forensic analysis is used to verify electrochemical measurements.

4.2 Experimental Procedure

All samples containing instrumented fibers are intended to observe the corrosive behavior of the fibers or steel wires embedded in concrete matrix. Some specimens were cast with low alloy steel wire of diameter 0.82mm. These steel wires were instrumented and embedded in concrete as a point of comparison to the zinc electroplated steel fibers. The instrumented fibers were measured 2 ways: 1) with a high impedance volt meter to determine the fiber potential vs a standard calomel reference electrode, 2) with a Gamry potentiostat machine to measure the linear polarization resistance of the instrumented fiber. Both measurement methods were used in tandem to determine the electrochemical behavior of samples. The corrosion potentials were measured by first connecting the reference electrode to one lead on a voltmeter; the other lead was connected to the instrumented fiber to be tested. The reference electrode was then suspended in the reservoir on top of the sample; or if the sample does not have a reservoir, the electrode was wrapped in a salt water soaked sponge then held on top of the concrete sample with a ring stand. Linear polarization resistance measurements were conducted with a Gamry potentiostat. The potentiostat was connected in a three electrode arrangement: one connection to the SCE reference electrode, a second connection to a titanium mix metal oxide mesh used as a counter electrode was made and placed between the concrete surface and the reference electrode. The third connection was attached to the instrumented fiber for measurement also known as the working electrode. After measurements, the linear region of the LPR graph close to the corrosion potential was

selected to determine the apparent linear polarization resistance. Instrumentation of fibers cast in concrete has not been done many times prior and standards are nonexistent. Instrumentation of steel fibers was an unintended variable shoved into the research presented in this section of the thesis.

For the samples cast with chlorides, samples for rapid chloride migration, and aqueous samples; the fiber instrumentation method varies. Many of the steel fibers and carbon wires were welded to 16 AWG silver plated copper wire with standard solder then the connection is coated with a thin layer of two part epoxy. Once epoxied, the instrumented fibers were cast into a concrete sample. Other fibers were simply wedged in between the strands of the 16 AWG wire and held together with friction before quickly being cast in a concrete sample. The last instrumentation method does not involve a connecting wire. The concrete samples were poked with fibers and carbon wires while the concrete was drying resulting in approx. ¼” of the fiber or carbon steel wire protruding from the concrete surface. The instrumented samples were maintained regularly to remove oxidation products from the exposed wire ends.

While all samples cast with instrumented fibers were tested for fiber potential and linear polarization measurements (both against a standard calomel reference electrode); the environment and concrete composition varied. Instrumented samples were cast with chlorides or without chlorides. Samples that were cast without chlorides were either left as a controlled reference, subject to modified migration, or subject to ponding for passive chloride transport. Samples cast with chlorides were intended to immediately initiate breakdown of the passive zinc electroplated layer and activate corrosion on the instrumented steel fibers. The purpose of exposing steel fibers to varying chlorides

within the concrete is to electrochemically observe the passive to active transition of the steel fibers and carbon steel wires at different concrete cover depths.

4.2.1 Instrumented samples cast with no chlorides

Cylindrical concrete samples cast without chlorides were intended to mimic the concrete characteristics of the mass produced highway drainage pipe. The target concrete composition was 284.8 kg/m³ cement, 59.3 kg/m³ fly ash, 1086.9 kg/m³ 3/8 rock, 776.6 kg/m³ sand, 131.1 kg/m³ water, 8.9 kg/m³ steel fibers. Like the fibers cast in the pipe, these instrumented fibers were expected to initially passivate. After the concrete casts have cured, some samples were left to remain passive (C1, C5, C6), some were subject to chloride diffusion via ponding (LWCA, LWCB, HWC, P1, P2) and others had chlorides migrated into them through modified RMT methods (B1, B2, MLWC1, MLWC2). The rapid migration samples were prepared to control depth as a variable. Concrete samples B1, B2, P1, P2, MLWC1, MLWC2 include instrumented fibers at specified depths. Using various molds and techniques, fibers and wires were set at various depths from 1cm to 4 cm from the surface. The accelerated chloride migration samples have directly simulated long term chloride deposition from one side; similar to deposition that would be observed after years in service. Fibers were instrumented at known depths; measurements were taken to determine the behavior of the fibers at each distance from the surface over the course of chloride deposition. After the measurements of corrosion potential and polarization resistance revealed obvious effects of chloride ingress, most samples were terminated and a forensic analysis was conducted to focus on the condition of the fibers. Forensic analysis has revealed the method of steel fiber corrosion; it has

helped determine the critical chloride content and physical properties of the fibers after the onset of corrosion.

4.2.1.1 C1, C5, C6 Control Samples

The first instrumented fibers presented here are the control samples; cast without chlorides to observe the electrochemical behaviors of the fibers under standard or safe environments. Sample C1 was cast on 2/27/2015 and samples C5 and C6 were cast on 2/20/2015. The samples were labeled well after their cast date.



Figure 4.1 Instrumented Samples without chlorides(Left to right:C1, C5, C6) Photograph

by Dietrich Vogel copyright 2016 by Dietrich Vogel

Shown in figure 4.1 are samples C1 (Left), C5 (Center), C6 (Right). These samples were instrumented controls without chlorides and low water to cementitious ratios. These samples have zinc electroplated steel fibers, the steel fibers were not subjected to chlorides and the concrete samples were experimental controls.

4.2.1.2 LWCA, LWCB, HWC Passive Transport Samples

These samples were cast without chlorides in 3X6” concrete molds, left to cure, and then a reservoir was added to passively transport chloride ions into the concrete. Samples LWCA, LWCB, HWC correspond to their water content. LWC stands for low water cement ratio (approaching dry cast) and HWC stands for high water to cement ratio. The high water cementitious ratio has a lower resistivity and ions can transport more freely in HWC than LWC. HWC was created to be a worse case scenario for passive chloride transport. The three samples were cast 2/27/2015 and they were subsequently ponded with 15% chloride solution starting 4/13/2015.



Figure 4.2 Instrumented samples cast without chlorides (Left to right: HWC, LWCA, LWCB) Photograph by Dietrich Vogel copyright 2016 by Dietrich Vogel

Figure 4.2 shows HWC (Left), LWCA (Center), LWCB (Right). The samples were 3” by 6” cylinders with two steel fibers and a carbon wire each; cast at a concrete cover depth of 20mm. After ponding, sample HWC was left outside 100M inland from

the ocean shoreline for 60 days. The LWC samples were maintained in the lab near 100% humidity. Since ponding, the samples have been exposed to a 15% NaCl solution suspended in the reservoir. Over time the fiber potential and the linear polarization resistance were measured and the steel fibers were forensically analyzed after termination.

4.2.1.3 P1, P2 Passive Transport Poke Samples

Instrumentation method may dictate the outcome of measurement due to mix metal corrosion. For the poked samples, wires were not a part of the experiment. The corrosion potential and linear polarization resistance measurements were taken by directly connecting the fibers to the measurement connections. The advantage of this type of connection was to remove the soldering and other metals from the electrochemical equation. One fall back of this method is that the oxygen and water were available at the surface of the fiber, which allowed for corrosion to propagate on the exposed surface. The first poke sample was cast 6/2/2015 with three steel fibers and three carbon steel wires. The second poke sample was cast on 6/4/2015 with 4 carbon steel wires and 4 steel fibers. Both samples were given reservoirs on 11/04/2015 so that the chlorides could begin to diffuse into the concrete. The reservoir was filled with 15% NaCl solution and was refilled when needed.



Figure 4.3 Instrumented samples with the poke method(Left to right: P2, P1) Photograph by Dietrich Vogel copyright 2016 by Dietrich Vogel

As seen in figure 4.3, poke samples P2 (left) and P1 (right). A red discoloration was seen around the fibers and wires due to the availability of water and oxygen in the atmosphere. Before measuring the corrosion potential, the ends of the fibers were lightly sanded to ensure solid metal connection. Because these are the samples with the most recent cast date, they did not have as many potential and linear polarization measurements.

4.2.1.4 MLWC A, MLWC B; Migration Cylinders

In order to observe a transition between initial passivity to activity in a short time, chlorides must be introduced rapidly using electricity. Two concrete cylinders (4 inches in diameter) were cast in low water to cement ratio cement with 6 zinc electroplated steel fibers and 3 carbon steel wires each. The zinc electroplated steel fibers were instrumented with wires and placed at 10mm, 20mm, and 30mm depths from the surface.

A variation in depth assisted in determining the chloride threshold; the chlorides will have different concentrations at different depths in the concrete.

The samples MLWCA, and MLWCB were each cast on 2/27/2015 and named after their composition: low water content, and their purpose: accelerated chloride migration. The fibers were cast in a 4" X 4" concrete cylinder mold. A mold was prepared ahead of time with holes in a 3X3 matrix pattern. Holes in a matrix pattern held fibers at their respective depths from the surface. After casting, the mold was removed and the concrete cylinders were left in high humidity to cure. In order to hold the salt solution, a reservoir was added to the top of each sample on 4/13/2015.



Figure 4.4 Instrumented Migration samples (Left to right: MLWCB, MLWCA)

Photograph by Dietrich Vogel copyright 2016 by Dietrich Vogel

Pictured in figure 4.4 are MLWCB (Left) and MLWCA (Right). The wires connecting the instrumented fibers were assembled in a matrix labeled by their index; 11 was the top left and 33 was the bottom right. The ponds for these samples were added

just before migration began on 4/12/2015 and filled with 15% NaCl. Stainless steel meshes were used as electrodes, the cylinder was placed in a container filled with calcium hydroxide on top of a stainless steel electrode. A 10V potential difference was induced for 24 hours; the initial migration was not immediately noticeable through potential measurements. Migration continued at 15V for 30 days until chlorides were observed to corrode the mesh in the calcium hydroxide solution. Post migration, the samples were left in elevated temperature and high humidity to facilitate the onset of electrochemical activity. After a month of exposure the samples were brought back to lab temperature and high humidity. Periodically, the samples were measured for fiber potential and linear polarization resistance until termination and fiber evaluation.

4.2.1.5 B1, B2; Migration Blocks

Because the previous samples were cast in a matrix pattern, there exists a possibility of shadow zones from migrating chlorides. Two other samples were cast with the intention of migration; they have the same length and width (130mm X 130mm), however sample B2 (30mm) has half the thickness as sample B1 (65mm). The sample B1 (*Figure 4.8*) was cast on 3/13/2015 with 4 steel fibers and 4 carbon steel wires each at a depth of 10mm, 15mm, 20mm, and 25mm from the surface of chloride exposure. Sample B2 (*figure 4.5*) was cast on 6/02/2015 with 3 steel fibers (cover depth 10mm, 12.5mm, 20mm) and 2 carbon steel wires (10mm, 20mm). Because the samples are intended for migration, reservoirs were added on 4/13/2015 to B1 and on 8/18/2015 to B2. The blocks were maintained at 100% humidity throughout curing and were maintained in high humidity.



Figure 4.5 Migration block samples. (Left to right: B2, B1) Photograph by Dietrich Vogel

copyright 2016 by Dietrich Vogel

Both block samples were fitted with reservoirs for modified chloride migration. Block B1 was subjected to 10V for 48 hours, then 12.5V for 15 days. The migration was terminated for block 1 because chlorides were observed to cause corrosion of the counter electrode mesh in the calcium hydroxide solution. Sample B2 was subject to a lower voltage over longer time, additionally B2 is significantly shorter than B1. Migration on B2 occurred at 2V for 23 days and was terminated once oxidation products from the counter electrode were observed in the calcium hydroxide solution. Both blocks were maintained in high temperature and humidity for 30 days post migration and measured regularly until early March 2016 when the samples were terminated. Sample B1 was carved on a milling machine so that concrete powder could be collected at various depths for a chloride profile determination. Sample B2 was sliced on a tile saw to separate fibers. The chloride profile for sample B2 was not determined.

4.2.2 Instrumented samples cast with chlorides C4, C7, C8

Presented to this point, instrumented samples had chlorides transported into the concrete over time via gravity, electro-migration and porosity. This section describes the behavior of fibers cast in concrete containing chlorides. Due to the chlorides, less water was needed to mix the concrete paste. Additionally, the chlorides cause the resistivity of the concrete to decrease which means that the ions transport within the concrete more easily. The samples C4 and C7 were cast on 2/20/2015 and sample C8 was cast on 3/26/2015; the samples cast with chlorides were composed of low water to cementitious ratio concrete.

Reliable measurements of these samples were not always possible as there was no solution reservoir initially, later ponds were added to the top of the samples to create a more conductive environment for the reference electrode when measuring potentials or LPR. The ponds were added on 8/18/2015 for samples C8 and C4; a solution reservoir was added for sample C7 on 9/03/2015.



Figure 4.6 Instrumented sample cast with chlorides(Left-C8, Center-C7, Right-C4)

Photograph by Dietrich Vogel copyright 2016 by Dietrich Vogel

In the figure 4.6 samples C8 (left), C7 (front center), and C4 (Right) were the three instrumented samples cast with chlorides. Samples C4 and C8 were larger than C7; there was increased concrete cover for fibers in the larger cylinders which inhibited the amount of oxygen and moisture that could transport to the fibers. Sample C7 was significantly smaller thus oxygen may be more available on the fiber surface from the bottom side.

4.3 Results and Discussion

An abundance of data was collected from the instrumented fibers embedded in concrete; potential measurements, linear polarization resistance (LPR) measurements and forensic analysis was conducted on 67 individual fibers. The goal of experimentation was to electrochemically observe the onset of corrosion for zinc electroplated steel fibers embedded in concrete. Corrosion potential measurements were indicators of electrochemical activity, LPR measurements were a proxy to determine corrosion rate,

and forensic analysis was used to compare steel fiber condition to the measurements which were taken over the course of a year.

4.3.1 C1, C5, C6 Control Samples

Casting instrumented samples in concrete without chlorides has provided a base control measurement for the steel fibers. Fibers embedded in concrete without chlorides were expected to form a passive layer; protecting the steel from corrosion. The formation of a zinc oxide layer is seen in the figures 4.7, 4.8, and 4.9. Initial electrochemical activity was observed in the fibers while the zinc was oxidizing; once the oxide layer covered the zinc then the corrosion potentials became significantly more positive.

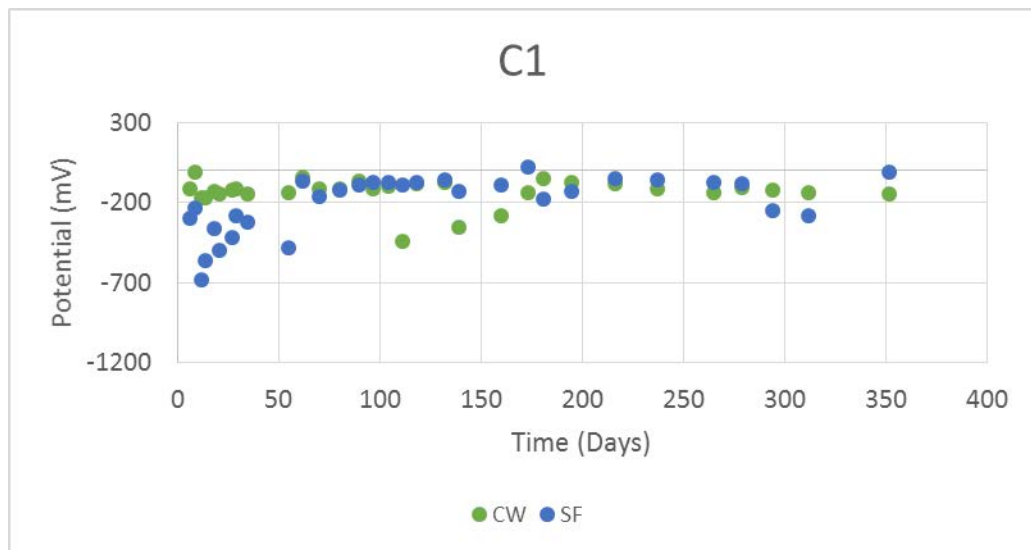


Figure 4.7 Corrosion potential graph of sample C1

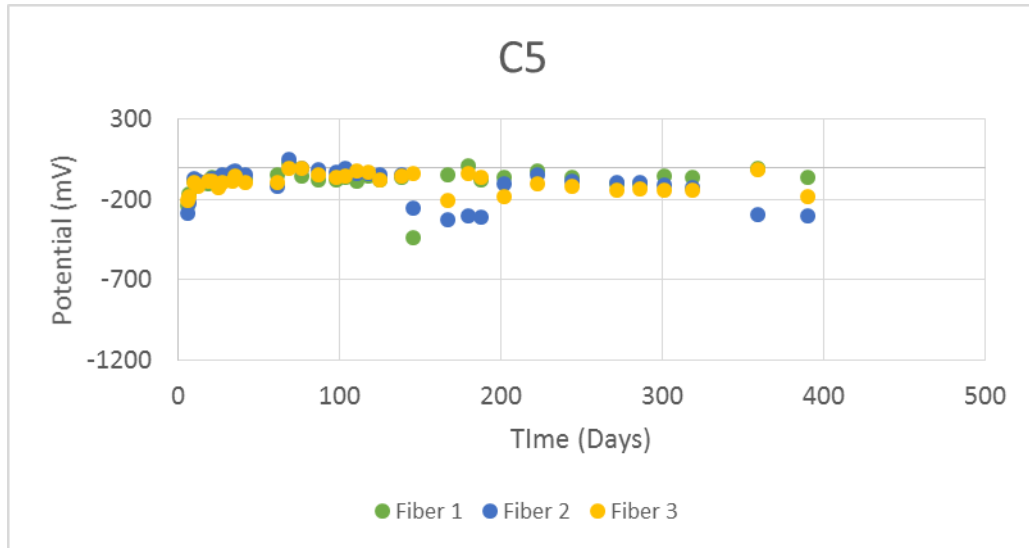


Figure 4.8 Corrosion potential graph of sample C5

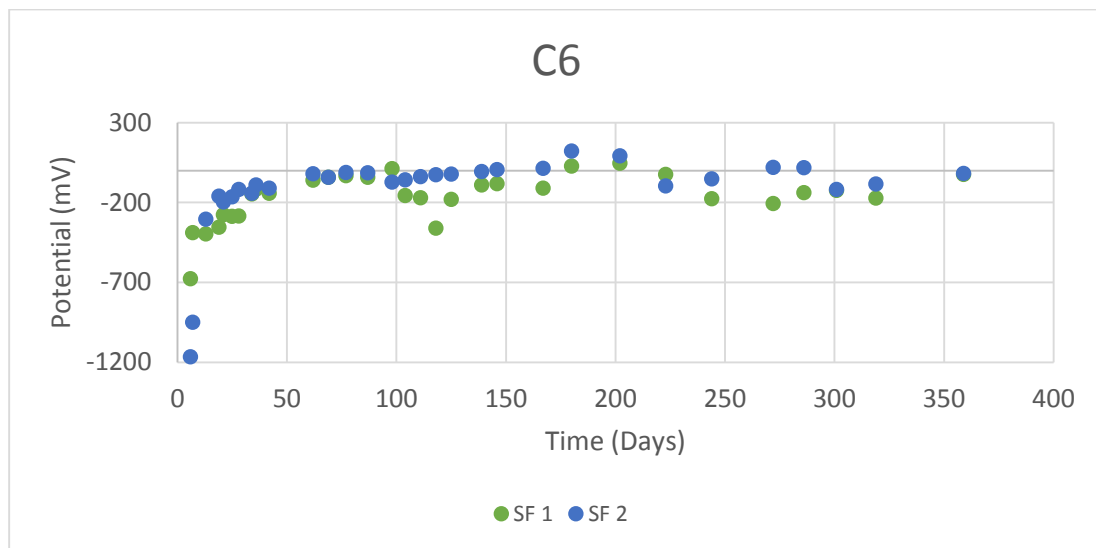


Figure 4.9 Corrosion potential graph of sample C6

The corrosion potential measurements of the three no chloride samples seen in figures 4.7, 4.8, 4.9 detail the same story; quick formation of a zinc oxide layer and then prolonged protection. The ASTM indicated that corrosion of carbon steel will occur at a corrosion potential less than -230 mV vs SCE electrode. There is no standard corrosion potential for steel fibers electroplated with zinc. Each fiber in the no chloride samples

were measured to be nobler than the corrosion potential set forth by the ASTM; an indication of electrochemical inactivity. LPR values were not measured because no corrosion activity was indicated by the corrosion potential measurements. The lack of corrosion suggested by the corrosion potential measurements was verified in the forensic analysis.



Figure 4.10 Fiber SF1 from sample C6 Photograph by Dietrich Vogel copyright 2016 by Dietrich Vogel



Figure 4.11 Carbon steel wire from sample C1 Photograph by Dietrich Vogel copyright 2016 by Dietrich Vogel

After cracking the concrete and extracting the fibers, examination of the fibers confirmed expectations. The fibers were completely free of red rust spots after exposure to high humidity for over a year. The fiber conditions shown in figures 4.10 and 4.11 served as a baseline for comparison with other samples. An unaffected zinc electroplated steel fiber was a uniform shade of matte grey; an unaffected carbon wire retained some shine.

4.3.2 LWCA, LWCB, HWC Passive Transport Samples

The next sample type was also cast without chlorides. Chlorides were gradually introduced to samples LWCA, LWCB, and HWC after day 50 via the ponded reservoir. The corrosion potentials were measured over the course of a year and values were plotted for each fiber seen in figures 4.12, 4.13, and 4.14.

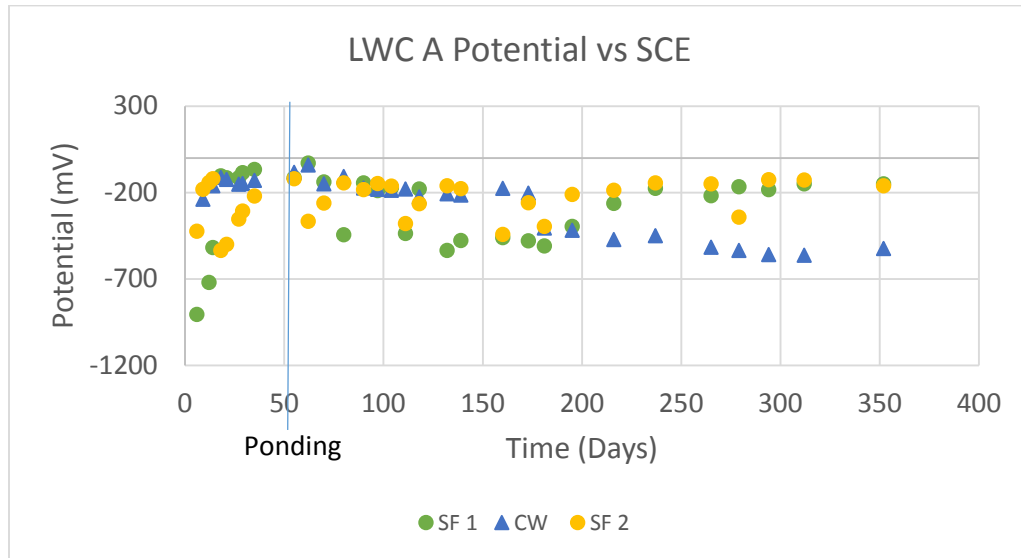


Figure 4.12 Corrosion potential graph of sample LWCA

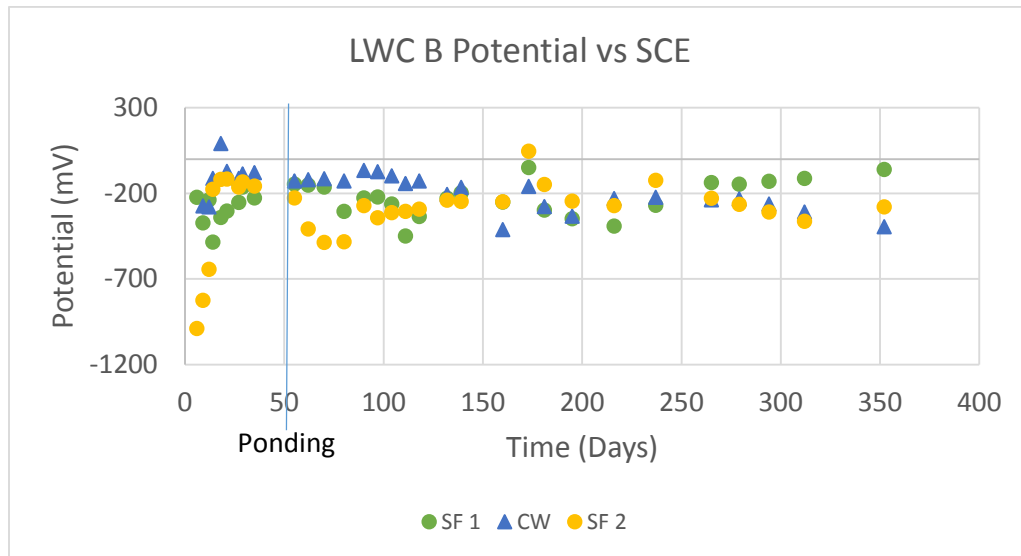


Figure 4.13 Corrosion potential graph of sample LWCB

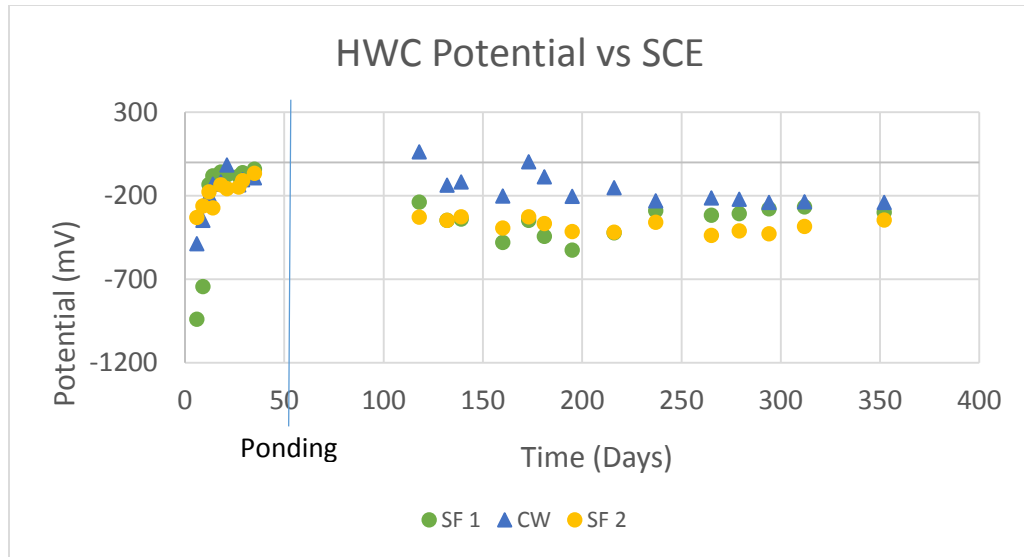


Figure 4.14 Corrosion potential graph of sample HWC

Corrosion potential measurements for the passive chloride migration samples initially mimicked the no chloride control samples. The steel fibers showed initial electrochemical activity in the zinc layer and then quick passivation of the fiber. Sometime after chlorides were introduced, slight dips were measured in some of the corrosion potentials indicating the presence of electrochemical activity. LPR measurements were plotted to gain a sense of the corrosion rate seen in figures 4.15, 4.16, and 4.17.

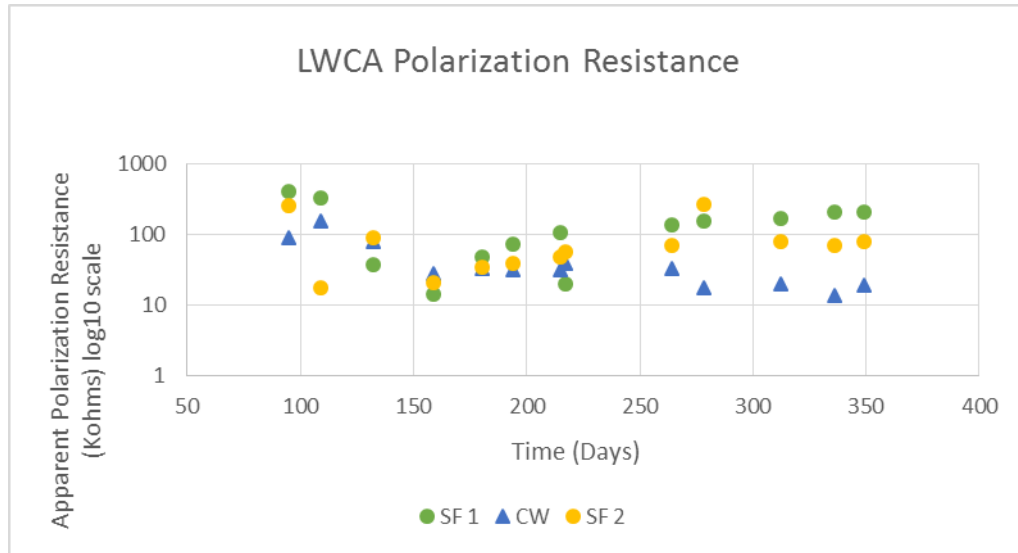


Figure 4.15 Apparent polarization resistance measurements graphed for sample LWCA

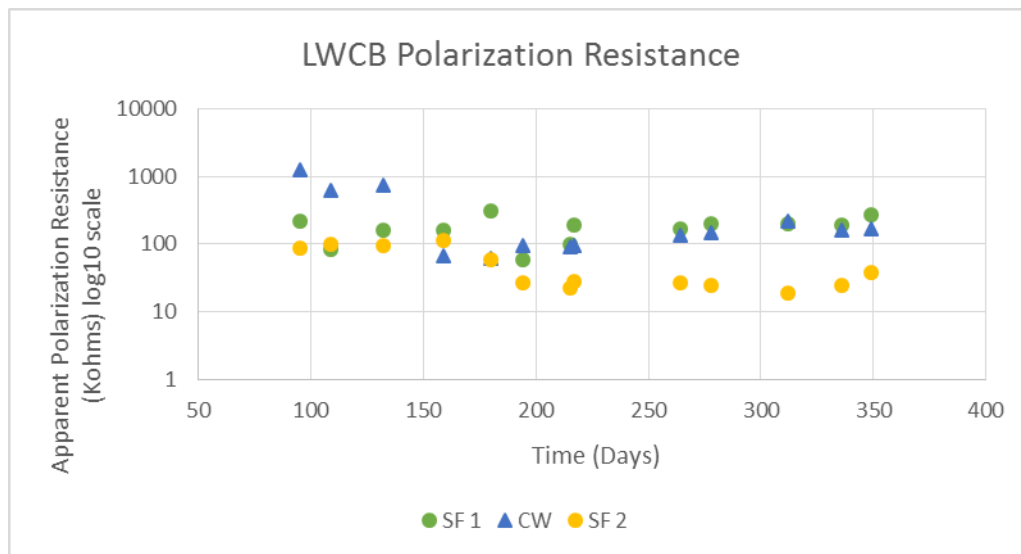


Figure 4.16 Apparent polarization resistance measurements graphed for sample LWCB

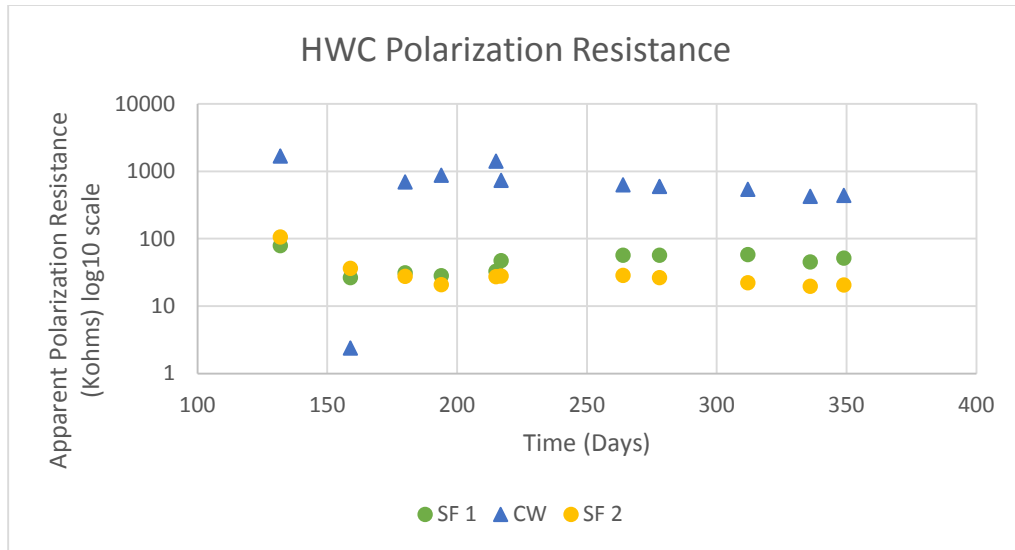


Figure 4.17 Apparent polarization resistance measurements graphed for sample HWC. For the samples LWCA, LWCB, and HWC LPR measurements revealed a very low corrosion rate. Analysis of the LPR measurements concluded that there would be very little or no corrosion found on the fibers during forensic analysis. For steel fibers of this size, an apparent polarization resistance less than 20Kohms is an indication of corrosion onset. Forensic analysis confirmed expectations; fibers were largely unaffected by corrosion initiated by the passive chloride migration.



Figure 4.18 Forensic analysis of fiber LWCA SF1. Photograph by Dietrich Vogel
copyright 2016 by Dietrich Vogel

Most steel fibers extracted from the LWC samples were largely passivated similarly to the no chloride control samples; no red rust was observed. The main difference was a

slightly darker matte grey surface condition seen in figure 4.18 for SF1 in cylinder LWCA when compared to the no chloride control fiber condition.

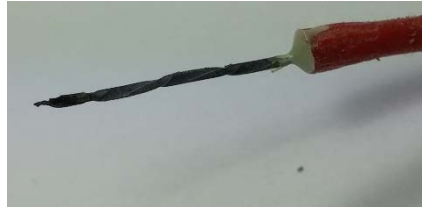


Figure 4.19 Forensic analysis of LWCB SF2 Photograph by Dietrich Vogel copyright 2016 by Dietrich Vogel

The second steel fiber in the LWCB sample was observed to corrode at the instrumentation site seen in figure 4.19. Because the fibers were soldered to the silver plated carbon wires, epoxy was used to isolate the connection from the concrete. For this fiber, the epoxy layer was not uniform and did not cover the entire solder area. The colder connection was exposed to the moisture and chlorides. Over time the fiber cross section was reduced at the crevice created by the solder joint. During extraction, the fiber broke where the cross section was reduced. This was an isolated occurrence of corrosion and occurred due to instrumentation error.



Figure 4.20 Forensic analysis of HWC SF2 Photograph by Dietrich Vogel copyright 2016 by Dietrich Vogel

Despite the presence of chlorides in the concrete around the fibers, the chloride threshold was not passed. Even in the sample HWC where the high water content decreases resistivity and increased the diffusivity of chlorides very minimal tarnishing was observed as seen in figure 4.20 depicting SF2 from cylinder HWC. Corrosion was only initiated in the LWCB SF2 due to instrumentation failure. The overwhelming majority of fibers were observed to have a similar matte grey color to the no chloride control fibers. The similarities to the control fibers indicate that chloride threshold has not been reached or that the zinc layer has initiated corrosion but the steel has not been exposed. Additional pictures from forensic analysis can be found in the appendix of the thesis.

4.3.3 P1, P2 Passive Transport Poke Samples

While the instrumentation of the steel fibers has influenced the electrochemical activity in some fibers; the lack of instrumentation had a greater effect on the fiber surface conditions. Because the fibers were not instrumented, they were protruding from the concrete for measurement purposes. Very soon after the chloride pond was added to the concrete, the ends of the fibers oxidized and the measurements were impossible to make because the fibers would disappear. Spillage of the chloride solution in the reservoir likely reached the exposed fibers causing corrosion. While they were still protruding the corrosion potentials were measured and the values were graphed in figures 4.21 and 4.22.

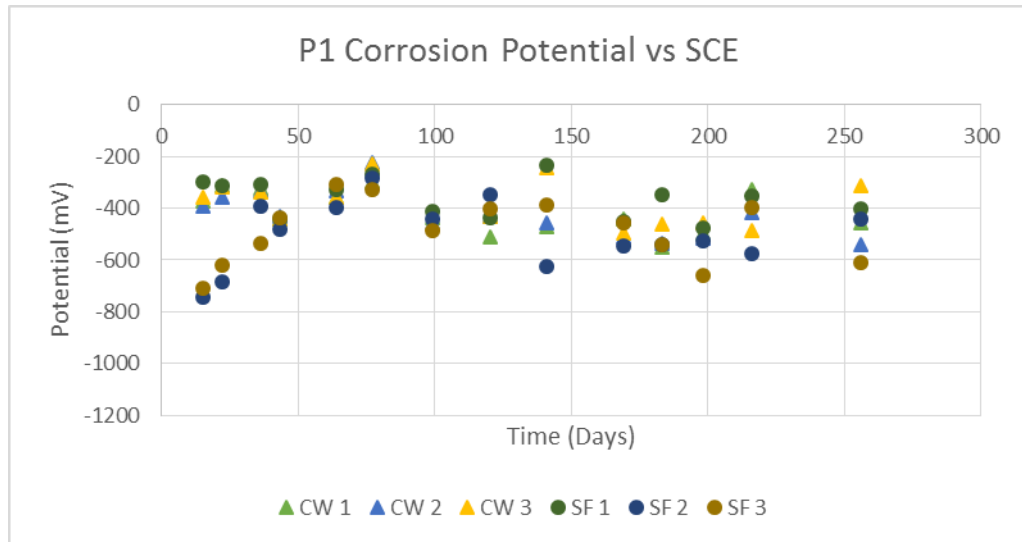


Figure 4.21 Corrosion potential for sample P1

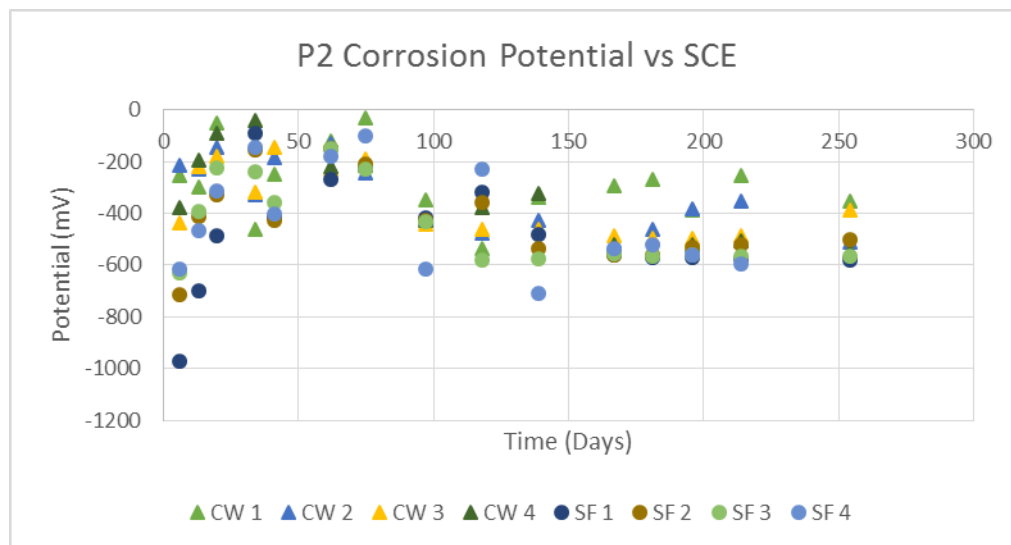


Figure 4.22 Corrosion potential for sample P2

The corrosion potential measurements detail the electrochemical activity in all the fibers poking out of the concrete. Every fiber had a corrosion potential below the ASTM corrosion line of -230 mV vs SCE. Even though the fibers were electrochemically active the LPR measurements suggested low corrosion rates as long as the fibers could be measured. Measurements from LPR tests are pictured in figures 4.23, and 4.24.

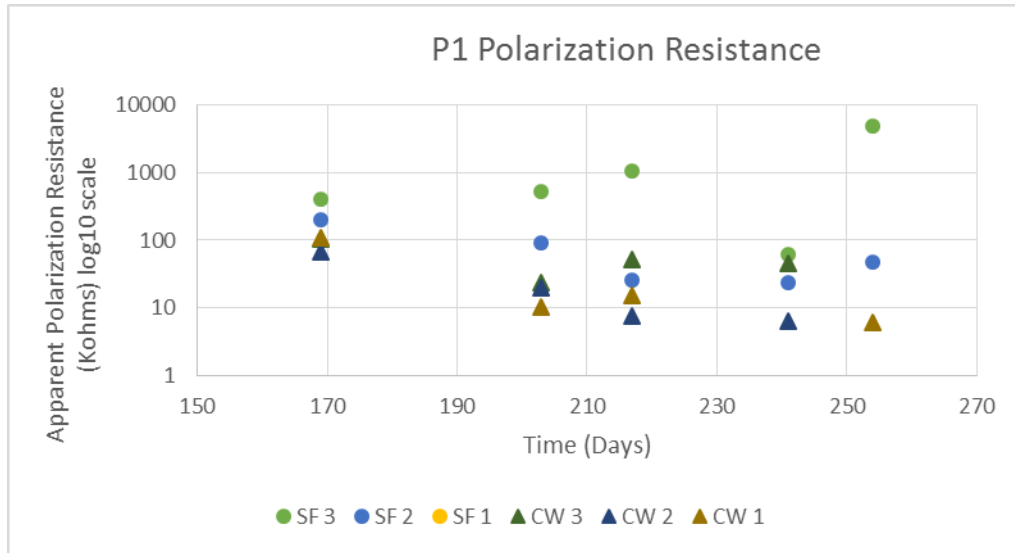


Figure 4.23 Apparent polarization resistance for sample P1

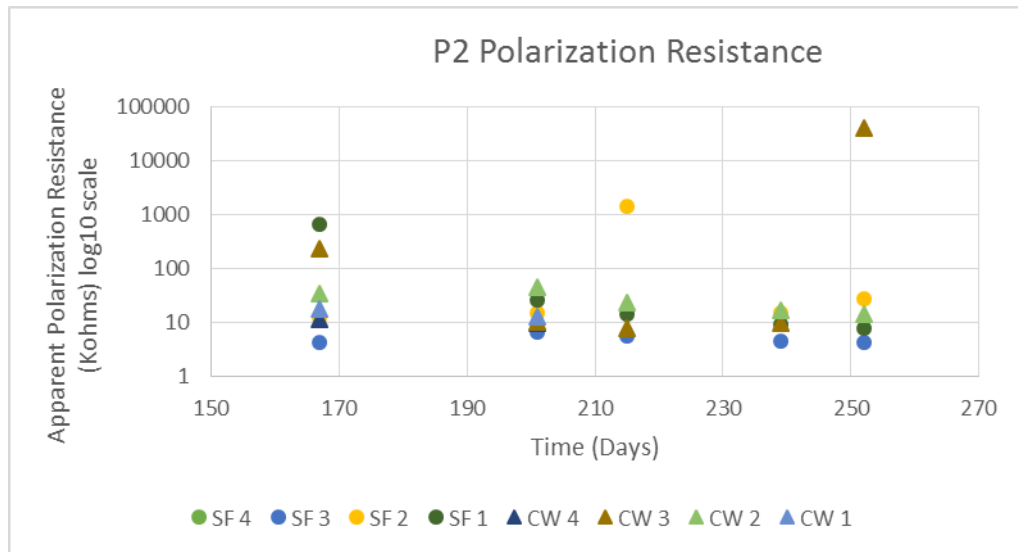


Figure 4.24 Apparent polarization resistance for sample P2

In the poked samples the LPR measurements suggest that the fibers are corroding slowly. The LPR measurements verify that the corrosion was taking place on the surface steel fiber and the majority of the fiber remained unaffected. Forensic analysis confirmed that the corrosion was only spotted on portions of fibers in close proximity to the surface.



Figure 4.25 Carbon steel wires protruding from sample P2 Photograph by Dietrich Vogel copyright 2016 by Dietrich Vogel

Oxidation was present at the surface due to the presence of moisture and oxygen. The fibers would get wet when the container was hydrated with aerosol spray. Corrosion on the fibers seen in figure 4.25 limited the measurements because rust needed to be removed before secure connections could be made with the fibers. The ends of the fibers were cleaned before each measurement with sand paper.



Figure 4.26 Forensic analysis of P1 CW1 Photograph by Dietrich Vogel copyright 2016 by Dietrich Vogel

The carbon steel wires extracted from the poked samples were very comparable; one of which is seen in figure 4.26. The wires were corroded on the side exposed to the

atmosphere and relatively untouched on the side covered by concrete mortar. The chloride threshold was passed on the edges but not under the concrete cover.



Figure 4.27 Forensic analysis of P2 SF 1 depth 40mm Photograph by Dietrich Vogel
copyright 2016 by Dietrich Vogel

One example of a poked steel fiber that exhibited corrosion on the concrete cover side was the SF 1 from sample P2 seen in figure 4.27. Despite the corrosion near the tip of the fiber, there were additional corrosion spots found along the length of the fiber. Despite other zinc electroplated fibers remaining passive, one zinc electroplated steel fiber has clearly passed the chloride threshold. At the last measurement, the fiber SF 1 from sample P2 had the lowest corrosion potential. The corrosion potential was a good indicator for electrochemical activity.



Figure 4.28 Forensic analysis of P2 SF2 depth 30mm Photograph by Dietrich Vogel
copyright 2016 by Dietrich Vogel

Although SF 1 exhibited some uniform corrosion, many of the steel fibers in the poked samples looked similar to figure 4.28. The oxidation products could be observed within

one half of the fiber surface but the majority of the fiber remains free of oxidation. Over time the corrosion would have progressed down the fiber length of the fiber.

4.3.4 MLWC A, MLWC B; Migration Cylinders

Two different attempts were made at modified rapid chloride migration through concrete with instrumented fibers; the first attempt involved cylinders MLWCA and MLWCB. The cylinders each contained 6 zinc electroplated steel fibers instrumented from both sides and 3 carbon steel wires instrumented from one side. The fibers were arranged in a 3x3 matrix pattern where the top row of three fibers were at 10mm cover depth and rows of fibers followed 10 and 20mm directly under. For forensic evaluation, the top 70mm was removed from the rest of the cylinder. A silver nitrate indicator confirmed chlorides to be in the concrete through 70mm cover distance. The corrosion potentials of each fiber was regularly monitored from both sides to ensure valid instrumentation. Corrosion potential measurements of the fibers in the migration cylinders are plotted in figures 4.29 and 4.30.

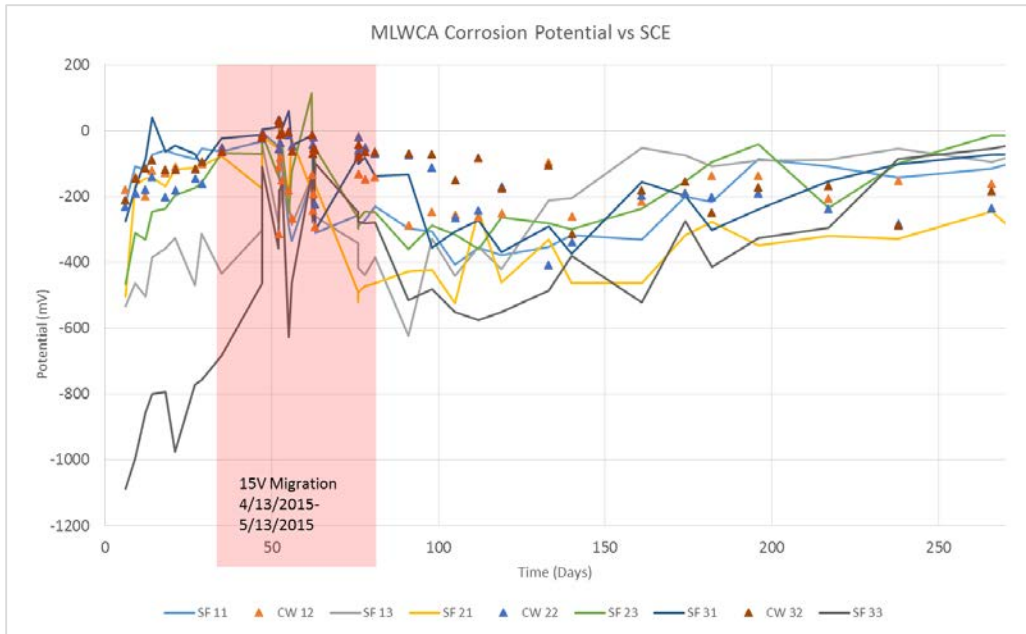


Figure 4.29 Corrosion potential for migration cylinder MLWCA

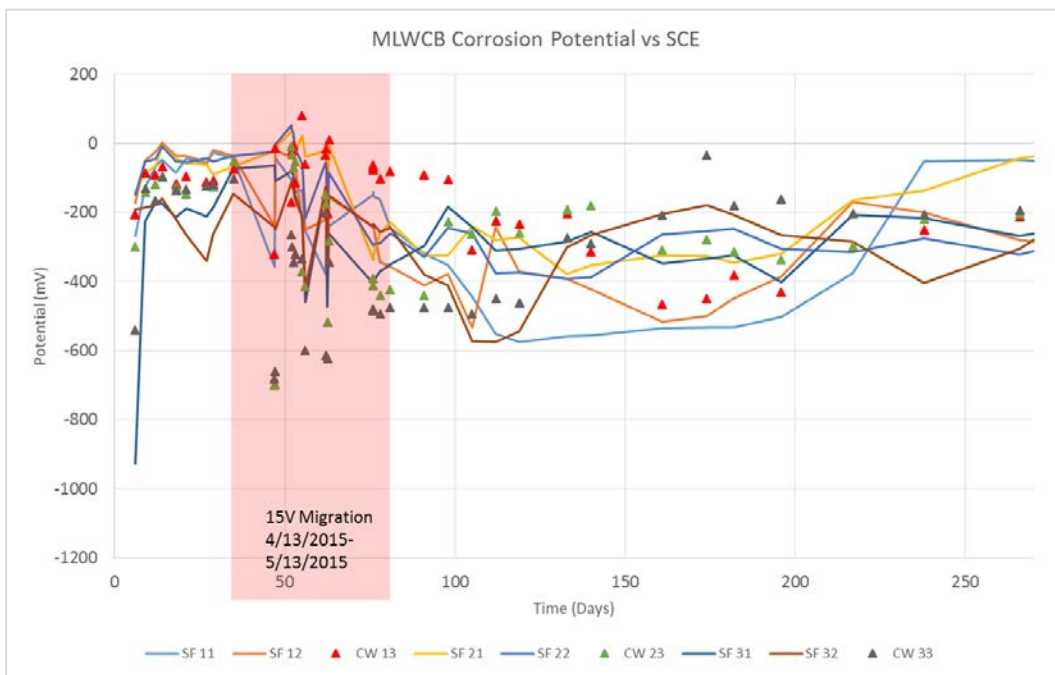


Figure 4.30 Corrosion potential for migration cylinder MLWCB

In large part the corrosion potentials of all the fibers in the migration cylinders indicate minimal electrochemical activity. Despite the confirmed presence of chlorides through

70mm cover distance the corrosion potentials of most fibers were above -200mv Vs SCE before the sample was terminated for analysis. The corrosion potentials indicated a lack of electrochemical activity.

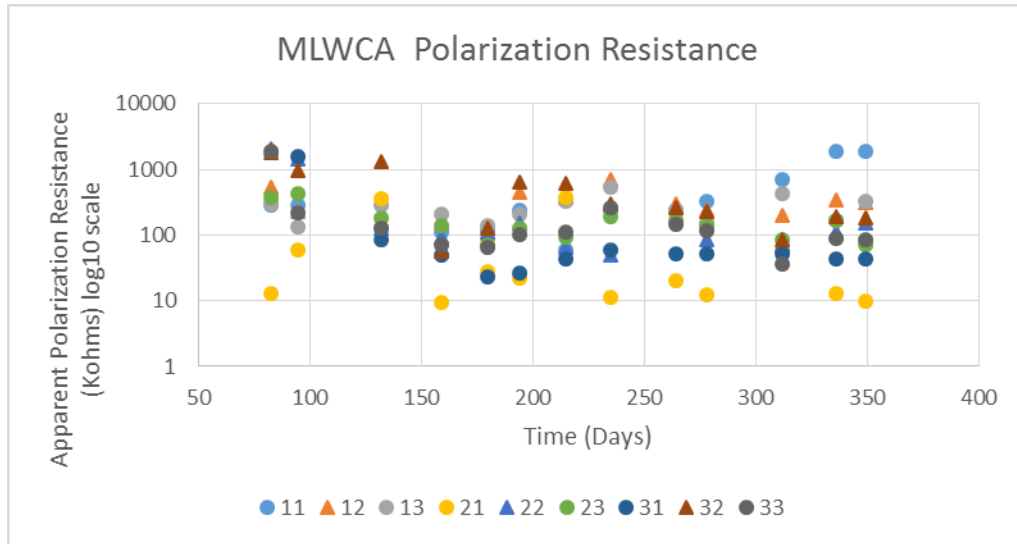


Figure 4.31 Polarization resistance for sample MLWCA

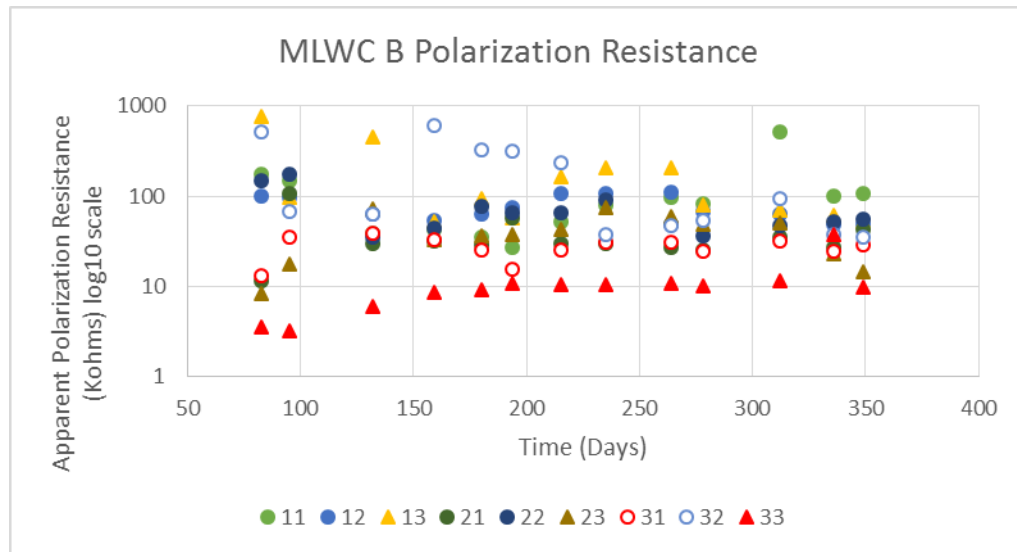


Figure 4.32 Polarization resistance for MLWCB

Like the corrosion potentials, the LPR measurements seen in figures 4.31 and 4.32, indicated high apparent polarization resistances. Many of the fibers at deeper cover

depths show a lower polarization resistance; the electrochemical activity at that depth may not be oxygen dependent. After a year of indoor environmental conditioning the fibers were extracted for analysis. Many of the fibers were free of any rust or tarnish. Despite the confirmed presence of chlorides the fibers remained free of steel corrosion indicated by red rust.



Figure 4.33 Forensic analysis of MLWCA SF 11; cover depth 10mm Photograph by Dietrich Vogel copyright 2016 by Dietrich Vogel

The figure 4.33 is a representative picture for the majority of the 12 steel fibers instrumented in the migration cylinder samples. Fibers embedded in the concrete that were subject to rapid chloride migration exhibited very little to no corrosion. The only tarnish spots on some fibers were at the instrumentation sites believed to be due to crevice corrosion effects.



Figure 4.34 Forensic evaluation of MLWCA SF 13; cover depth 10mm Photograph by Dietrich Vogel copyright 2016 by Dietrich Vogel

Figure 4.34 is an example of a cross section reduction due to fiber instrumentation. The entire solder joint was not coated in epoxy and moisture penetrated the crevice. The electrochemical activity of the cross section reduction was observed as dips in the corrosion potential and LPR measurements but the majority of the zinc coated fiber remained free of corrosion.



Figure 4.35 Forensic evaluation of MLWCB 32; cover depth 30mm Photograph by Dietrich Vogel copyright 2016 by Dietrich Vogel

The most active fiber observed out of the 12 zinc steel fibers tested (figure 4.35) was extracted from the deepest cover depth. Forensic analysis concluded that the fiber was oxidizing but no significant cross section was lost. Oxidation products were black and tarnished the matte grey appearance of the fiber in isolated spots. At the same cover depth, in the same cylinder another steel fiber resembles a no chloride control. Figure 4.36 details a completely passivated steel fiber at the same depth as a steel fiber that was tarnished.



Figure 4.36 Forensic analysis of MLWCB SF 31; cover depth 30mm Photograph by Dietrich Vogel copyright 2016 by Dietrich Vogel

Despite the corrosion onset in another fiber at the same depth some fibers have a higher chloride threshold or lower oxygen concentration thus only a zinc layer may be oxidizing.

4.3.5 B1, B2; Migration Blocks

A second attempt at rapid chloride migration with instrumented fibers involved two blocks. Blocks were constructed to hold fibers at different depths without stacking fibers vertically. There were no metal impediments above the fibers at their various cover depths. The blocks were of different thickness and subject to RMT of different parameters. Chlorides were verified to penetrate both blocks completely indicated by

silver nitrate spray. Over the course of experimentation the blocks were measured for corrosion potential and the values are graphed in figures 4.37 and 4.38.

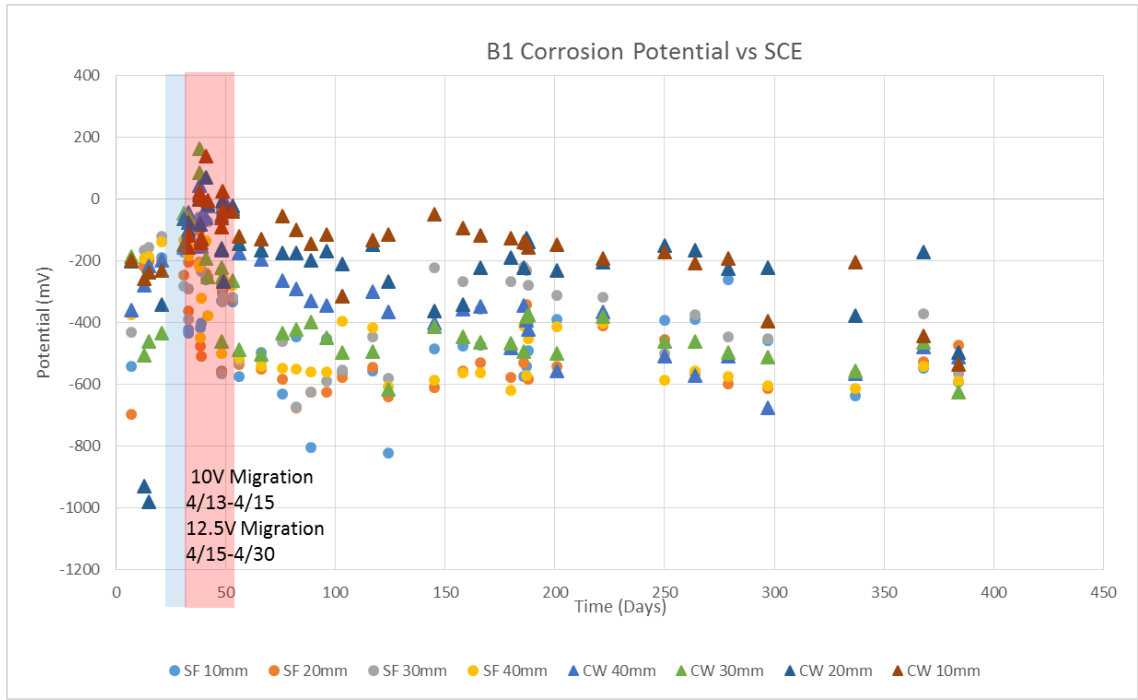


Figure 4.37 Corrosion potential for migration block B1

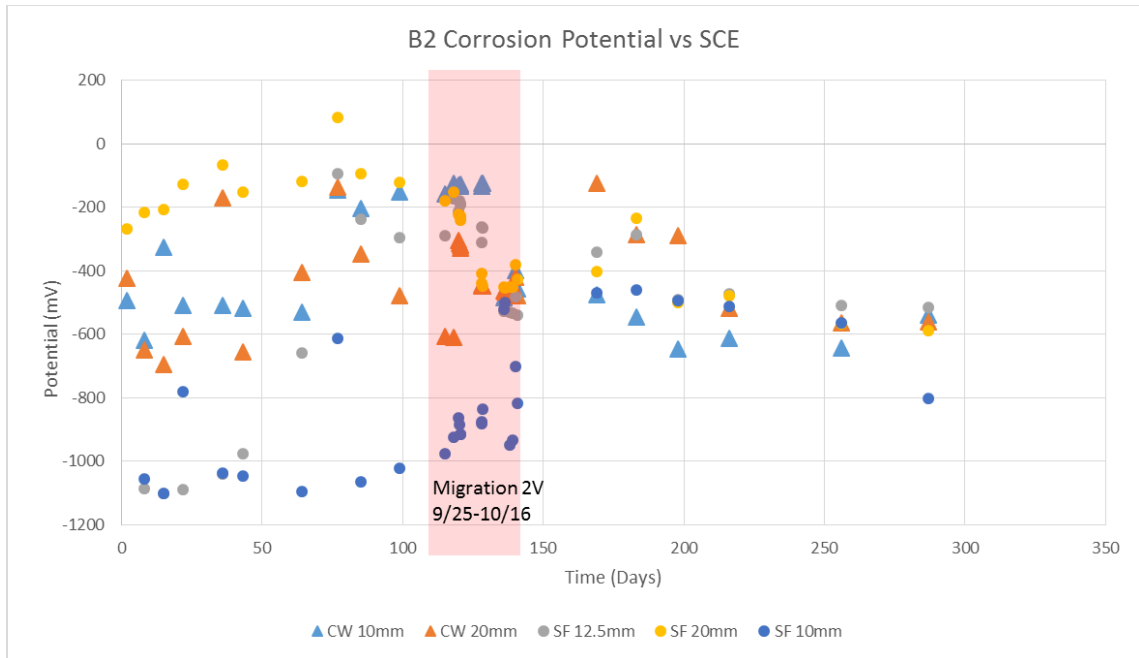


Figure 4.38 Corrosion potential for block B2

The corrosion potentials for all of the fibers indicate the presence of corrosion at the time of sample termination; the potentials were measured to be less than -230 vs. SCE. At the last set of measurements, the potentials of all fibers were below -400 vs SCE. Over time the fibers exhibited different behaviors from the migration cylinders. After the chloride migration, the corrosion potentials in the zinc electroplated steel fibers continued to decrease over time. The measurements of the apparent polarization resistance were examined to confirm the electrochemical activity measured with the corrosion potentials.

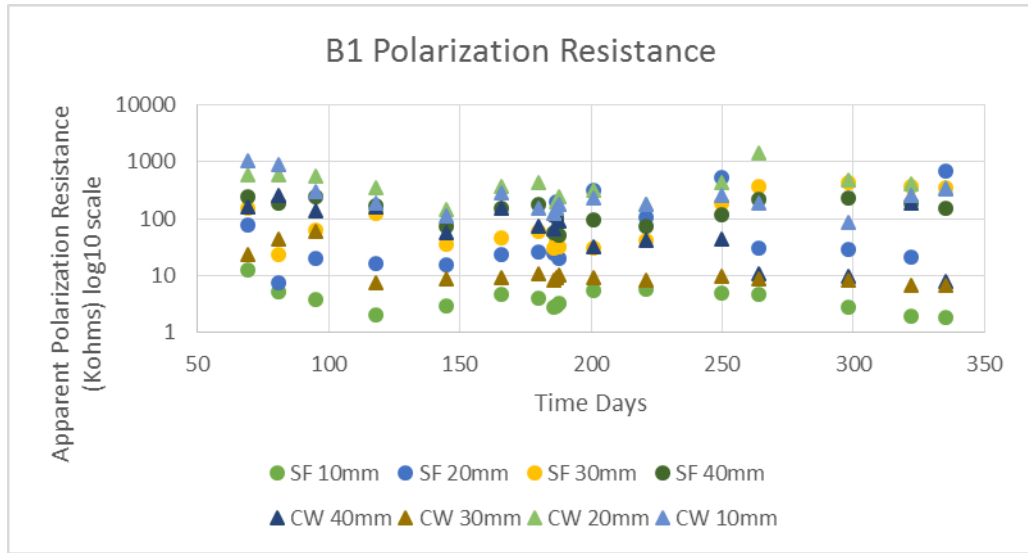


Figure 4.39 Polarization resistance for migration block B1

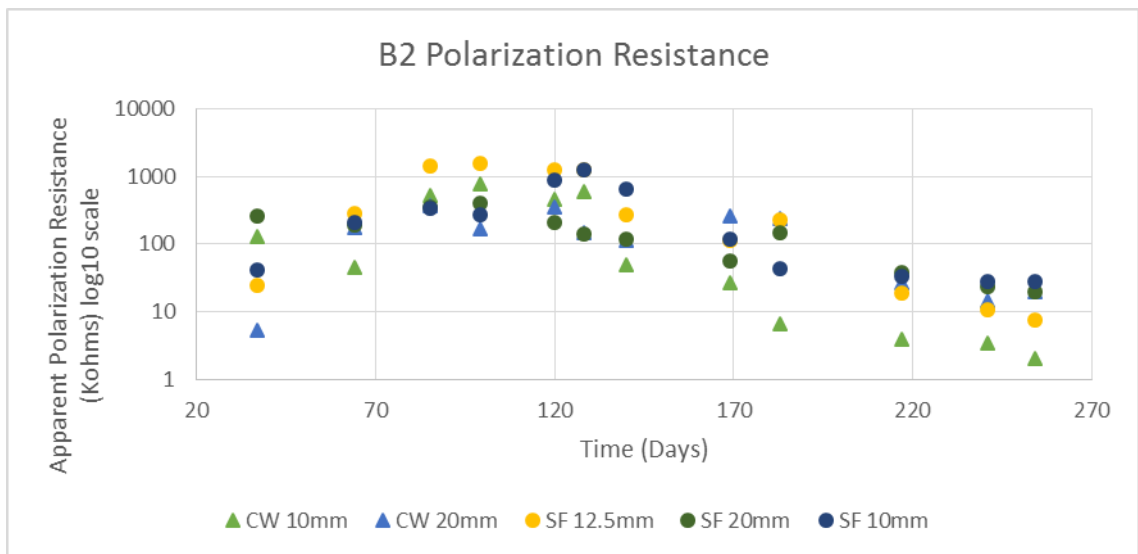


Figure 4.40 Polarization resistance for migration block B2

Graphs of the polarization resistance seen in figures 4.39 and 4.40 confirm the trend that was observed in the corrosion potential measurements. After the migration period, many of the zinc electroplated steel fibers continued to decrease in apparent polarization resistance. The polarization resistance of fibers in block B1 was measured over a large

range of values throughout experimentation. The spread in values indicate a large range in electrochemical activity within the same sample.



Figure 4.41 Forensic analysis of B1 SF1; cover depth 10mm Photograph by Dietrich Vogel copyright 2016 by Dietrich Vogel

Many of the steel fibers extracted from the block samples showed red rust stains. In figure 4.41, a steel fiber at the most shallow depth did not observe any red oxidation products but rather an overall color change. The matte grey observed in the no chloride control samples was not observed, the fibers in the blocks were seen to have turned a darker color. The darkest colors could be observed around the ends of the fibers. Loss in cross section was not measured or observed.



Figure 4.42 Forensic analysis of B1 SF2; cover depth 20mm Photograph by Dietrich Vogel copyright 2016 by Dietrich Vogel

The steel fiber at the 20mm cover depth seen in figure 4.42 consistently had one of the lowest corrosion potentials. It is no surprise that the fiber observed the most corrosion. Nearly 1 cm is missing from the fiber and its cross section is diminished near the center. A portion of the fiber was completely oxidized; the oxidized portion of the fiber crumbled to dust when separated from the mortar. Because a portion of the fiber was missing, the most recent high apparent polarization resistance measurement was due to a sudden decrease in measured fiber cross sectional area.



Figure 4.43 Forensic analysis of B1 SF3; cover depth 30mm Photograph by Dietrich Vogel copyright 2016 by Dietrich Vogel

Slightly further from the surface the corrosion in the steel fiber is observed to cover less of the fiber surface area seen in figure 4.43. Either the individual fiber has a higher chloride threshold than its neighbor or the cover distance restricted oxygen flow differently from other fibers. Despite the presence of oxidation products, a loss in cross section was not observed or measured.



Figure 4.44 Forensic analysis of B1 SF4; cover depth 40mm Photograph by Dietrich Vogel copyright 2016 by Dietrich Vogel

The deepest steel fiber of the block samples seen in figure 4.44 observed some oxidation but no cross section loss. Oxidation that was observed was found on the edges of the helix twist and near the fiber ends where crevice effects from the wire came into play.



Figure 4.45 Forensic analysis of B2 SF 3; cover depth 12.5mm Photograph by Dietrich Vogel copyright 2016 by Dietrich Vogel

Fibers in the sample B2 were subject to a smaller block thickness. Fibers were observed to have very minimal oxidation that was localized near the ends. The fiber in the center of the block (figure 4.45) was observed to have the same matte grey as the no chloride control samples. For the fiber pictured in figure 4.45, the chloride threshold was likely not reached.

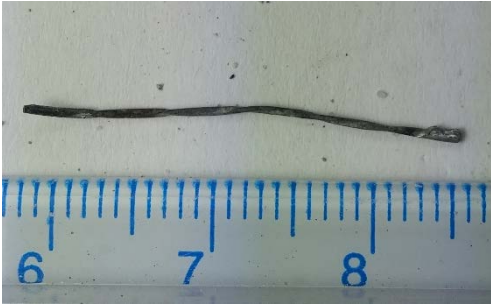


Figure 4.46 Forensic analysis of B2 SF 5; cover depth 10mm Photograph by Dietrich Vogel copyright 2016 by Dietrich Vogel

At a lower cover depth in sample B2, SF5 seen in figure 4.46 was found to have slightly more oxidation. Corrosion potential measurements predicted that there would be more evidence of electrochemical activity. A combination of decreased cover depth and the presence of chlorides allowed the fiber to pass its chloride threshold to initiate corrosion. Despite some oxidation, the cross section of the fiber was not significantly diminished.

4.3.6 Instrumented samples cast with chlorides C4, C7, C8

Concrete cylinders were cast with salt solution as the water used to mix the cementitious materials. Casting the samples with chlorides was a simple bypass for chloride deposition. Because the chlorides were already present in the concrete, the chloride threshold of each fiber only depended on the presence of oxygen and moisture. The corrosion potential measurements were an indication of electrochemical activity and their graphs are presented in figures 4.47, 4.48, and 4.49.

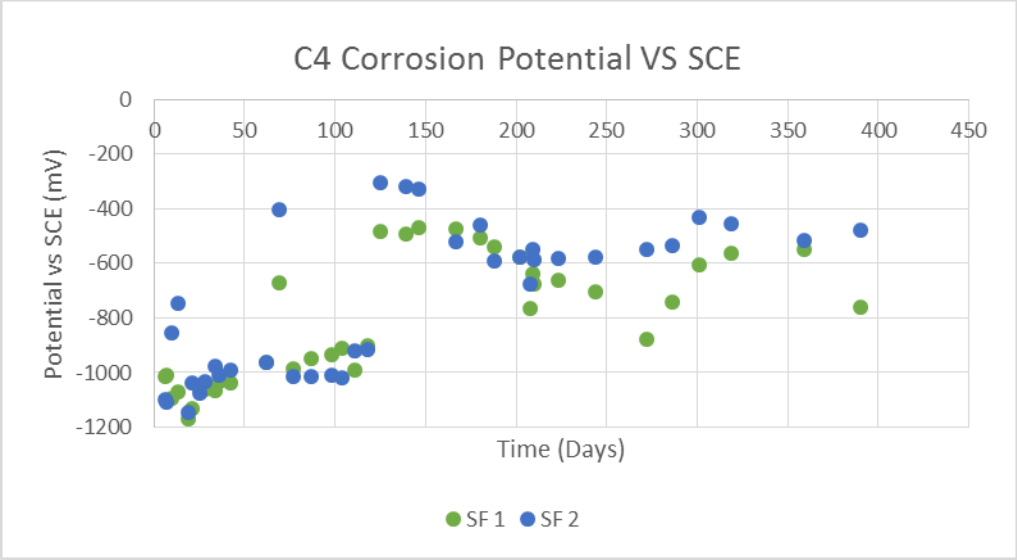


Figure 4.47 Corrosion potential of chloride cylinder C4

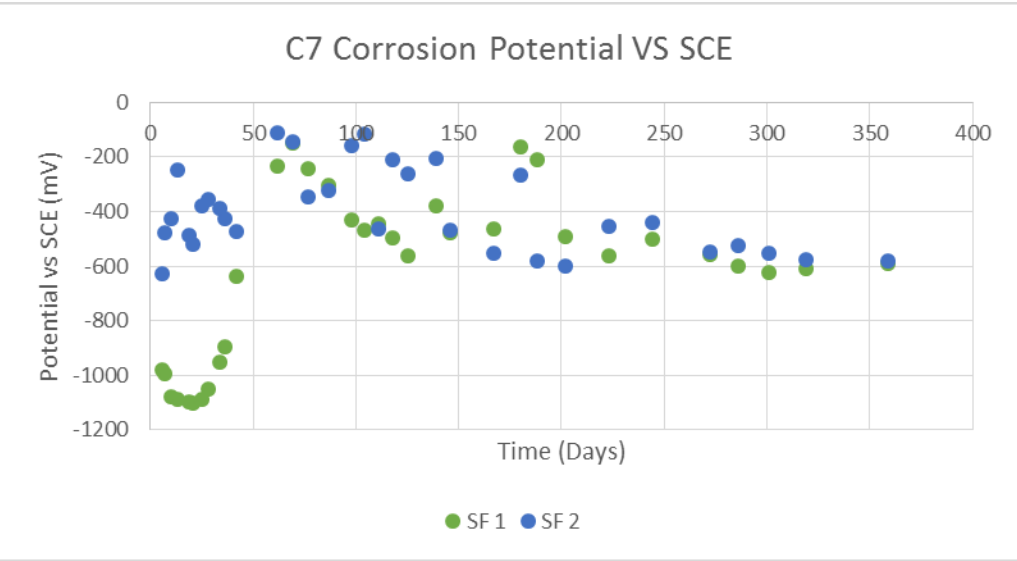


Figure 4.48 Corrosion potential of chloride cylinder C7

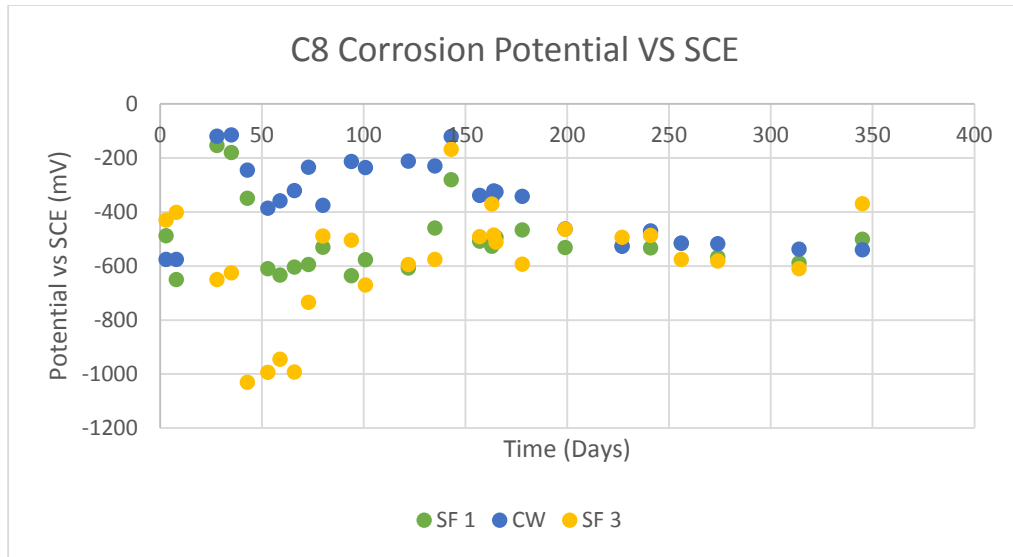


Figure 4.49 Corrosion potential of chloride cylinder C8

Steel fiber passivation was a slow and uncertain process in the samples cast with chlorides. The zinc electro coat was not able to form a passive layer around all of the steel fiber samples. Zinc was seen to be active at corrosion potentials below -1000mV; for sample C4 the zinc layer was active for over 100 days. Despite the thickness of the zinc electro coat, the chloride concentration was high enough to dissolve or not allow the zinc to form a protective oxide layer. Although the passive layer was being dissolved, the steel fiber corrosion rates were very small. LPR measurements confirmed the high polarization resistance for the steel fibers and their graphs are presented in figures 4.50, 4.51, and 4.52.

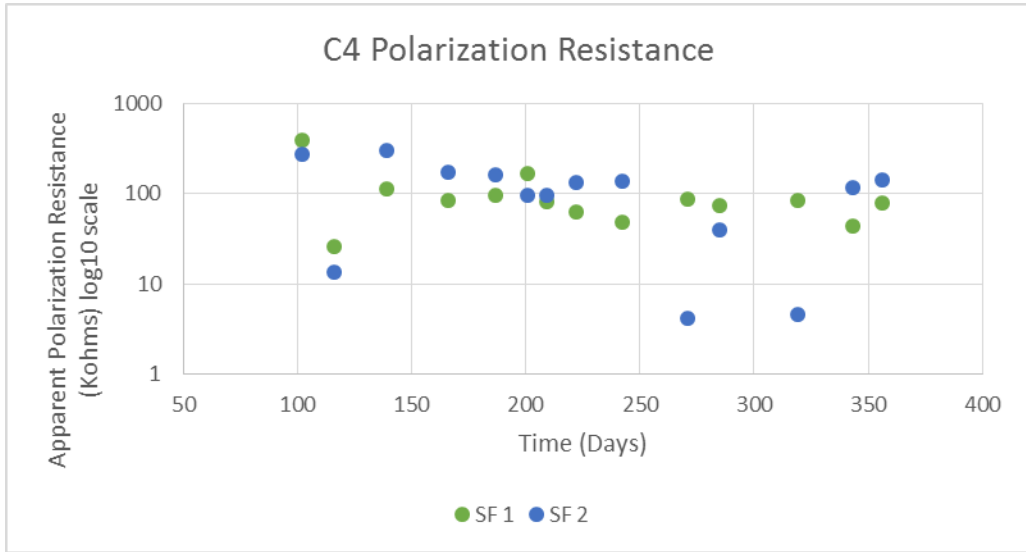


Figure 4.50 Apparent polarizations resistance for chloride cylinder C4

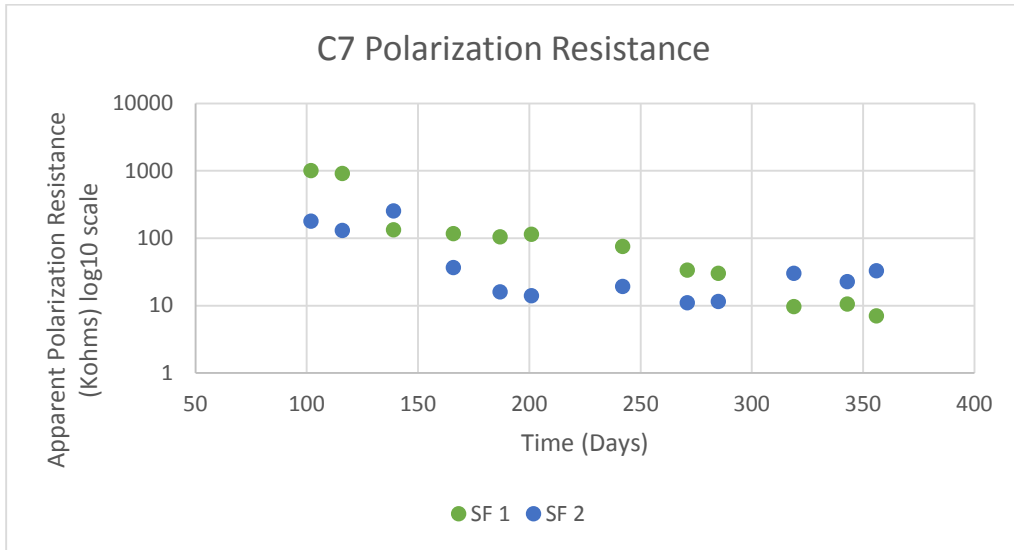


Figure 4.51 Apparent polarizations resistance for chloride cylinder C7

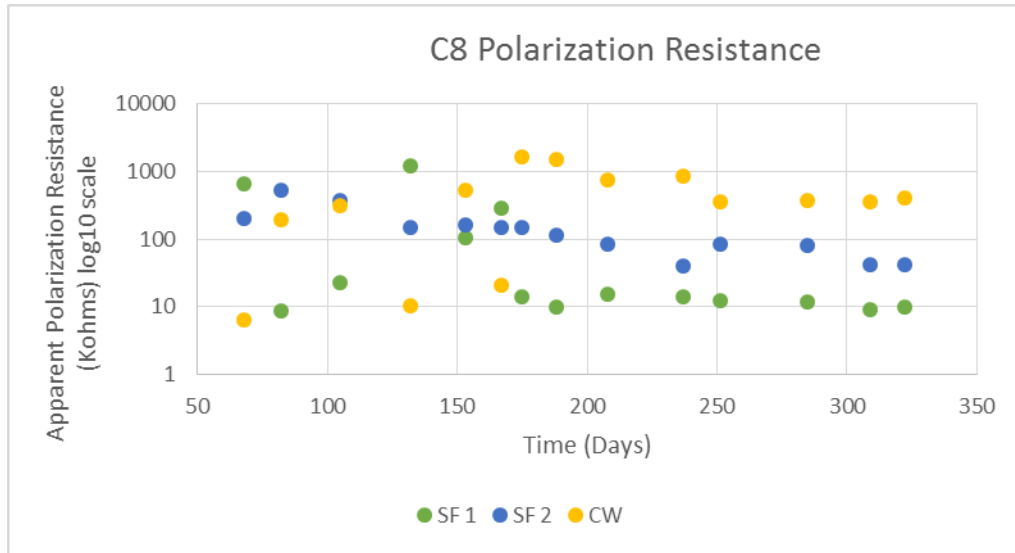


Figure 4.52 Apparent polarizations resistance for chloride cylinder C8

According to the corrosion potential curves, all fibers contained in the samples cast with chlorides should observe some degree of corrosion. Corrosion potential detailed that corrosion was initiated in the fibers from the time of casting. Despite the presence of chlorides and the onset of corrosion; the apparent polarization resistance measurements reveal a modest corrosion rate. Entering the fiber forensic analysis, corrosion of the steel fibers was expected but the amount of corrosion onset was uncertain.



Figure 4.53 Forensic analysis of sample C4 SF 1 on top, SF 2 on the bottom Photograph by Dietrich Vogel copyright 2016 by Dietrich Vogel

Corrosion propagation of the steel fibers was observed for the instrumented fibers in sample C4. Despite the low corrosion potential very little oxidation was observed. The fibers were discolored from the no chloride control matte grey but there was no observable significant loss in cross section as seen in figure 4.53. Parts of the fiber were tarnished with black specs and the mortar was difficult to remove from the fiber. LPR measurements proved true; the fiber exhibited some electrochemical activity but it progressed modestly.



Figure 4.54 Forensic analysis of chloride cylinder C7 pictured left SF 1 pictured right SF2 Photograph by Dietrich Vogel copyright 2016 by Dietrich Vogel

While the instrumented fibers in the concrete cylinder C4 did not exhibit clear signs of oxidation, fibers in sample C7 were observed to have red oxidation spots on both fibers seen in figure 4.54. Oxidation products on the fibers indicated that the chloride threshold was passed. Corrosion was initiated on both fibers but the corrosion did not propagate long enough for significant cross section loss to be observed. Although the chloride content was less in sample C7 than sample C4, the fibers exhibited more corrosion. Because the chloride threshold depends on oxygen availability, the smaller cover distance in sample C7 could explain the increase in fiber oxidation.



Figure 4.55 Forensic analysis of sample C8 SF1 Photograph by Dietrich Vogel copyright 2016 by Dietrich Vogel

After analyzing the electrochemical measurements, the most activity was observed in the SF 1 from sample C8 seen in figure 4.55. One end of the fiber remained completely corrosion free while the other end showed significant cross section loss. Crevice corrosion between the fiber and the instrumentation connection caused the electrochemical activity and the cross section loss. With the exception of the poorly instrumented end, the majority of SF 1 from cylinder C8 remained the matte grey observed in the no chloride control sample except for the area a few millimeters from the end.



Figure 4.56 Forensic analysis of C8 SF 2 Photograph by Dietrich Vogel copyright 2016 by Dietrich Vogel

SF 1 from sample C8 was observed to have corrosion at an instrumented end; SF2 seen in figure 4.56 from sample C8 was observed to have oxidation products near the

middle of the fiber. Oxidation products without the influence of a crevice was the result of a zinc oxide layer breakdown, consumption of the remaining zinc until steel exposure, and an indication that the chloride threshold was reached. The chloride content of the cylinder C8 was the lower boundary of the chloride threshold.

4.4 Conclusions

- The chloride threshold was reached for some fibers at cover depths deeper than fibers that have not reached the chloride threshold or that still retain a zinc coating
- The chloride threshold does not depend on chlorides alone; oxygen and moisture play an important role in corrosion initiation
- The corrosion potential of corroding zinc on the steel fibers is between -1000 and -1200mV
- The mixed corrosion potential of steel fibers occurs between -350mV and -600mV
- When a fiber has a significant loss of cross section the apparent polarization resistance increases drastically

5 EXPERIMENTAL PROGRAM: CHLORIDE THRESHOLD DETERMINATION FOR ZINC ELECTROPLATED STEEL FIBERS IMMERSED IN SIMULATED PORE SOLUTION

5.1 Introduction

Corrosion activation of the steel fibers embedded in concrete was observed using corrosion potential and LPR measurements. Once a certain combination of chloride concentrations, oxygen and moisture have reached the fiber; corrosion can initiate and propagate. Incrementally adding chlorides to concrete is a difficult process. A fourth experiment was developed to observe fiber behavior over increasing chloride concentrations. Simulated concrete pore solution tests consisted of instrumented fibers immersed in high pH solutions. The experiment was modeled after a study performed by Raupach and Dauberschmidt on the critical chloride content of steel wires. Expected values for chloride thresholds found for steel without a zinc coating by Raupach and Dauberschmidt were 15 mmol/l for 12.6 pH solution and under 500 mmol/l for 13.3pH solution. Increasing the pH was found to increase the chloride threshold. The objective of the simulated pore solution testing was to find the chloride threshold for a zinc electroplated steel fiber in 12.6 pH, 13.3pH solutions.

Each sample included carbon steel wires and zinc electroplated steel fibers. The fibers were positioned around the reference electrode and held in place by the container lid. Also imbedded in the lid and immersed in the solution was a titanium mix metal oxide mesh used as a counter electrode for LPR measurements. The aqueous tests were

structured to first develop a passive layer around the instrumented fiber. The passive layer was indicated by consistently relatively positive potential measurements, high polarization resistance, and a small current range on the LPR measurements. Then, slowly the chlorides were introduced. Throughout the experiment the potentials were monitored daily and the LPR was measured before every chloride addition. Chlorides were added until a breakdown of the passive layer was measured and corrosion was observed. Indications of passive layer breakdown were decaying or dipping fiber potential measurements; and large current ranges for LPR measurements.

5.2 Experimental Procedure

Three separate containers stored separate groups of fibers in 12.6 pH, 13.3 pH, and mortar coated fibers in 13.3pH solutions.

5.2.1 A1- Bare Fibers; pH 12.6

Sample A1 consisted of four bare zinc electroplated steel fibers and two carbon steel wires. The fibers were prepared by first soldering them to a 4 inch piece of silver coated copper wire. Then the connection was epoxied to ensure a solid connection and to protect the solder joint from the environment. After the epoxy, shrink wrap was added to the connection to keep water out of that area. A 1 liter container was prepared with 8 wire sized holes in the lid and a center hole for a SCE reference electrode. The sample was initiated on 10/06/2015 in a 12.6pH solution. The solution was made up of 2 g/L CaOH_2 and deionized water. For preparation, 1 g of calcium hydroxide was measured and mixed with 500mL of DI water. Then instrumented fibers were threaded through the holes in the lid and the fibers were immersed in the solution. After every measurement, the contents of the container were agitated to ensure a homogeneous concrete pore

simulation solution. The fiber potential with respect to a saturated calomel reference electrode was measured regularly and linear polarization resistance measurements were conducted before each chloride addition.

The chlorides were added to the 12.6 pH solution in spaced out intervals. The chlorides were added incrementally so that the solution contained the following: first 8 milli-molar, then 10, 20, 30 and lastly the critical content should be reached by 40 milli-molar. The additions of salt were as follows: 0.4675g, 0.1169g, 0.5844g, 0.5844g, 0.5844g. After the additions were confirmed to surpass the chloride threshold, fibers were removed. Fibers were visually inspected and analyzed for degree of corrosion.

5.2.2 A2- Bare Fibers; pH 13.3

Sample A2 consisted of four bare zinc electroplated steel fibers and three carbon steel wires. The fibers were prepared by first soldering them to a 4 inch piece of silver coated copper wire. Then the connection was epoxied to ensure a solid connection and to protect the solder joint from the environment. After the epoxy, shrink wrap was added to the connection to keep water out of area. A 1 liter container was prepared with 8 wire sized holes in the lid and a center hole for a SCE reference electrode. The sample was initiated on 10/15/2015 in a 13.3 pH solution. The solution was made up of 3.7 g/L sodium hydroxide, 10.5 g/L potassium hydroxide, and 2 g/L calcium hydroxide. A 500mL solution was prepared and the fibers were equipped in the prepared lid; then the experiment was initiated when the fibers entered the solution. The corrosion potential of each fiber were measured daily and the LPR measurements before each chloride addition. The chlorides were be added incrementally so that the solution contains the following: first 40 milli-molar, then 100, 250, lastly the critical content should have been reached by

500 mili-molar. Further additions were needed through 600, 700 and 800mmol/l. The critical chloride content was much higher in higher alkaline. Once the concentration was passed, the fibers were removed and examined forensically.

5.2.3 A3- 13.3 pH mortar coating on fibers

Sample A3 consisted of three zinc electroplated steel fibers and three carbon wires covered in mortar. The fibers were prepared by first soldering them to a 4 inch piece of silver coated copper wire. Then the connection was epoxied to ensure a solid connection and to protect the solder joint from the environment. After the epoxy, shrink wrap was added to the connection to keep water out of area. The shrink wrap on these fibers was intentionally left long to cover the fiber. Before the wrap was heated, a mortar paste was mixed and packed around the fiber in the shrink wrap. The mortar paste was made with 10g of cement, 10g of sand, 2g fly ash, and 10mL of tap water. The resulting instrumented fibers were left to dry for a weekend and then the wrap was removed. A one liter container was prepared with 8 wire sized holes in the lid and a center hole for a SCE reference electrode. The sample was initiated on 10/26/2015 in a 13.3 pH solution. The solution was made up of 3.7 g/L sodium hydroxide, 10.5 g/L potassium hydroxide, and 2 g/L calcium hydroxide. A 500mL solution was prepared and the fibers were equipped in the prepared lid; then the experiment was initiated when the fibers entered the solution. The potential of each fiber, measured daily and the LPR measurements before each chloride addition. The chlorides were be added incrementally so that the solution contains the following: first 40 mili-molar, then 100, 250, lastly the critical content was reached by 500 mili-molar. Then the fibers were extracted for forensic analysis.

5.3 Results and Discussion

Simulated pore solution samples were designed to pinpoint the chloride threshold of the zinc electroplated steel fibers. Each sample was subject to incremental chloride additions until the fibers exhibited electrochemical activity in the corrosion potential and the apparent polarization resistance. For the pH 12.6 fibers, the critical chloride concentration expected to break down the passive layer was 0.015 moles per liter. In the 13.3 pH samples, 0.5 moles per liter was expected as the chloride threshold. The expectations were based off of research completed by Raupach and Dauberschmidt on similar diameter carbon steel fibers in simulated pore solution. Fibers in the lower pH simulated pore solution were expected to have a lower chloride threshold than higher pH solutions. An abundance of hydroxide ions stimulate the insolubility of the steel fiber protective layer; less hydroxide ions more soluble passive layer. In high pH, the zinc is very electrochemically active. Electrochemical activity was observed through corrosion potential and LPR measurements. Passing the chloride threshold was determined as a sudden drop in corrosion potential or a sudden decrease in apparent polarization resistance.

5.3.1 A1- Bare Fibers; pH 12.6

Instrumented fibers placed in simulated pore solution were regularly monitored for electrochemical activity. Because the chloride threshold depended on oxygen and moisture, corrosion could have initiated at any time between chloride additions. Corrosion potential measurements detailed the chloride additions and the sharp drop in fiber potential after the chloride threshold was reached.

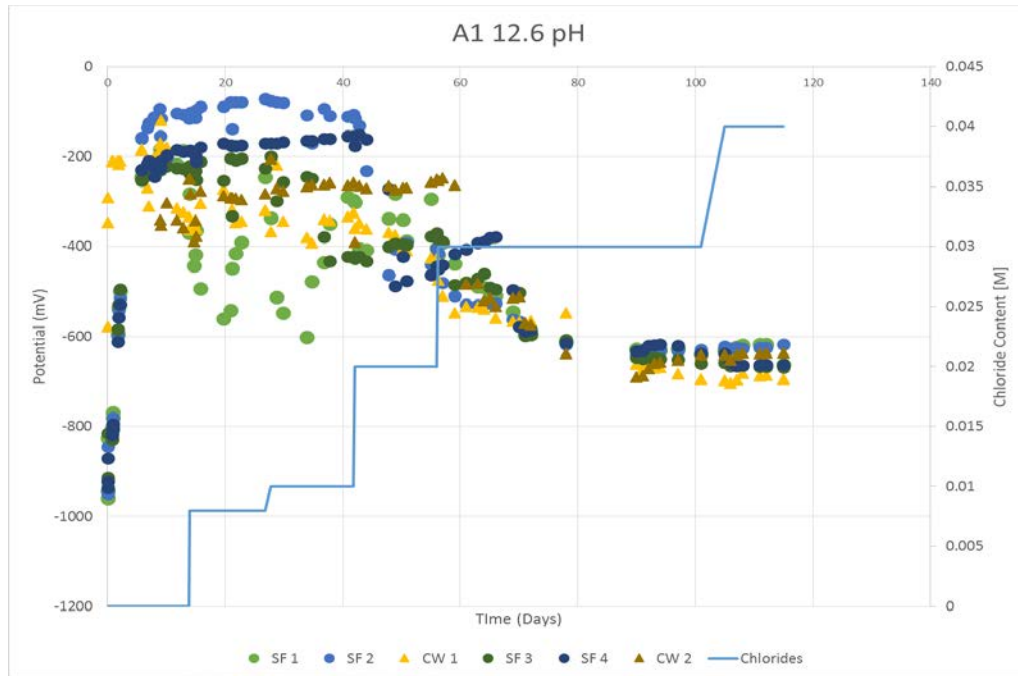


Figure 5.1 Corrosion potential for simulated pore solution A1

At pH 12.6, the first fiber to indicate electrochemical activity was SF 1 after the first chloride addition of 0.008 moles per liter or 8 mmolar. It was not until the chloride concentration reached 20mmolar that the other steel fibers observed a drop in potential. In figure 5.1, the steel fibers were all shown to be electrochemically active when the chloride concentration passed 0.02 moles per liter. After the chloride threshold was surpassed, the fibers corrosion potential settled between -600 and -700mV.

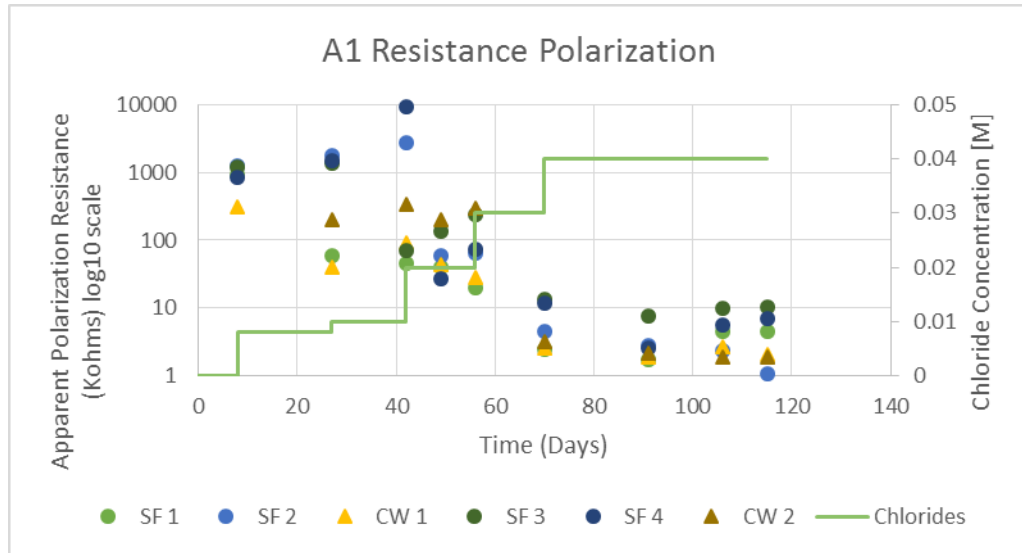


Figure 5.2 Apparent polarization resistance measurements for simulated pore solution sample A1

The graph of apparent polarization resistance in figure 5.2 confirmed the chloride threshold found using the corrosion potential. After the addition of chlorides to change the concentration to 20mmolar, the apparent polarization resistance values dropped and remained low. Once the LPR measurements confirmed the presence of electrochemical activity, the sample was terminated and the fibers extracted.



Figure 5.3 Forensic analysis for A1 SF2 Photograph by Dietrich Vogel copyright 2016 by Dietrich Vogel

Figure 5.3 depicts the extracted zinc electroplated steel fiber SF 2. The fiber was uniformly corroded and the cross section was diminished throughout the length of the fiber. The cross section loss has shortened the fiber and oxidation products were seen on the entirety of the fiber surface. The chloride threshold was passed at 20mmolar and the fiber remained active until extraction.



Figure 5.4 Forensic analysis for A1 SF 5 Photograph by Dietrich Vogel copyright 2016 by Dietrich Vogel

The zinc electroplated steel fiber seen in figure 5.4 was more representative of the other three fibers conditions. Three of the four steel fibers in the specimen were corroded near the hilt of the fiber. Corrosion started near the instrumentation connection between the fiber and the instrumentation wire possibly due to the presence of crevices. Because the epoxy or shrink wrap did not completely cover the connection, corrosion was able to start around the crevices between materials. Despite the localized corrosion, the majority of the fiber remained corrosion free. Although the chloride threshold was passed, the fibers did not undergo uniform corrosion; rather suffered from local crevice attacks and local corrosion on the few millimeters below the connection.

5.3.2 A2- Bare Fibers; pH 13.3

Concrete pH is known to be near 13.3; a higher pH simulated pore solution was a closer comparison to the concrete environment. An abundance of hydroxide ions were

expected to passivate the carbon steel wire but keep the zinc electroplated steel fibers active. It appears that the zinc oxide layer observed in the concrete cast samples remained at the surface of the fibers immersed in simulated pore solution. In comparison to the 12.6 pH solution (15mmolar), the chloride threshold was expected to be near 500mmolar in the higher pH solution. A 30g salt addition to one half liter was equivalent to a 500mmolar solution. The chlorides were added incrementally for over 180 days.

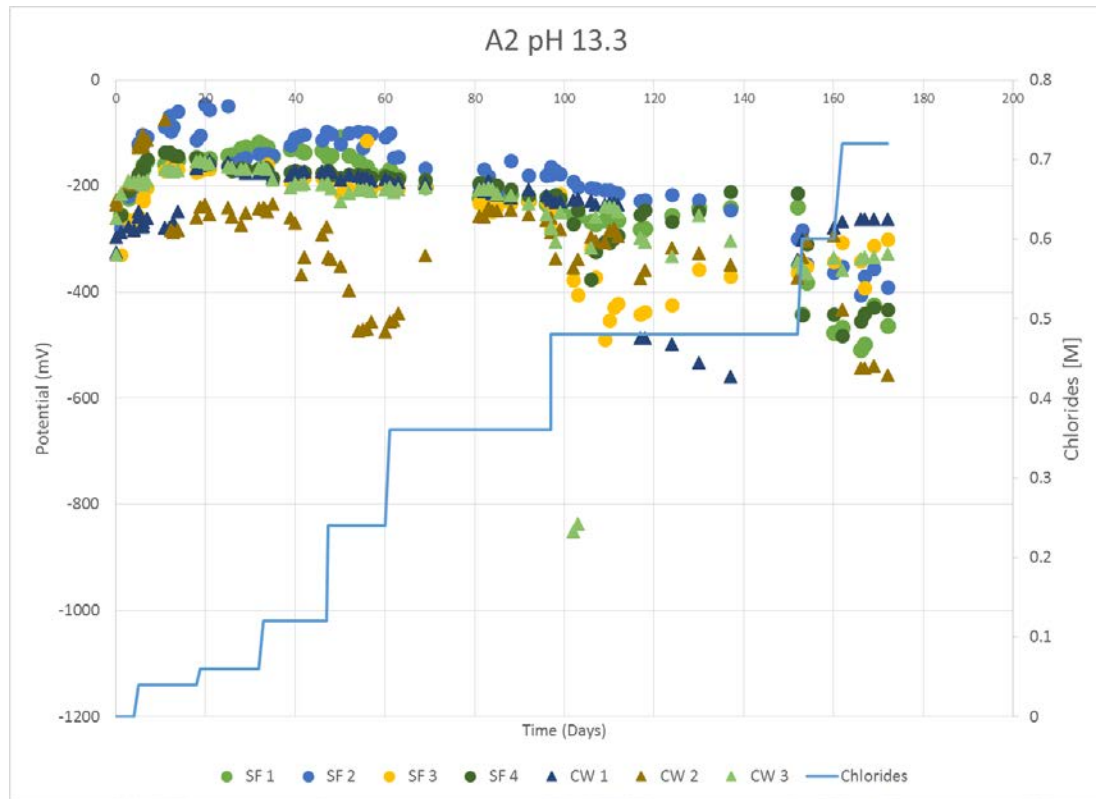


Figure 5.5 Corrosion potential for simulated pore solution A2

Soon after day 100 at a chloride concentration of 480mmolar, the first steel fiber was measured to have a corrosion potential dip; an indicator of corrosion. While one fiber (figure 5.5 SF 3) showed electrochemical activity other three steel fibers remained passive until day 160 where the fiber potentials begin to tail off and not drop suddenly.

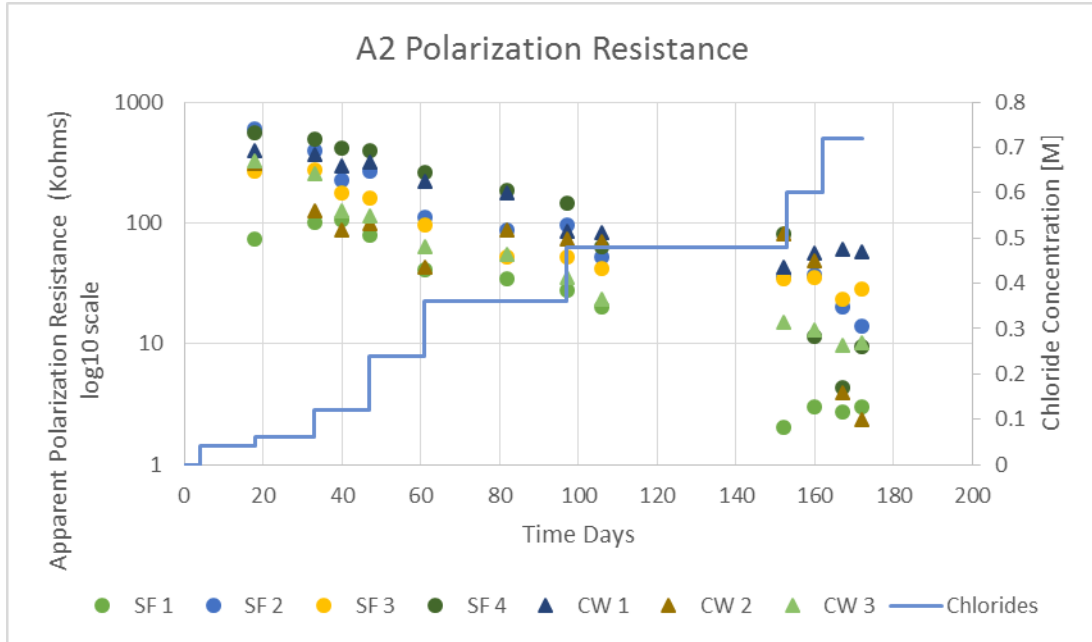


Figure 5.6 Apparent polarization resistance measurements for simulated pore solution sample A2

According to the LPR measurements displayed in figure 5.6, the apparent polarization resistance values were slowly trending downward. The first jump in polarization resistance occurred before the 600mmolar addition for fiber SF 1. At 480mmolar one of the 4 fibers indicated that the chloride threshold was reached. An upper limit of the chloride threshold was not able to be determined because two of the fibers did not indicate electrochemical activity past the 720mmolar chloride addition.

5.3.3 A3- 13.3 pH mortar coating on fibers

Placing bare fibers in the simulated pore solution ensured a complete surface area coverage for hydroxide ions. Mortar was placed on fibers to simulate the natural concrete cover while the fiber was immersed in the high pH solution. The mortar interaction with the fiber was a point of comparison with the other high pH simulated

pore solution. The water to cementitious ratio was high and the mortar did not completely cover the instrumented fibers.

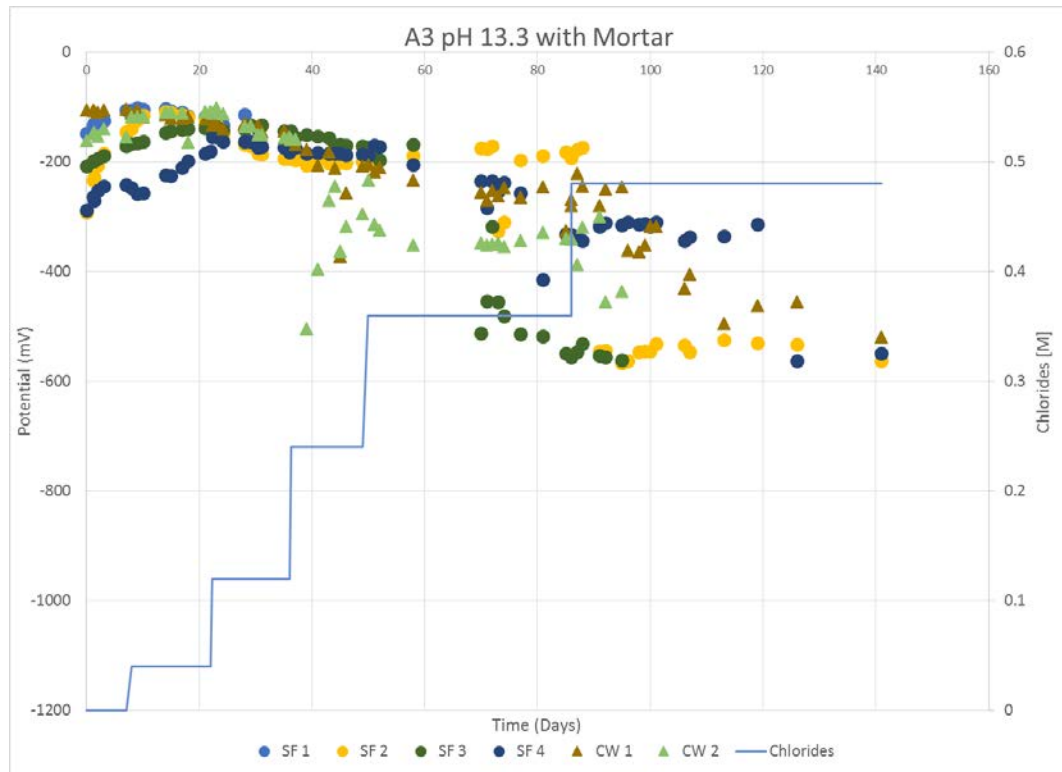


Figure 5.7 Corrosion potential for simulated pore solution A3

Corrosion potential measurements were grouped tightly until the chloride concentration reached 360mmolar. Figure 5.7 depicts the moment that the chlorides started to dissolve the passive layer. The transient began after the 240 mmolar chloride addition for one of the carbon steel wires. Just after day 60 three out of four steel fibers had a drop in potential. The fourth zinc electroplated steel fiber reached the chloride threshold after the 480mmolar chloride addition.

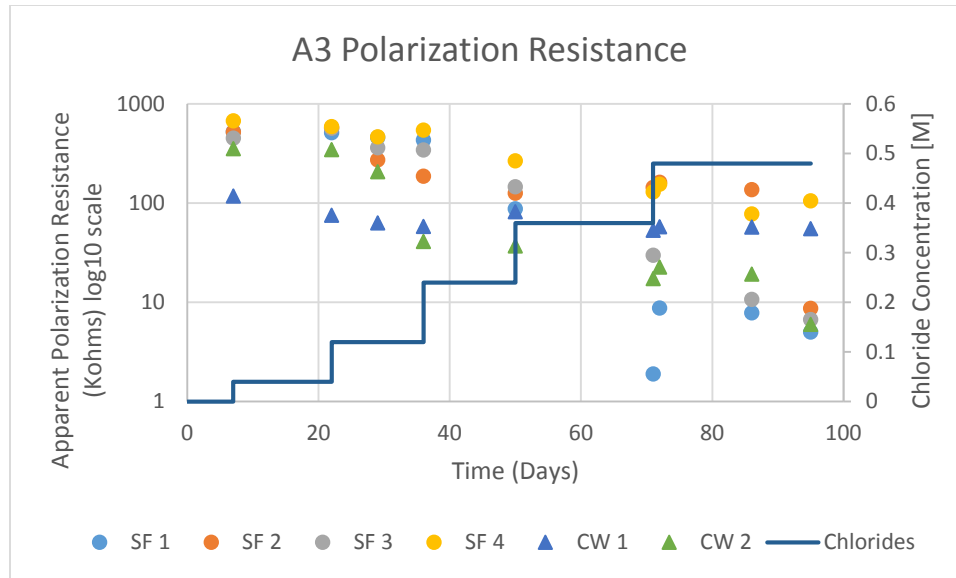


Figure 5.8 Apparent polarization resistance measurements for simulated pore solution sample A3

Similar to the sample A2 (figure 5.6) the polarization resistance values began to slowly decline as chlorides were introduced into the solution. After day 60, drops in apparent polarization resistance indicated electrochemical activity in the SF 1, 3 4. The LPR measurements confirm the chloride threshold for the zinc electroplated steel fibers coated in mortar was between 360 and 480mmolar. Despite the confirmation that corrosion has been initiated, the apparent polarization resistance values for the fibers suggest a moderate corrosion rate. Forensic analysis was expected to determine how much of the fiber was corroded after it had passed the chloride threshold. Analysis has shown that the fibers were most affected by corrosion where the mortar created a crevice. Non homogeneous fiber coverage was observed to stimulate corrosion propagation.



Figure 5.9 Forensic analysis of simulated pore solution A3 SF 1 Photograph by Dietrich Vogel copyright 2016 by Dietrich Vogel

Crevice corrosion was a common source of corrosion initiation and propagation observed in fibers cast with mortar. Because compaction around the fiber was not properly achieved, parts of the mortar paste cover crumbled from the fiber surface upon immersion. Figure 5.9 is a representative example of the effects of the crevice corrosion. Non uniform concrete cover lowered the chloride threshold in comparison to bare fiber immersion.

5.4 Conclusions

- For 12.6pH simulated pore solution, the chloride threshold for zinc electroplated steel fibers was between 10 and 20mmolar
- For 13.3pH simulated pore solution, the lower limit to the chloride threshold was 480 mmolar
- For 13.3pH simulated pore solution, the chloride threshold for zinc electroplated steel fibers coated in mortar was between 360 and 480 mmolar
- The chloride threshold is a range of chloride concentrations that strongly depends on the environment pH

- Non homogeneous fiber surface cover decreases the chloride threshold for zinc electroplated steel fiber

6 SUMMARY AND CONCLUSIONS

6.1 Summary

Results from the experimentation presented in this thesis satisfied the research objectives. Dry-cast concrete used in the highway drainage pipe was characterized with resistivity and non-steady state migration coefficient measurements. The steel fibers embedded in the concrete drainage pipes were electrochemically analyzed for their corrosion potential and linear polarization resistance vs a saturated calomel reference electrode. Zinc electroplated steel fibers embedded in concrete and immersed in simulated pore solution had the chloride threshold passed after varying chloride exposures.

In the first experimental program; concrete was conditioned with chlorides to stimulate varying degrees of corrosion and then the flexural strength was compared to a no chloride control. Beams from flexural strength testing were evaluated for chloride penetration distance and the failure faces were forensically analyzed for fiber amount and condition. Results concluded that the chloride induced corrosion propagation weakened the steel fibers resulting in brittle fractures. Some fibers within the chloride penetration region remained free of red rust stains indicative of steel fiber corrosion.

In the second experimental program; fibers extracted from pipe section cores were re-cast in concrete cylinders. The cylinders were subject to varying chloride concentrations; 4 cylinders were cast with chlorides, 2 cylinders were subject to chloride

electro-migration, and two cylinders were no chloride controls. Over time, the cylinders were observed visually through sliced disk sections. Slices exposed to lab humidity or placed in a Ziploc bag did not exhibit steel fiber corrosion propagation. Corrosion propagation was only observed on slices cast with chlorides left outdoors. Results from this experimental program conclude that the chloride threshold and corrosion propagation are highly dependent on concrete moisture content and oxygen availability at the surface of the fiber. This study confirms good interfacial transition zone covering the zinc electroplated steel fibers.

The third experimental program contained instrumented steel fibers embedded in concrete. The instrumented fibers were subject to varying chloride concentrations. Some cylinders were cast with chlorides, others were subject to chloride electro-migration, few cylinders were subject to passive chloride diffusion and no chloride exposure. The fibers were measured for corrosion potential and linear polarization resistance vs SCE. Over time measurements indicated when fibers have become electrochemically active and surpassed the chloride threshold. The fibers were extracted from the concrete samples and forensically analyzed. Fiber condition was compared to the measurements to determine when the chloride threshold was passed and what the mixed corrosion potential was at that point. Results concluded that the zinc electroplated on the steel fibers produces a protective oxide layer which can be broken down by the right concentration of chlorides. After the passive layer was broken down, the steel fibers corroded at a mixed potential of to -350 to -600mV vs SCE.

In the last experimental program the chloride threshold was pinpointed in simulated concrete pore solutions. Instrumented fibers were suspended in 12.6 and 13.3 pH

solutions. Incrementally, chlorides were added to increase the chloride concentration in the solution. Instrumented fibers were regularly measured for corrosion potential and apparent polarization resistance. Once the measurements indicated that the fibers were electrochemically active and that corrosion has propagated, the samples were terminated and steel fibers were forensically analyzed. The results from this experimental program concluded the chloride threshold for 12.6 and 13.3 simulated pore solution. An additional conclusion was that the chloride threshold depends on the solution pH and the surface area exposure for the fiber.

6.2 Conclusions

6.2.1 Fracture Analysis of Zinc Electroplated Steel Fibers Embedded in Dry-cast Concrete Pipes Exposed to Varying Chlorides

- Upon the presence of corrosion propagation, the modulus of rupture for concrete reinforced with zinc electroplated steel fibers is adversely affected
- The fiber reinforcements resist corrosion propagation in the presence of chlorides alone; corrosion propagation is only possible in the presence of oxygen and humidity when the chloride concentration exceeds the threshold.
- Oxidation products from corroded fibers appear to have traveled through the concrete pore structure which may make identifying fibers difficult
- The moisture content of concrete greatly affects ion diffusion and concrete resistivity
- Some fibers in the chloride penetration zone did not reach the chloride threshold or the zinc layer was not completely consumed

6.2.2 Visual Analysis of Zinc Electroplated Steel Fibers Embedded in Concrete Exposed to Varying Chloride Concentrations

- Chlorides, oxygen, and moisture are required for corrosion propagation of zinc electroplated steel fibers embedded in concrete
- The initial oxidation products create a stronger bond between the steel fiber and cement matrix

6.2.3 Electrochemical Analysis of Zinc Electroplated Steel Fibers Embedded in Concrete Exposed to Varying Chlorides

- The corrosion propagation is highly oxygen dependent; concrete moisture and pore structure affect oxygen transport and the rate of corrosion propagation
- The mixed corrosion potential of steel fibers occurs between -350mV and -600mV vs SCE

6.2.4 Chloride Threshold Determination for Zinc Electroplated Steel Fibers Immersed in Simulated Pore Solution

- For 12.6pH simulated pore solution, the chloride threshold for zinc electroplated steel fibers was between 10 and 20mmolar
- For 13.3pH simulated pore solution, the lower limit to the chloride threshold was 480 mmolar
- For 13.3pH simulated pore solution, the chloride threshold for zinc electroplated steel fibers coated in mortar was between 360 and 480 mmolar
- The chloride threshold is a range of chloride concentrations that strongly depends on the environment pH

- Non homogeneous fiber surface cover decreases the chloride threshold for zinc electroplated steel fibers

7 APPENDIX



Figure 7.1 No chloride exposure pipe section



Figure 7.2 Chloride exposure to the pipe exterior post RMT



Figure 7.3 Chloride exposure to pipe interior post RMT



Figure 7.4 Pipe sections CE (left) and CI (right) subject to environmental conditioning



Figure 7.5 Beam NC1 post ASTM C78

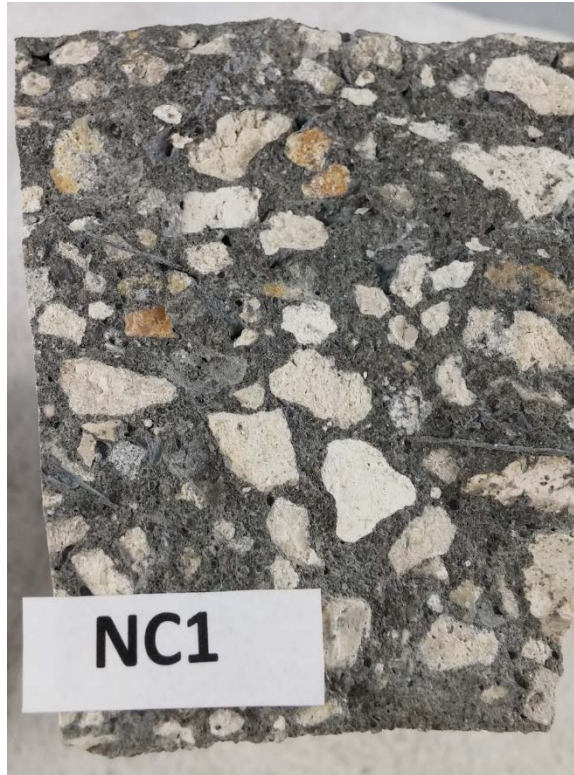


Figure 7.6 Failure plane 1 for beam NC1

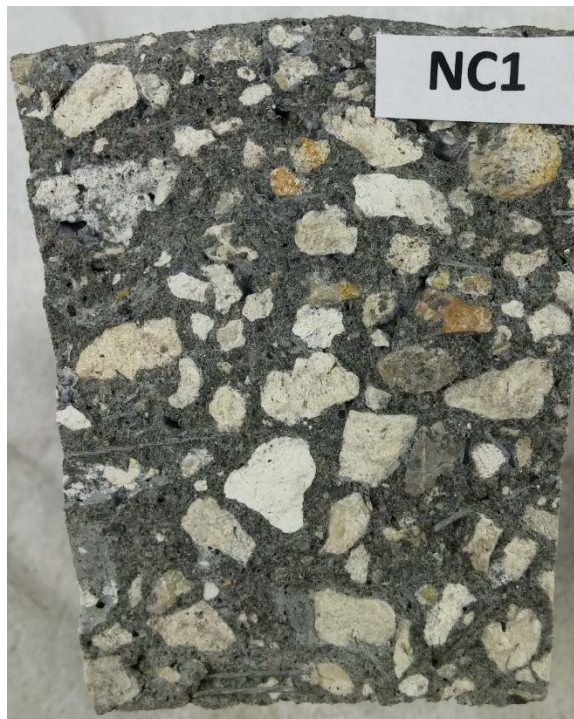


Figure 7.7 Failure plane 2 for beam, NC1



Figure 7.8 Combined failure planes for NC1



Figure 7.9 Beam NC2 post ASTM C78



Figure 7.10 Failure plane 1 for beam NC2



Figure 7.11 Failure plane 2 for beam NC2



Figure 7.12 Combined failure planes NC2



Figure 7.13 Beam crack comparison NC2



Figure 7.14 Beam NC3 post ASTM C78



Figure 7.15 Failure plane 1 for beam NC3



Figure 7.16 Failure plane 2 for beam NC3



Figure 7.17 Combined failure planes NC3



Figure 7.18 Beam CE1 post ASTM C78



Figure 7.19 Combined failure planes CE1



Figure 7.20 Beam crack comparison CE1



Figure 7.21 Beam CE1 sprayed with silver nitrate



Figure 7.22 Beam CE2 post ASTM C78



Figure 7.23 Failure plane 1 for beam CE2



Figure 7.24 Failure plane 2 for beam CE2



Figure 7.25 Companion failure faces CE2



Figure 7.26 Beam CE2 crack comparison



Figure 7.27 Beam CE3 post ASTM C78



Figure 7.28 Failure plane 1 for beam CE3



Figure 7.29 Failure plane 2 for beam CE3



Figure 7.30 Companion failure faces for beam CE3



Figure 7.31 Crack comparison for beam CE3



Figure 7.32 Beam CI1 post ASTM C78



Figure 7.33 Failure plane 1 for beam CI1

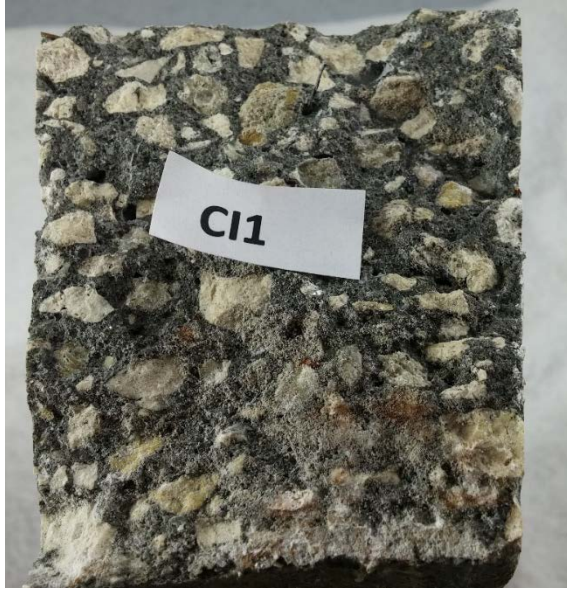


Figure 7.34 Failure plane 2 for beam CI1



Figure 7.35 companion failure planes for beam CI1



Figure 7.36 Failure plane from beam CI1 sprayed with silver nitrate



Figure 7.37 CI 2



Figure 7.38 Failure plane 1 for beam CI2



Figure 7.39 Failure plane 2 for beam CI2



Figure 7.40 Companion failure faces for beam CI2

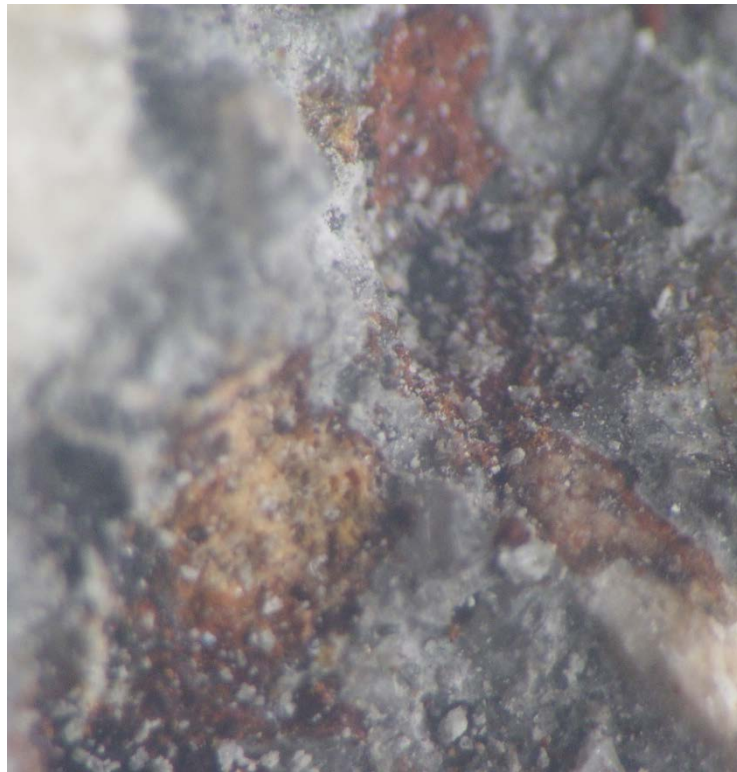


Figure 7.41 Microscope picture of a brittle fracture in beam sample CI2



Figure 7.42 companion face to the previous picture



Figure 7.43 microscopic picture of corrosion propagation on a pullout failure fiber



Figure 7.44 Beam C13 post ASTM C78



Figure 7.45 Failure plane 1 for beam CI3



Figure 7.46 Failure plane 2 for beam CI3

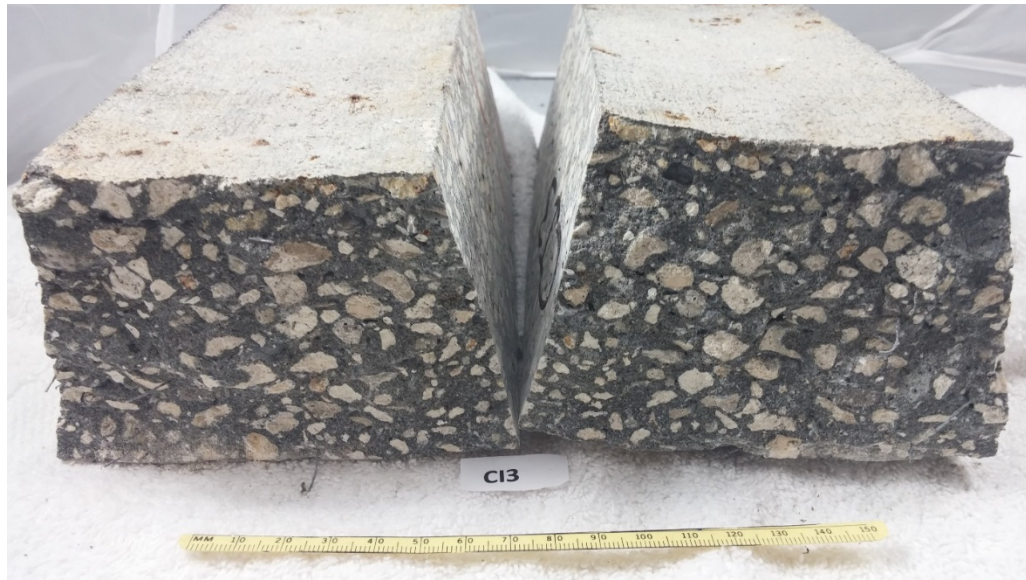


Figure 7.47 companion failure planes for beam CI3



Figure 7.48 Beam SW1 post ASTM C78



Figure 7.49 Failure plane 1 for beam SW1



Figure 7.50 Failure plane 2 for beam SW1



Figure 7.51 Companion failure faces for beam SW1



Figure 7.52 Beam SW2 post ASTM C78

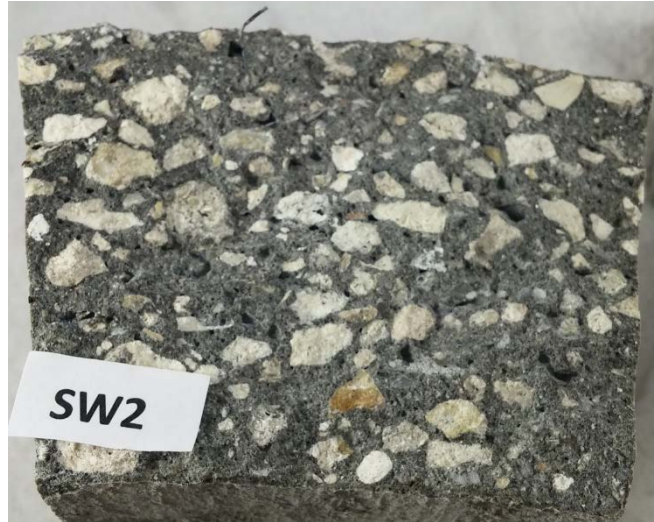


Figure 7.53 Failure plane 1 for beam SW2



Figure 7.54 Failure plane 2 for beam SW2



Figure 7.55 Companion failure planes for beam SW2



Figure 7.56 Beam S1 post ASTM C78



Figure 7.57 Failure plane 1 for beam S1



Figure 7.58 Failure plane 2 for beam S1



Figure 7.59 companion failure planes for beam S1



Figure 7.60 Beam S2 post ASTM C78



Figure 7.61 Failure plane 1 for beam S2



Figure 7.62 Failure plane 2 for beam S2



Figure 7.63 Companion failure planes for beam S2



Figure 7.64 Remaining pipe section pieces NC, CI, CE (left to Right)



Figure 7.65 Concrete mold with 4 inch diameter and 8 inch length



Figure 7.66 Slice 1 From NCB after being sprayed with silver nitrate



Figure 7.67 Slice 4 From NCB after being sprayed with silver nitrate



Figure 7.68 Slices approximately 2mm thick from RMT sample 2 after elevated temperature conditioning



Figure 7.69 Fibers extracted from slice 8mm to 10mm cover depth RMT sample 2



Figure 7.70 Slices approximately 2mm thick from RMT sample 3 after elevated temperature conditioning



Figure 7.71 Fibers extracted from slice 8mm to 10mm cover depth RMT sample 3



Figure 7.72 Slices approximately 2mm thick from RMT sample B after elevated temperature conditioning



Figure 7.73 Fibers extracted from slice 8mm to 10mm cover depth RMT sample B



Figure 7.74 Slices approximately 2mm thick from RMT sample C after elevated temperature conditioning

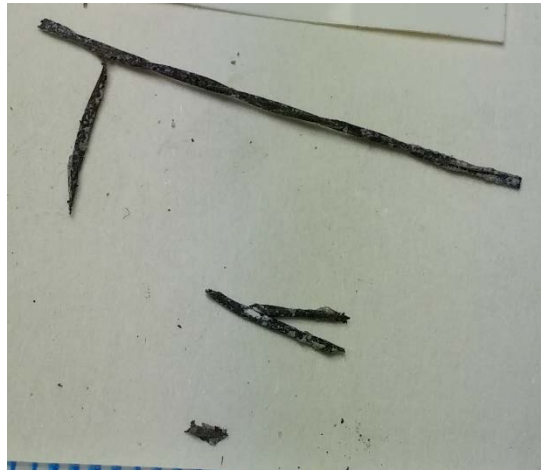


Figure 7.75 Fibers extracted from slice 8mm to 10mm cover depth RMT sample C



Figure 7.76 Non-instrumented no chloride control samples NC and NCI



Figure 7.77 Four slices from sample NCI

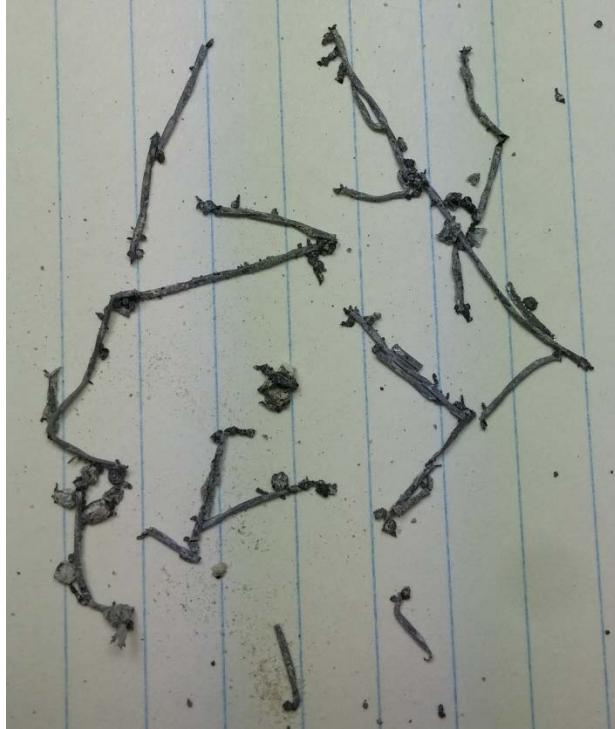


Figure 7.78 Fibers extracted after a NCI slice was crushed immediately after cutting



Figure 7.79 Three slices from sample NC

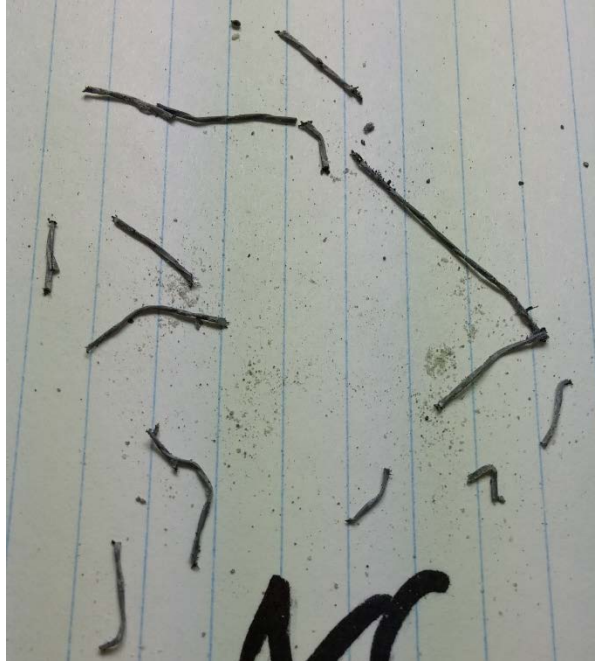


Figure 7.80 Fibers extracted after a NC slice was crushed immediately after cutting



Figure 7.81 Slice NC exposed outdoors 5 weeks after cutting



Figure 7.82 Slice NC exposed outdoors 5 weeks after cutting side 2



Figure 7.83 Fibers extracted from slice NC left outdoors



Figure 7.84 Slice NCI exposed outdoors 5 weeks after cutting



Figure 7.85 Slice NCI exposed outdoors 5 weeks after cutting side 2



Figure 7.86 Fibers extracted from slice NCI left outdoors



Figure 7.87 Slice NC exposed to lab humidity 5 weeks after cutting



Figure 7.88 Slice NC exposed to lab humidity 5 weeks after cutting side 2

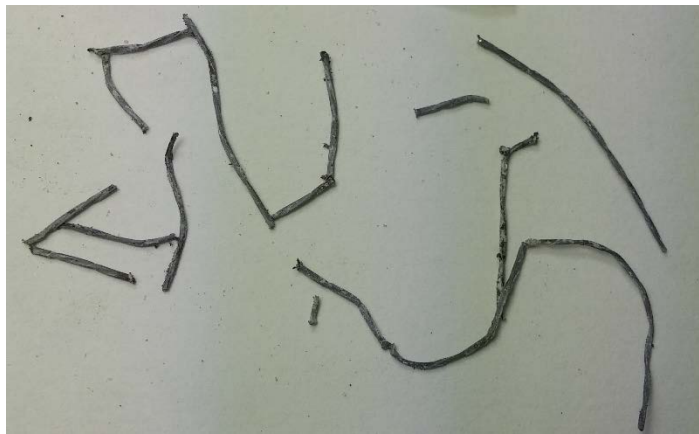


Figure 7.89 fibers extracted from slice NC left in lab humidity



Figure 7.90 Slice NCI exposed to lab humidity 5 weeks after cutting



Figure 7.91 Slice NC exposed to lab humidity 5 weeks after cutting side 2

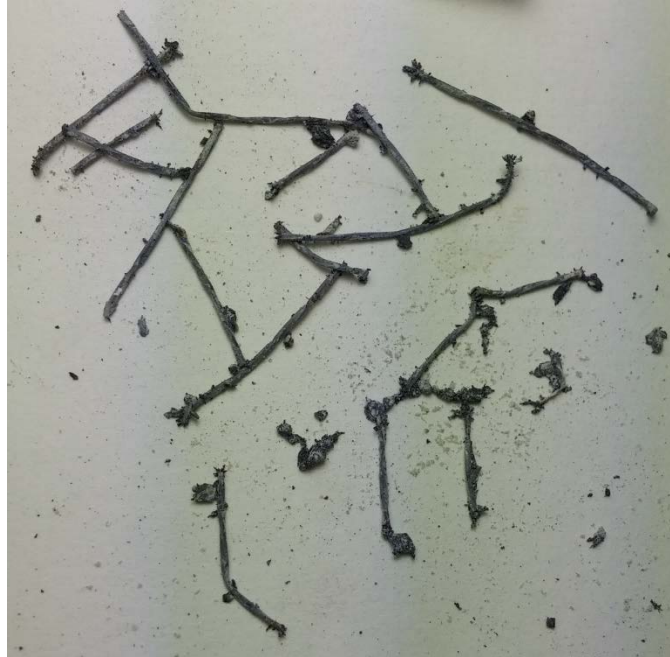


Figure 7.92 Fibers extracted from slice NCI after lab humidity exposure



Figure 7.93 Slice NC exposed to high moisture and low oxygen for 5 weeks after cutting



Figure 7.94 Slice NC exposed to high moisture and low oxygen for 5 weeks after cutting side 2

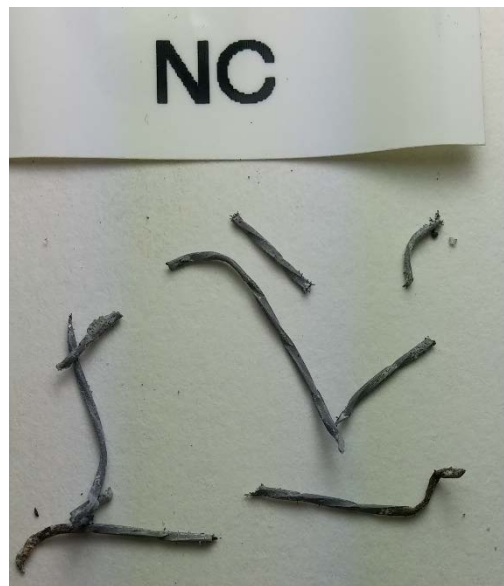


Figure 7.95 Fibers extracted from slice NC exposed to high moisture and low oxygen

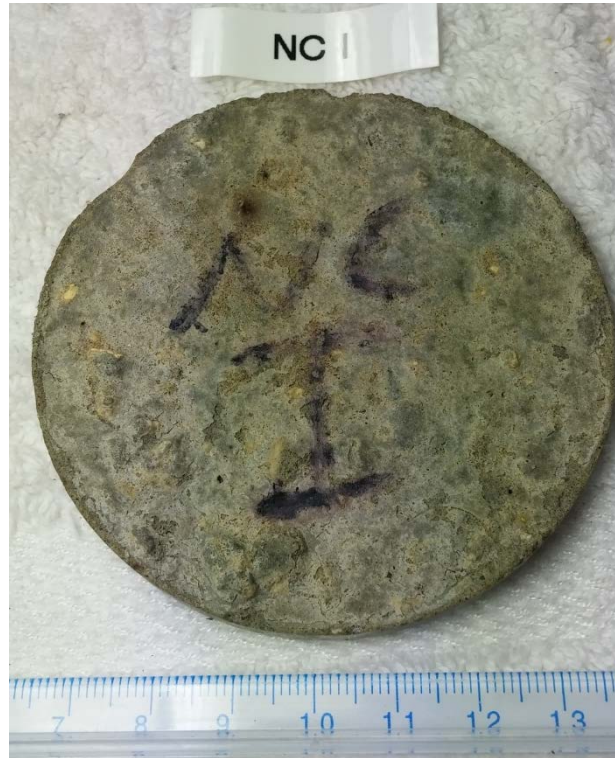


Figure 7.96 Slice NCI exposed to high moisture and low oxygen for 5 weeks after cutting



Figure 7.97 Slice NCI exposed to high moisture and low oxygen for 5 weeks after cutting side 2



Figure 7.98 Fibers extracted from slice NCI exposed to high moisture and low oxygen

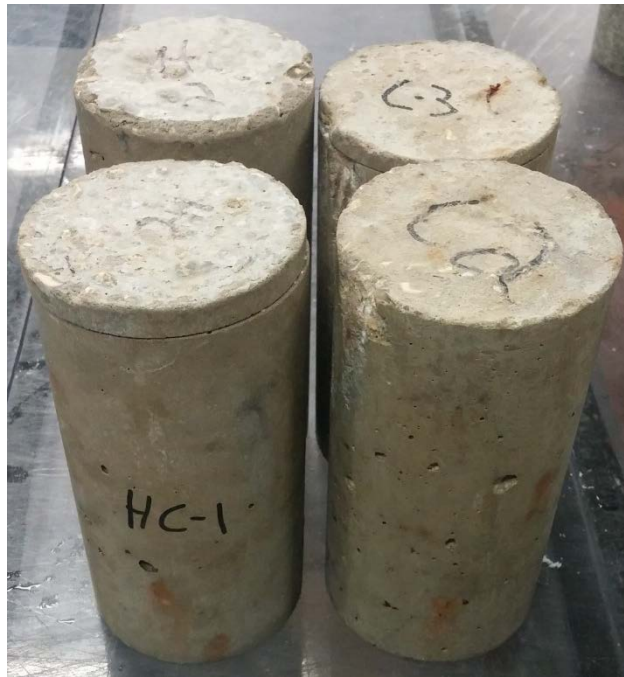


Figure 7.99 Non-instrumented samples cast with chlorides



Figure 7.100 Four slices taken from high chloride sample HC1

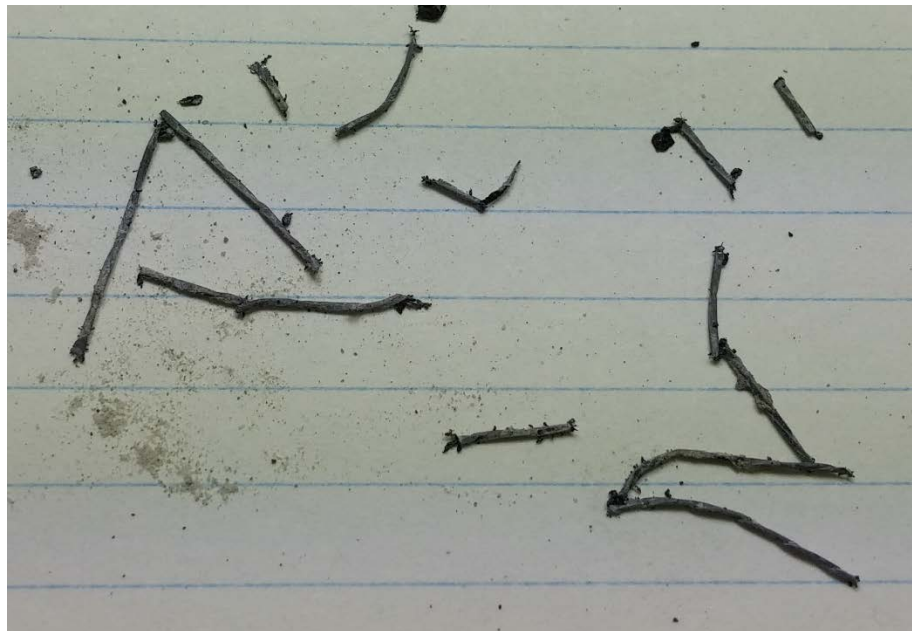


Figure 7.101 Fibers taken from a crushed slice immediately after cutting



Figure 7.102 Slice HC1 after 5 weeks of outdoor exposure



Figure 7.103 Slice HC1 after 5 weeks of outdoor exposure side 2

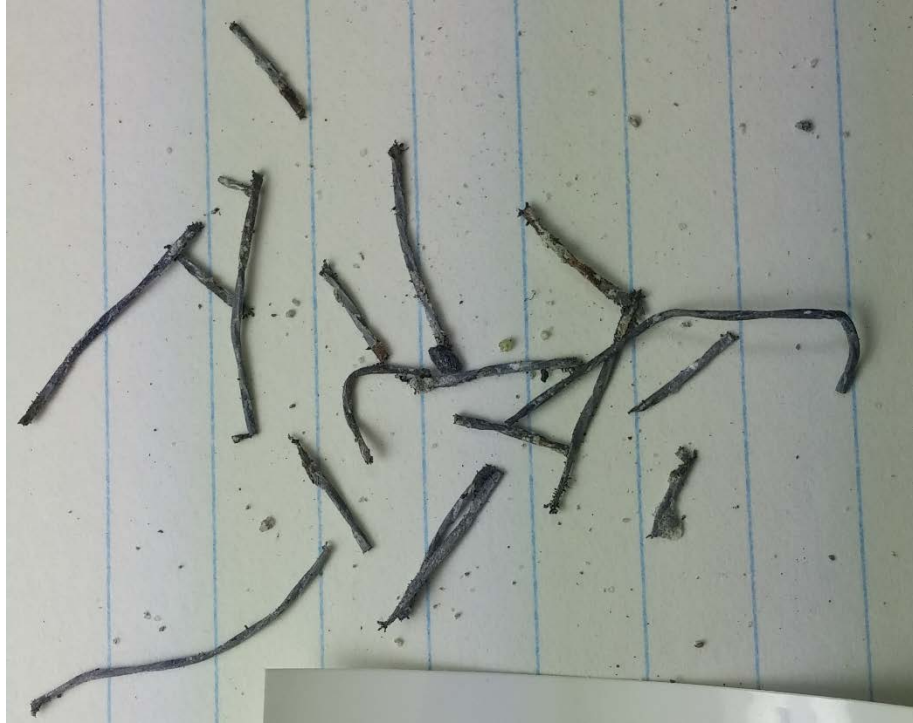


Figure 7.104 fibers extracted from the HC1 slice left outdoors



Figure 7.105 Slice HC1 after 5 weeks of lab humidity exposure



Figure 7.106 Slice HC1 after 5 weeks of lab humidity exposure side 2



Figure 7.107 Fibers extracted from slice HC1 exposed to lab humidity



Figure 7.108 Slice HC1 after 5 weeks of high moisture and limited oxygen exposure



Figure 7.109 Slice HC1 after 5 weeks of high moisture and limited oxygen exposure side

2

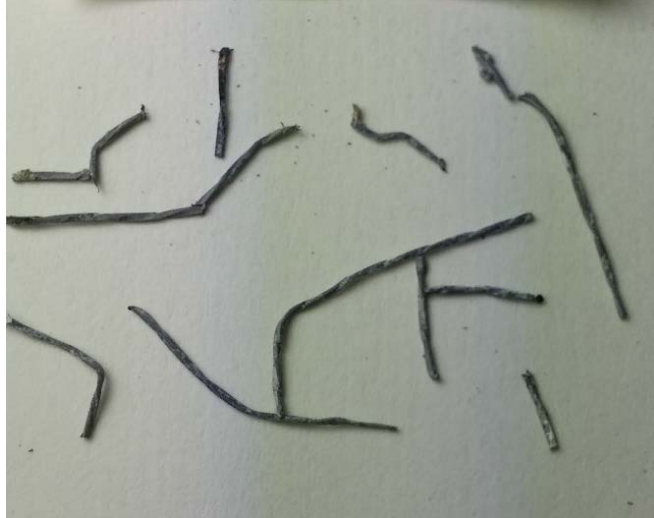


Figure 7.110 Fibers extracted from slice HC1 exposed to high humidity and low oxygen



Figure 7.111 Four slices from cylinder HC2 4 months after casting

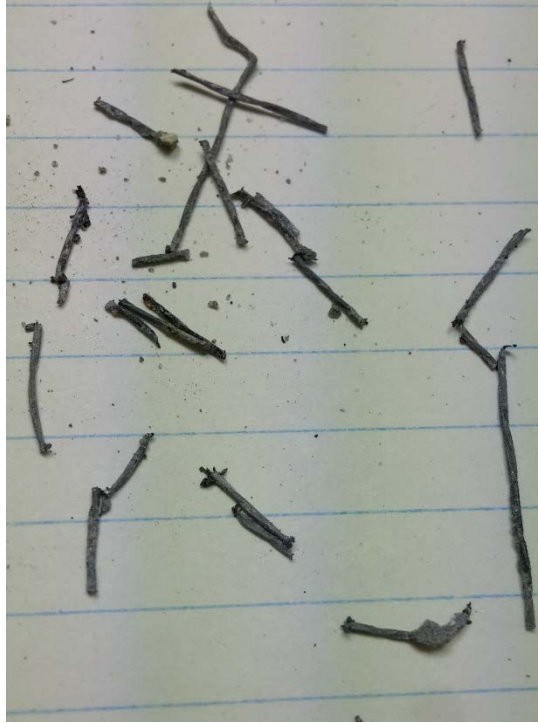


Figure 7.112 fibers extracted from a slice immediately after cutting



Figure 7.113 Slice HC2 after 5 weeks of outdoor exposure



Figure 7.114 Slice HC2 after 5 weeks of outdoor exposure side 2

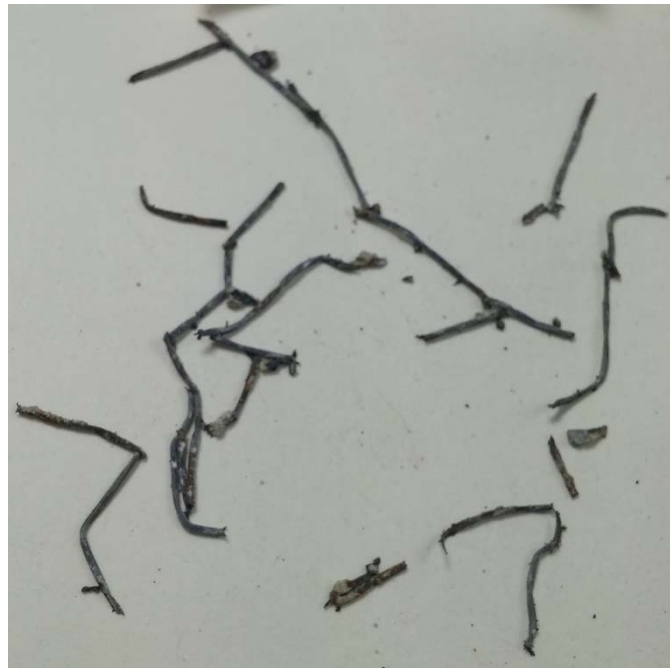


Figure 7.115 Fibers extracted from slice HC2 left outdoors



Figure 7.116 Slice HC2 after 5 weeks of lab humidity exposure



Figure 7.117 Slice HC2 after 5 weeks of lab humidity exposure side 2



Figure 7.118 Fibers extracted from the HC2 slice left in lab humidity



Figure 7.119 Slice HC2 after 5 weeks of high moisture and low oxygen exposure



Figure 7.120 Slice HC2 after 5 weeks of high moisture and low oxygen exposure side 2

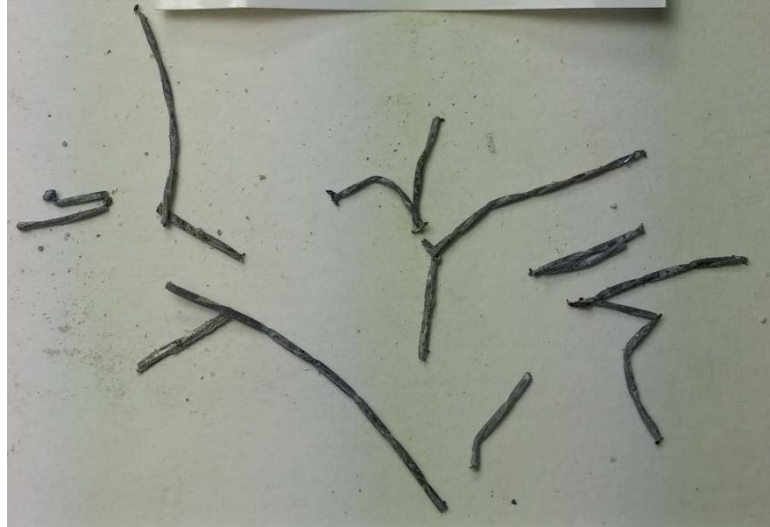


Figure 7.121 Fibers extracted from slice HC2 exposed to high moisture and low humidity



Figure 7.122 Four chloride slices from sample C2 taken 6 months after casting.

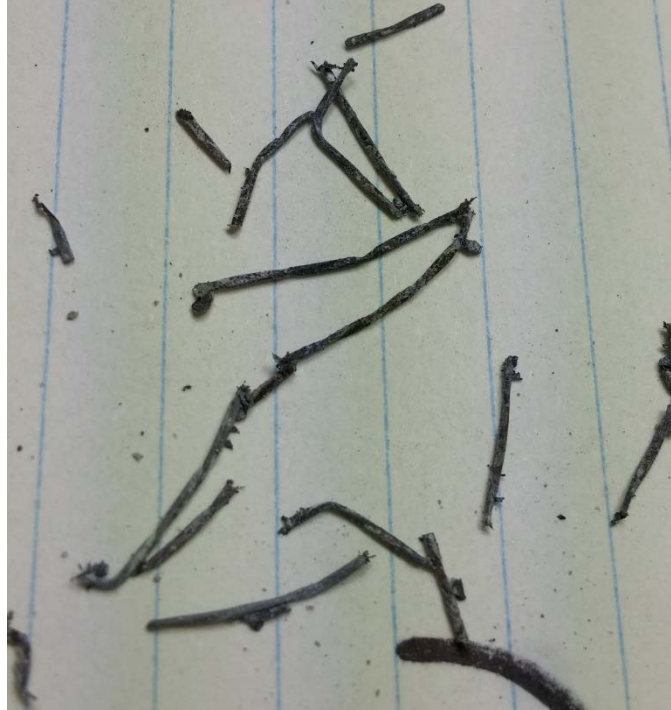


Figure 7.123 Fibers extracted from a slice C2 immediately after cutting



Figure 7.124 Slice C2 after 5 weeks of outdoor exposure



Figure 7.125 Slice C2 after 5 weeks of outdoor exposure side 2



Figure 7.126 Fibers extracted from slice C2 left outdoors



Figure 7.127 Slice C2 exposed to lab humidity for 5 weeks after cutting



Figure 7.128 Slice C2 after 5 weeks of outdoor exposure side 2

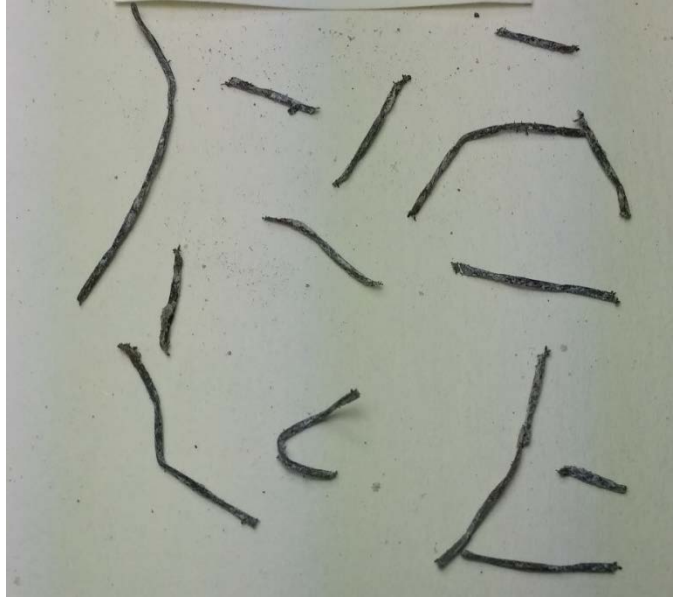


Figure 7.129 Fibers extracted from slice C2 after lab humidity exposure



Figure 7.130 Slice C2 exposed to high moisture and low oxygen for 5 weeks after cutting



Figure 7.131 Slice C2 exposed to high moisture and low oxygen for 5 weeks after cutting side 2



Figure 7.132 Fibers extracted from slice C2 exposed to high moisture and limited oxygen



Figure 7.133 Four slices from cylinder C3 cut 6 months after casting with chlorides

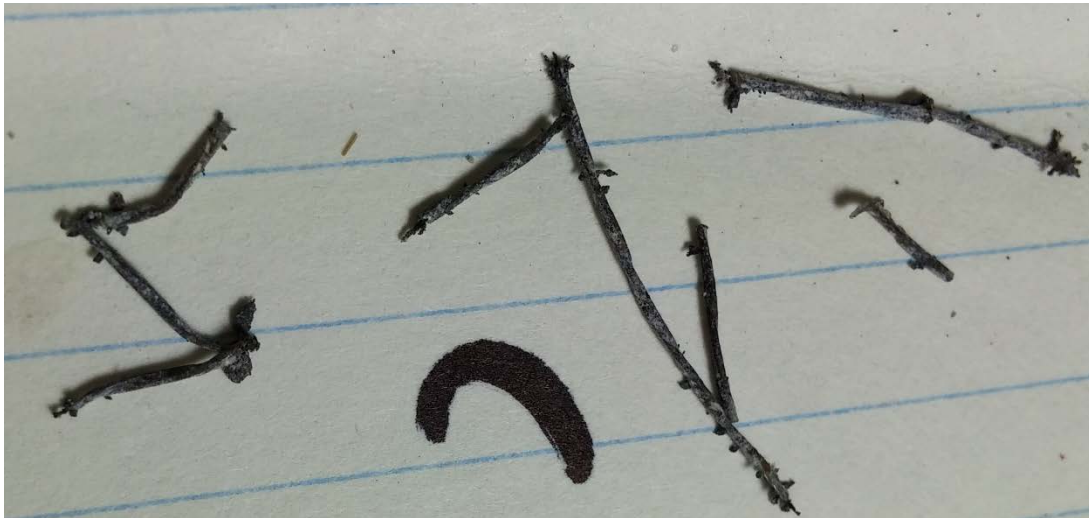


Figure 7.134 fibers extracted from a slice immediately after cutting

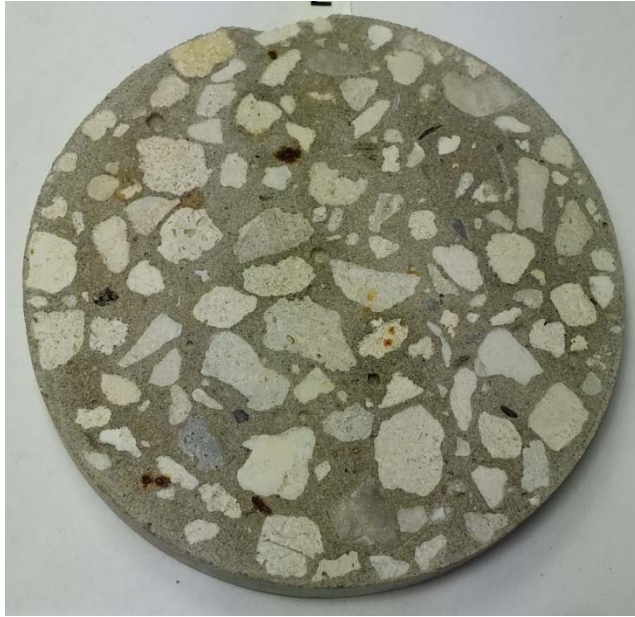


Figure 7.135 Slice C3 exposed outdoors for 5 weeks after cutting



Figure 7.136 Slice C3 exposed outdoors for 5 weeks after cutting side 2



Figure 7.137 Fibers extracted from slice C3 left outdoors



Figure 7.138 Slice C3 exposed to lab humidity for 5 weeks after cutting



Figure 7.139 Slice C3 exposed to lab humidity for 5 weeks after cutting side 2

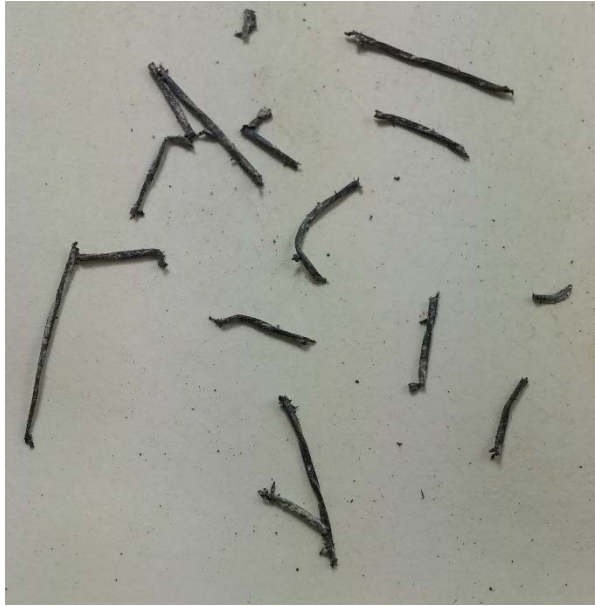


Figure 7.140 Fibers extracted from slice C3 exposed to lab humidity



Figure 7.141 Slice C3 exposed to high moisture and low oxygen for 5 weeks after cutting



Figure 7.142 Slice C3 exposed to high moisture and low oxygen for 5 weeks after cutting side 2



Figure 7.143 Fibers extracted from slice C3 exposed to high moisture and low oxygen



Figure 7.144 All samples cast by the researcher used in the experimental programs



Figure 7.145 Instrumented cylinders cast without chlorides for experimental control



Figure 7.146 No chloride cylinder C1



Figure 7.147 CW1 from C1



Figure 7.148 SF1 from C1



Figure 7.149 Cylinder C6



Figure 7.150 SF1 from C6



Figure 7.151 SF2 from C6



Figure 7.152 Cylinders subject to passive chloride migration HWC right, LWCA center and LWCB right

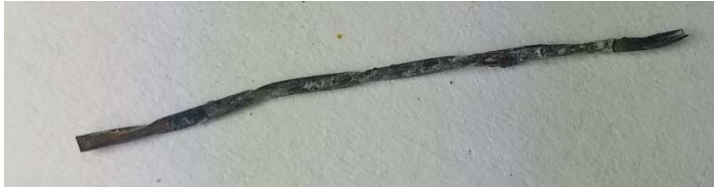


Figure 7.153 SF 1 from cylinder LWCA



Figure 7.154 CW from LWCA



Figure 7.155 SF 2 from LWCA



Figure 7.156 LWCB after pond removal



Figure 7.157 SF1 from cylinder LWCB

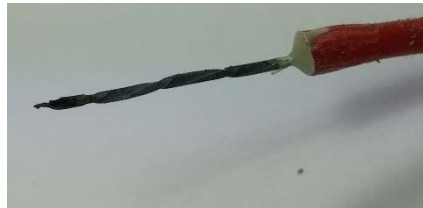


Figure 7.158 SF2 from LWCB



Figure 7.159 CW from LWCB



Figure 7.160 SF1 from HWC



Figure 7.161 CW from HWC



Figure 7.162 SF2 from HWC



Figure 7.163 Poke instrumentation cylinders P1 left P2 right



Figure 7.164 Carbon steel wires from poke sample P1 9 months after casting



Figure 7.165 CW1 at 40mm cover depth from sample P1



Figure 7.166 CW2 at 30mm cover depth from sample P1



Figure 7.167 CW3 at 20mm cover depth from sample P1



Figure 7.168 Steel fiber face from poke sample P1



Figure 7.169 SF1 at 40mm cover depth from sample P1



Figure 7.170 SF2 at 30mm cover depth from sample P1



Figure 7.171 SF3 at 20mm cover depth from sample P1



Figure 7.172 Carbon steel wires exposed on sample P2 8 months after casting



Figure 7.173 CW1 at 40mm cover depth from sample P2



Figure 7.174 CW2 at 30mm cover depth from sample P2



Figure 7.175 CW3 at 20mm cover depth from sample P2



Figure 7.176 CW4 at 10mm cover depth from sample P2



Figure 7.177 steel fibers while exposed from sample P2



Figure 7.178 SF1 40mm cover depth sample P2



Figure 7.179 SF2 30mm cover depth sample P2



Figure 7.180 SF3 20mm cover depth sample P2



Figure 7.181 SF4 10mm cover depth sample P2



Figure 7.182 MLWC1 left and MLWC2 right while ponded



Figure 7.183 SF 11 cover depth 10mm from MLWC1



Figure 7.184 CW 12 cover depth 10mm from MLWC1



Figure 7.185 SF 13 cover depth 10mm from MLWC1



Figure 7.186 SF 21 cover depth 20mm from MLWC1



Figure 7.187 CW 22 cover depth 20mm from MLWC1



Figure 7.188 SF 23 cover depth 20mm from MLWC1



Figure 7.189 SF 31 cover depth 30mm from MLWC1



Figure 7.190 CW 32 cover depth 30mm from MLWC1



Figure 7.191 SF 33 cover depth 30mm from MLWC1



Figure 7.192 SF 11 cover depth 10mm from MLWC2



Figure 7.193 SF 12 cover depth 10mm from MLWC2



Figure 7.194 CW 13 cover depth 10mm from MLWC2



Figure 7.195 SF 21 cover depth 20mm from MLWC2



Figure 7.196 SF 22 cover depth 20mm from MLWC2



Figure 7.197 CW 23 cover depth 20mm from MLWC2



Figure 7.198 SF 31 cover depth 30mm from MLWC2



Figure 7.199 SF 32 cover depth 30mm from MLWC2



Figure 7.200 CW 33 cover depth 30mm from MLWC2



Figure 7.201 Sample B1 left and sample B2 right shown with reservoir ponds



Figure 7.202 SF1 at 10mm cover depth taken from sample B1



Figure 7.203 Instrumented SF2 at 20mm cover depth taken from sample B1



Figure 7.204 SF2 at 20mm cover depth taken from sample B1



Figure 7.205 SF3 at 30mm cover depth taken from sample B1

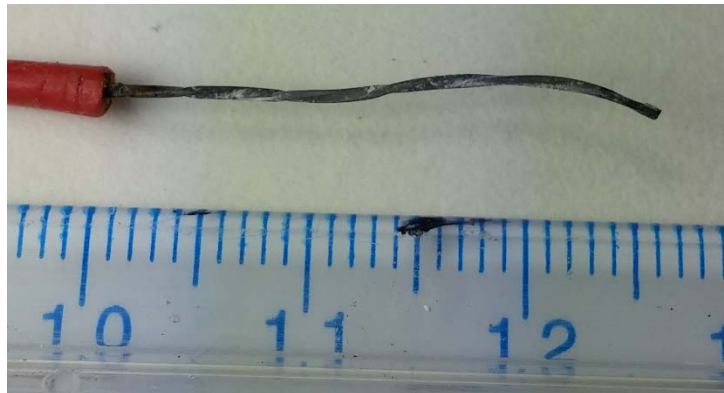


Figure 7.206 Instrumented SF4 at 40mm cover depth taken from sample B1



Figure 7.207 SF4 at 40mm cover depth taken from sample B1



Figure 7.208 CW1 at 40mm cover depth taken from sample B1



Figure 7.209 Instrumented CW2



Figure 7.210 CW2 at 30mm cover depth taken from sample B1 much of the fiber was destroyed by the milling process to obtain a chloride profile



Figure 7.211 CW 3 at 20mm cover depth taken from sample B1



Figure 7.212 CW 4 at 10mm cover depth taken from sample B1



Figure 7.213 Sample B2 after the first step of forensic analysis



Figure 7.214 Instrumented CW1 at 10mm cover depth taken from sample B2



Figure 7.215 Instrumented CW2 at 20mm cover depth taken from sample B2



Figure 7.216 Instrumented SF1 at 12.5mm cover depth taken from sample B2



Figure 7.217 SF1 at 12.5mm cover depth taken from sample B2



Figure 7.218 Instrumented SF2 at 20mm cover depth taken from sample B2



Figure 7.219 SF2 at 20mm cover depth taken from sample B2



Figure 7.220 Instrumented SF3 at 10mm cover depth taken from sample B2



Figure 7.221 SF3 at 10mm cover depth taken from sample B2



Figure 7.222 Samples cast with chlorides C8 left, C7 center, and C4 right



Figure 7.223 SF1 from sample C4

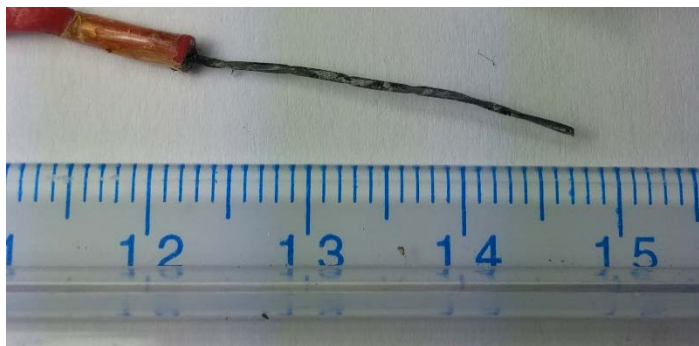


Figure 7.224 SF2 with instrumentation from sample C4



Figure 7.225 SF2 from sample C4

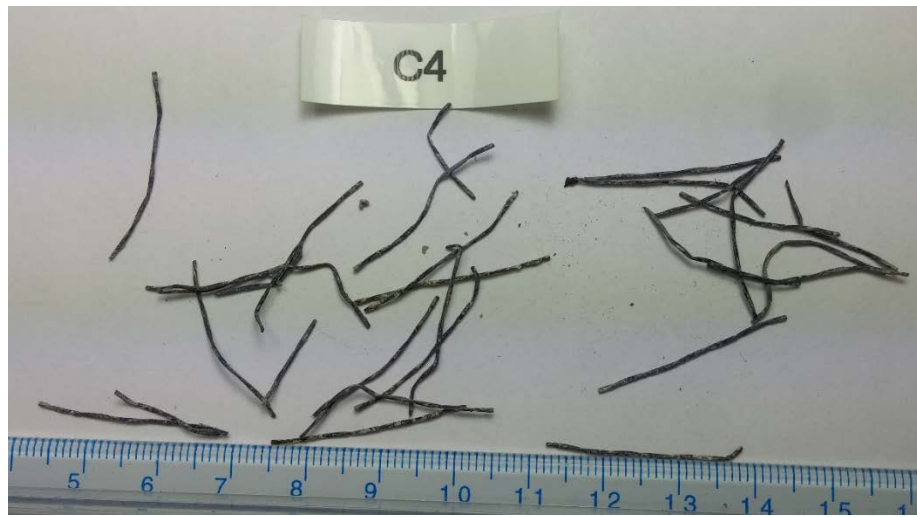


Figure 7.226 Assorted non-instrumented fibers embedded in sample C4



Figure 7.227 SF1 and SF2 from sample C4



Figure 7.228 Sample C7 before forensic analysis



Figure 7.229 Both steel fibers from sample C7, SF1 left, SF2 right



Figure 7.230 Steel fiber 1 from sample C7



Figure 7.231 Steel fiber 2 from sample C7



Figure 7.232 Carbon steel wire embedded in C8 with instrumentation



Figure 7.233 Carbon steel wire embedded in C8 without instrumentation



Figure 7.234 SF1 from sample C8



Figure 7.235 SF2 from sample C8



Figure 7.236 Assorted non-instrumented fibers embedded in sample C8



Figure 7.237 Simulated pore solution samples A1 A2 A3 left to right



Figure 7.238 Fiber group from simulated pore solution A1



Figure 7.239 A1 fiber 1



Figure 7.240 A1 fiber 2



Figure 7.241 A1 fiber 3



Figure 7.242 A1 fiber 4



Figure 7.243 A1 fiber 5



Figure 7.244 A1 fiber 6



Figure 7.245 Fiber group immediately after immersion sample A3



Figure 7.246 A3 fiber 1 coated in mortar



Figure 7.247 A3 fiber 1



Figure 7.248 A3 fiber 2 coated in mortar post immersion



Figure 7.249 A3 fiber 2



Figure 7.250 A3 fiber 3 coated in mortar post immersion



Figure 7.251 A3 fiber 3 without mortar



Figure 7.252 A3 fiber 4 after immersion



Figure 7.253 A3 fiber 4



Figure 7.254 Carbon steel wire coated in mortar; A3 fiber 5



Figure 7.255 Carbon steel wire: A3 fiber 5

8 REFERENCES

1. Judy Brewer. *"The History of Concrete"*. Dept. of Materials Science and Engineering, University of Illinois, Urbana-Champaign. Published online in 2007: <http://matse1.matse.illinois.edu/concrete/hist.html>
2. "Hot-Dip Galvanized Reinforcing Steel A Concrete Investment". *International Zinc Association*. Brochure published in 2006, <http://www.galvanizedrebar.com>
3. Basham, Kim. *Choices in Corrosion Resistant Rebar*. Published in "Concrete Construction" magazine, October 1999
4. Halvorsen, Kesler, Robinson, Stout. ACI Committee 544. "Report on the Physical Properties and Durability of Fiber-Reinforced Concrete" American Concrete Institute. Published 1976-1978
5. "Top 10 Reasons: To Design with Helix Micro Rebar vs. Rebar/Mesh" *Precise Forms, INC.* published 2007.
http://www.preciseforms.com/literature/PFI_Top%2010%20Reasons%20to%20Design%20with%20Helix.pdf
6. Raupach, M and Dauberschmidt, C. "Critical Chloride Content for the Corrosion of Steel Fibers in Artificial Concrete Pore Solutions". American Concrete Institute. SP-212-11, P165-179, published 2003
7. MANGAT, P. and MOLLOY, B. T. (2000). Size effect of reinforcement on corrosion initiation. In: *5th RILEM Symposium on Fibre-Reinforced Concretes (FRC)*, Lyon, France, September 13-15, 2000. 691-701.

8. FM 5-578, Florida Method of Test For Concrete Resistivity as an Electrical Indicator of its Permeability. FDOT, 2004.
9. NT BUILD 492, Concrete, Mortar, and Cement-based Repair Materials: Chloride Migration Coefficient from Non-steady-State Migration Experiments. NORDTEST, 1999.
10. ASTM C78 / C78M-15b, Standard Test Method for Flexural Strength of Concrete (Using Simple Beam with Third-Point Loading), ASTM International, West Conshohocken, PA, 2016, www.astm.org
11. BD545-41, Durability of Fiber-Reinforced Concrete in Florida Environments. FDOT, July 2009